Improved Processes to Remove Naphthenic Acids

Final Technical Report

(From October 1, 2002 to September 30, 2005)

Principle Authors

Aihua Zhang, Qisheng Ma, Kangshi Wang,
Yongchun Tang (co-PI), William A. Goddard (PI),

Date Report was issued: December 9, 2005

Name and Address of Submitting Organization

California Institute of Technology
1200 East California Blvd.,
Pasadena, CA91125

Disclaimer

This report was prepared as an account of work sponsored by an agency of the United States Government. Neither the United States Government nor any agency thereof, nor any of their employees, makes any warranty, express or implied, or assumes any legal liability or responsibility for the accuracy, completeness, or usefulness of any information, apparatus, product, or process disclosed, or represents that its use would not infringe privately owned rights. Reference herein to any specific commercial products, process, or services by trade name, trademark, manufacturer, or otherwise does not necessarily constitute or imply its endorsement, recommendation, or favoring by the United States Government or any agency thereof. The views and opinions of authors expressed herein do not necessarily state or reflect those of the United States Government or any agency thereof.

Abstract

In the past three years, we followed the work plan as we suggested in the proposal and made every efforts to fulfill the project objectives. Based on our large amount of creative and productive work, including both of experimental and theoretic aspects, we received important technical breakthrough on naphthenic acid removal process and obtained deep insight on catalytic decarboxylation chemistry. In detail, we established an integrated methodology to serve for all of the experimental and theoretical work. Our experimental investigation results in discovery of four type effective catalysts to the reaction of decarboxylation of model carboxylic acid compounds. The adsorption experiment revealed the effectiveness of several solid materials to naphthenic acid adsorption and acidity reduction of crude oil, which can be either natural minerals or synthesized materials. The test with crude oil also received promising results, which can be potentially developed into a practical process for oil industry. The theoretical work predicted several possible catalytic decarboxylation mechanisms that would govern the decarboxylation pathways depending on the type of catalysts being used. The calculation for reaction activation energy was in good agreement with our experimental measurements.

Table of Content

Improved Processes to Remove Naphthenic Acids

List of Figures

List of Tables

1. Introduction

Liquid petroleum, or crude oil, is a complex mixture of organic compounds predominately composed of hydrocarbons, and often contains large amounts of other compounds such as organic and inorganic sulfur species, chloride and nitrogen compounds, trace metals and naphthenic acids. The name naphthenic acid (NA) derives from the first observation of the acidity in naphthenic-based crude from the Baku Region, of Russia in 1920's [1]. The chemical composition of NAs is extremely complex and a great variety of structures and compositions fall within the classification of NA [2, 3]. In general, NA is characterized by a carboxylic acid functional group attached to a hydrocarbon molecule, and a generalized chemical formula of $R(CH_2)_nCOOH$ can be applied where R is a cyclopentane ring and n is typically greater than 12. However, a multitude of other acidic compounds are also present, and the chemistry of petroleum related naphthenic acids has yet been completely characterized. The presence of NA compounds contributes to the acidity of crude oils and is one of the major sources of corrosion in oil pipelines and distillation units in oil refineries [4-6]. Consequently, crude oils with high naphthenic acid concentrations are considered to be of poor quality and marketed at a lower price.

Total acid number (TAN), defined as the number of milligrams of KOH required neutralizing the acidity of one gram oil, is a commonly accepted criterion for the oil acidity, although its correlation with corrosive behavior is still controversial [7]. Based on this measurement, oils with a TAN number greater than 0.5 are classified as highly acidic. High TAN crude oils are commonly encountered in California, Venezuela, the North Sea, Western Africa, India, China and Russia.

Removing NA compounds from crude oils is regarded as one of the most important processes in heavy oil upgrading. Current industrial practices either depend on dilution or caustic washing methods to reduce the TAN number of heavy crude oils [8]. However, neither of these approaches is entirely satisfactory. For instance, blending a high TAN crude oil with a low TAN one may reduce the naphthenic acid content to an acceptable level, but the acidic compounds remain and the value of the low TAN oil is diminished. Caustic treatment can substantially remove NAs, but the process generates significant amounts of wastewater and emulsions that are problematic to treat. In particular, once an emulsion is formed, it is very difficult to remove.

Accordingly, the objective of this study was to develop a low-temperature and cost effective methods, including catalytic and adsorptive approaches, to remove naphthenic acids from crude oil. In detail, our objectives are 1) to develop a novel decarboxylation process to convert naphthenic acid compounds into non-corrosive components and 2) to remove naphthenic acid via a chemical adsorptive process by using solid adsorbents.

Catalytic decarboxylation is a well-established chemical reaction in organic and biochemical processes that has been widely applied in organic synthesis and even applied to the identification of coal structure through oxidative decarboxylation [9]. Cu-based catalysts, predominately employed homogeneously, are commonly used [10,11], and in some cases, the presence of organic nitrogen compounds is also necessary [12]. Additionally, there are reports that ZrO_2 can promote the catalytic decarboxylation of acetic acid in supercritical water (673K, 25-40MPa) [13]. Tungsten complexes facilitate catalytic decarboxylation of cyanoacetic acid through homogeneous catalysis [14]. Zeolite has also been applied in the catalytic decarboxylation of benzoic acid but the reaction occurred at around 400°C [15]. Nevertheless, most of these studies are limited to the delicate catalyst system such as transition metal complexes, which have relatively low stabilities at the increased temperatures. The application of them to crude oil is not practical.

Developing a low cost effective adsorptive process to remove naphthenic acid is also of great importance in this work. The naphthenic acid, existing in complex mixture of organic compounds, can be selectively extracted and condensed through solid adsorbents. If the two processes can reach a complementary for each other, it would be an ideal concept for the process design.

Theoretical calculation consists of one of the major works for this project. It plays an important role in explaining experimental phenomena, predicting reaction or change trends, and providing theoretic instruction to the designs of the catalysts or adsorbents.

In the past three years, we followed the work plan as we suggested in the proposal and made every efforts to fulfill the project objectives. We conducted a large amount of experimental and theoretical work to develop effective and practical decarboxylation catalyst/adsorbents and also try to obtain profound understanding on catalytic decarboxylation and naphthenic acid removal process.

2. Methodologies

2.1 Experimental methods for model compounds and mixed acid solution

2.1.1   Model carboxylic acids and mixed acid solution

A set of carboxylic acids, including 2-naphthoic acid ($C_{10}H_7COOH$), cyclohexane carboxylic acid ($C_6H_{11}COOH$) and cyclohexane propionic acid ($C_6H_{11}C_2H_5COOH$) were selected as the model compounds to represent aromatic and saturated NAs. Naphthoic acid was used in most catalytic tests due to its proper physical property and similarity to the acidic compounds most often encountered in crude oils.

A mixed hydrocarbon-acid solution was also prepared by dissolving five organic acids in dodecane to more closely model actual NA compositions in oils. The five acids were cyclohexane carboxylic acid (CHCA), cyclopentane carboxylic acid (CPCA), benzoic acid (BA), C_5H_{11}-CHCA and C_7H_{15}-BA, and their weight concentrations in dodecane were 2.471%, 1.927%, 0.871%, 1.099%, and 1.107% respectively. The structures and physical properties of the carboxylic acids used in this study were listed in Table 1.

2.1.2   Catalyst materials and catalyst preparation

Four types of solid catalysts, which are alkaline earth metal oxides, oxidative metal oxides, zeolite and supported precious metal, were involved in this study. These catalysts were either commercial available or prepared through specified procedure.

Commercially available compounds such as MgO, CaO, Ag_2O, Cu_2O, MnO_2 were used in this study. For MgO, it was calcined at 800°C for 10hrs prior to use for activation.

Several supported metal catalysts such as Pt/SiO_2, Ni/Al_2O_3 and Cu/SiO_2 were also tested in the reactions involving the model acid or mixed hydrocarbon-acid solution. These supported metal catalysts were prepared by impregnating their salt solutions such as H_2PtCl_6, $NiCl_2$ and $CuCl_2$ on the supports followed by hydrogen reduction at 400°C for 1hr.   The typical concentrations of metals on supports were 0.5wt%.

A strong acidic zeolite, ZSM-5 type zeolites were applied in this work. The materials were obtained from ZEOLYST and the products data were shown in Table 2. The high SiO_2/Al_2O_3 ratios indicate their strong acidities. Before the running, all of the three zeolites were activated at 450°C overnight. With this treatment, the ammonium type zeolites (CBV 3024E and CBV 8014E) could be converted to their hydrogen type.

Table 1: Structures and properties for several carboxylic acids

Carboxylic Acids	Structures	Molecular Weight	MP(°C)	BP(°C)
2-Naphthoic acid		172.18	185.5	>300
Cyclohexane carboxylic acid		128.17	31.5	232.5
Cyclohexanepropionic acid		156.22	16.0	276.5
Cyclopentane carboxylic acid		114.14	4.0	216.0
Benzoic acid		122.12	122.4	249.2
Trans-Pentylcyclohexanecarboxylic acid		198.31	51-53	110.0
4-Heptyl benzoic acid		220.31		
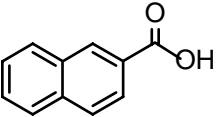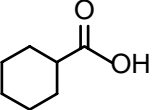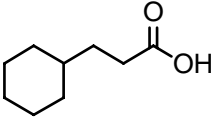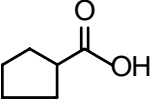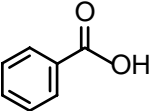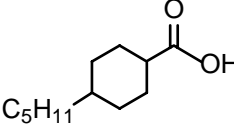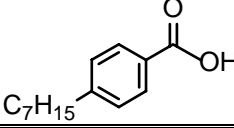
Table 2: Data of ZSM-5 type zeolites

Catalyst	SiO_2/Al_2O_3 Mole ratio	Nominal cation form	Na_2O Weight %	Surface Area (m^2/g)
CBV 3020E	30	Hydrogen	0.10	400
CBV 3024E	30	Ammonium	0.05	400
CBV 8014E	80	Ammonium	0.05	425

The zeolites were activated overnight at 450°C prior to use.

Supposing this treatment can convert ammonium type zeolite to hydrogen type zeolite.

Powder catalysts were mainly used in batch reactions, while granular ones with an average particle size of 28-65 mesh were loaded into a tubular flow reactor in order to reduce the resistance to flow during oil addition.

2.1.3   Sealed glass tube batch reaction – reactor, operation and analysis

This method was specially developed for the purpose of fast screening for the large amounts of catalyst candidates due to its simplicity, simultaneous availability for multiple reactors.

About 2- ml sealed glass tube batch reactors were used for single model compound reaction and the larger ones (~9ml) for mixed hydrocarbon-acid solution reactions. Approximately 50 milligrams of acid and 10 milligrams catalyst were sealed in a glass tube under vacuum. While doing this, the lower portion of the tubes were immersed in liquid N_2 or dry ice to prevent the unexpected reaction caused by heating. For the safety reason, all the sealed glass tubes were inserted into metal sockets to prevent the unexpected explosion during the reaction. The metal sockets were then fixed on a self-made cart and were ready for the reaction. At last, the cart was placed in oven and the reaction can be started under controlled reaction condition. During the reactions, the tubes were agitated by a reciprocal shaker which connects with the cart through a long stick in order to maintain a well mixed system. The reactions were typically carried out in the temperature range of 200 to 300°C for 4 hours.

Analytical methods – After reaction, the tubes were connected to a vacuum line, where the total produced gas was collected and quantified using a standard gas transfer method [16]. Then a subsample of the collected gas was analyzed with a GC-TCD+FID (HP 6890 series), which was directly connected to the vacuum line. This setup allowed for the quantification of the individual gaseous components, from which the yields of CO_2 and other products could be calculated. The reaction residues including unreacted reactants were recovered by washing the tube with chloroform, and the solution was then subjected to another GC-FID analysis with a selected temperature program in order to determine the extent of acid conversion and byproduct formation. For unknown products, GC-MS (Hewlett-Packard G1800A GCD System) was employed for structure identification. A capillary column, HP INNOWAX (30m, 0.32mmID, 0.5 μ film thickness) was selected for the analysis of hydrocarbons, acids, ketones etc.

2.2 Experimental methods for crude oil

2.2.1 Crude oil sample

All the crude oil tests were performed with a crude oil sample that was provided by ChevronTexaco, which is our industrial collaborator for this project. This particular crude oil is typical of many acidic, sour, and viscous oil with TAN, sulfur-content and the API gravity values of 4.7, 1.84% and 14.2 (60°F) respectively.

2.2.2 Total acid number measurement

Determination of the Total Acid Number is a key technology for this project. Following the procedure of ASTM standard method D664, we developed the in-lab TAN measurement method. Briefly, this measurement involves a non-aqueous acid-base potentiometric titration using a specific solvent mixture including toluene 50.0%, *iso*-propanol 49.5% and water 0.5% (v/v) with which to dissolve the oil samples. A mV/pH meter (Oakton PH510 Series) was used to record the potential change. The major operation steps consist of the followings.

- Preparation of potassium acid phthalate ($KHC_8H_4O_4$ or KHP) standard solution – heat KHP in oven at 80°C for about 10hrs to remove moisture. Accurately weigh the heated KHP and dissolve it into CO_2-free pure water in a flask. Add water to the graduation of the flask and then calculate the mole concentration of the prepared solution.

- Preparation of alcoholic potassium hydroxide solution – Add 6g of KOH to approximately 1L of anhydrous iso-propanol. Boil gently for 30min to increase the solubility of KOH in the solution. Store the solution overnight and then standardize the solution with the prepared KHP solution.

- Standardization of alcoholic KOH solution – Standardize the solution with potentiometric titration of weighed quantities of KHP dissolved in CO_2-free water.

- Preparation of oil sample – Dissolve 1-5g oil sample in 125ml titration solvent (500ml toluene/495ml anhydrous iso-propanol/5ml water), filter the sample and transfer the prepared solution to a 250ml beaker, which is used as the titration vessel.

- Titration of KOH to oil sample – Add suitable amount of KOH alcoholic solution and wait until a constant potential has been observed, then record the solution used and meter readings. When the sample was titrated close to the inflection point, add less drops of KOH and record the meter carefully. For each set of samples, make a blank titration of the titration solvent.

- Calculation – Plot the volumes of KOH solution added versus the corresponding electrode potential (mv). Mark the inflection points A and B for oil sample and solvent

only, which should reflect the largest potential changes for a unit KOH. Calculate the TAN as the equation

$$\text{Acid number, mg KOH/g} = (A\text{-}B) \times M \times 56.1/W \tag{1}$$

M: Concentration of alcoholic KOH solution, mol/L
W: Sample mass, g

   Two typical titration curves for KOH to KHP and KOH to oil were shown in Figure 1. In each case, the inflection points were clearly observed. The results we measured were consistent with the data obtained from The Oil Analysis Lab. An excellent agreement was achieved between our measurements with the data obtained from The Oil Analysis Lab (which provides commercial services for oil products). The reproducibility of our measurements was also well established.

   For an oil sample with the addition of 2% cyclohexane propanoic acid, the measured TAN is very close to the calculated value.

   Calculated TAN: 11.52;   Measured TAN: 11.03;   Mea/Cal: 95.7%

	In our lab	Oil Analysis Lab
TAN	4.35 (1st), 4.29 (2nd)	4.35 (1st), 4.38 (2nd)
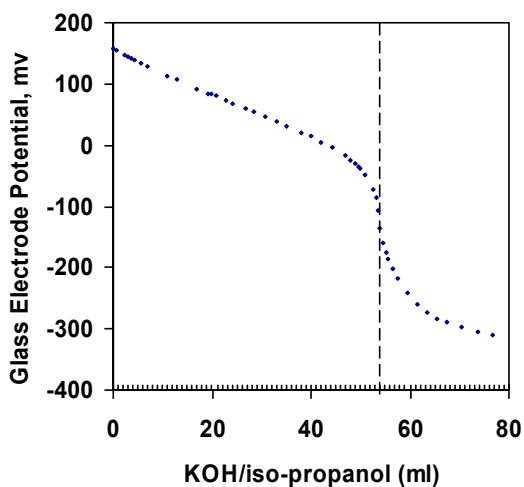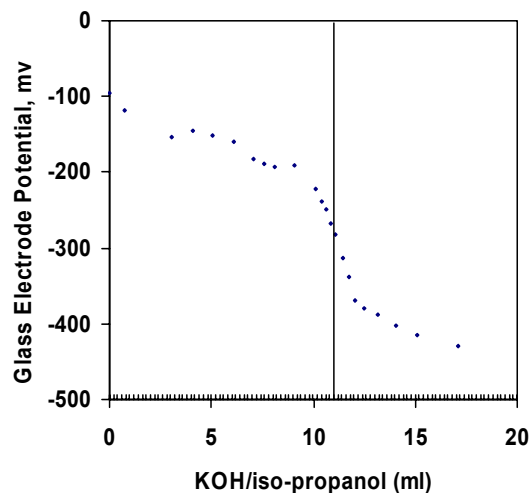
(a)   (b)

Figure 1: (a) Titration curve of potassium acid phthalate to KOH/iso-propanol solution; (b) Titration curve of KOH/iso-propanol solution to oil sample.

2.2.3 Viscosity measurement

Brookfield DV-I viscometer was used for the oil viscosity measurement. Through selecting different spindles and speeds, it allowed to measure the viscosity of the fluids in large scale (100~26 mcP). During the measurement, the fluid vessel was heated by a water bath which pumped out the water constantly. For the oil samples, most of the measurements were carried out at 40°C and 70°C.

2.2.4 Stainless steel autoclave batch reaction – reactor, operation and analysis

Various steel autoclave batch reactors were used for crude oil tests. The geometries and reactor volumes were different depending on the purposes of the experiments. For most oil tests, tubular and bottle shaped autoclaves were used which have reaction volumes of about 3~5 ml and 50 ml respectively.

A highly acidic, sour, and viscous crude oil produced in California, USA provided by ChevronTexaco was used in our studies. Due to the relative low concentration of naphthenic acid in the oil, the amount of the CO_2 produced through decarboxylation would be small and difficult to be detected. Instead, we used a semi-quantitative FTIR analysis as a means to monitor the decarboxylation reaction. The typical IR adsorption of C=O in RC=OOH (~ 1700cm^{-1}) was monitored to represent the change of naphthenic acid components in crude oil. A Perkin Elmer 16PC FT-IR spectrometer was used for this purpose.

During the reactions, the reactors were also fixed on the cart and the reactors were agitated by the shaker as the operation described in Experimental 1.3. The reactions were typically carried out in the temperature range of 200~300°C for 4 hrs. After the reactions, the reactors were taken out from the oven and the caps should be opened carefully because of the possible gas pressure. Then the oil/catalyst was poured out and subjected to oil-catalyst separation. Three methods, thermal filtration, solvent dissolving followed by filtration and centrifuge separation were commonly used for the separation purpose. Dichloromethane, which was an excellent solvent for crude oil, was commonly used to in this work.

For the catalysts and oil samples collected after the reaction, various measurements such as XRD, elementary analysis for C, H, O and S, TAN, viscosity were conducted and the results will be discussed in the next sector.

2.2.5   Fixed-bed flow through reaction – apparatus and operation

Flow tests for crude oil and mixed-acid solution were conducted in a reaction line, as shown in Figure 2. An HPLC pump was used to pump decane to a transfer vessel at a constant flow rate. Crude oil placed in the other side of the transfer vessel was pushed out by decane through a transfer piston and into a stainless steel reactor (0.4cm ID and 29cm in length) where the catalytic tests took place. Two pressure gauges were placed in line to monitor the flow status. The granular catalyst with an average particle size of 28~65 mesh was loaded in the central part of the reactor. Quartz wool, glass beads and metal screens were also sequentially packed at both sides of the catalyst layer to reduce the deal volume and protect the catalyst from moving. When flow tests with mixed-acid solution were conducted, a stainless loop placed in a dry-ice trap was inserted between the reactor and collector to cool down the volatile products. The oil samples can be collected continuously from the outlet of the line at variable time intervals. After the reaction, the oil was purged with high-purity N_2 to remove the oil residue. All the transfer, tubing lines and valves were heated to about 80°C to keep the oil at a manageable viscosity.

To obtain a clear observation of RC=OOH change during the experiment, 2% model carboxylic acid (cyclohexane pentanoic acid) was added to crude oil in some experiments to boost the peak strength of RC=OOH in some experiments.

For the oil samples collected at different reaction times, TANs and viscosities were measured using the methods described above.
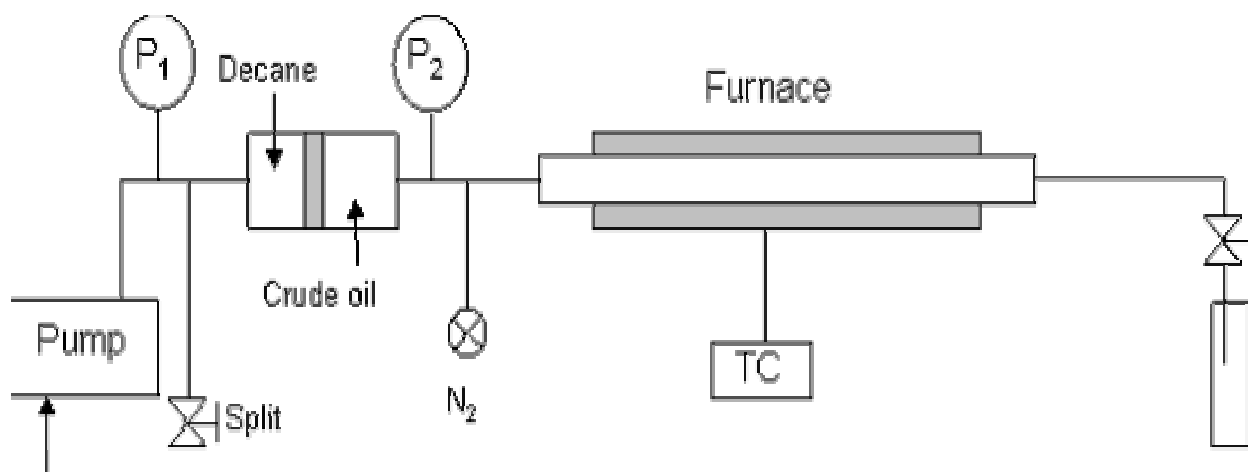
Figure 2: Fixed-bed flow reaction system from crude oil and mixed-acid solution

2.3   Adsorbent and adsorption measurement

2.3.1   Adsorptive application of clay minerals

The purpose of this study is to investigate whether clay minerals have the potential for catalytic and adsorptive applications for the removal of naphthenic acid. Clay minerals are aluminosilicates that predominate in the clay fractions of soils at the intermediate to advanced stages of weathering. These materials are stacked, polymeric sandwiches of tetrahederal and octahedral sheet structures with a layered structure as shown in Figure 3. The 1:1 layer type consists of one tetrahederal sheet fused to an octahederal sheet. The 2:1 layer type has two tetrahederal sheets fused to an octahederal sheet. Their major components are silica, alumina, and water, frequently with appreciable quantities of iron, alkali, and alkaline earth cations [17]. Natural clays usually have high cation-exchange capacity (CEC) and surface areas. In addition, they are inexpensive and environmentally friendly. Clay is one of the most important of the natural industrial substances. It is available in every country of the world and is commercially produced in nearly every state in the United States.

Clay minerals may interact with many organic compounds to form complexes of varying stabilities and properties. Clay organic interactions are multivariable reactions involving the silicate layers, the inorganic cations, water and the organic molecules. The chemical affinity between the acid compound and the solid surface depends on structure (molecular weight, chain length, etc) of the acid molecule, functional groups present in the acid molecule such as hydrophobic groups (-C-C-C-C-), electronegative groups (-C=O, -C-O-C-, -OH), π bonds (-C=C-, aromatic rings), and configuration of the acid molecule [18]. Adsorption of organic molecules on minerals such as clays has already been considered as a major process in the diagenesis and maturation of organic matter to petroleum. Surface functional groups in clay minerals play a significant role in adsorption processes. Surface functional groups can be organic (e.g. carboxyl, carbonyl, phenolic) or inorganic molecular units. The major inorganic surface functional groups in soils are the siloxane surface associated with the plane of oxygen atoms bound to the silica tetrahedral layer of a phyllosilicate and hydroxyl groups that are associated with the edges of inorganic minerals such as kaolinite, amorphous materials, metal oxides, oxyhydroxides, and hydroxides [19].
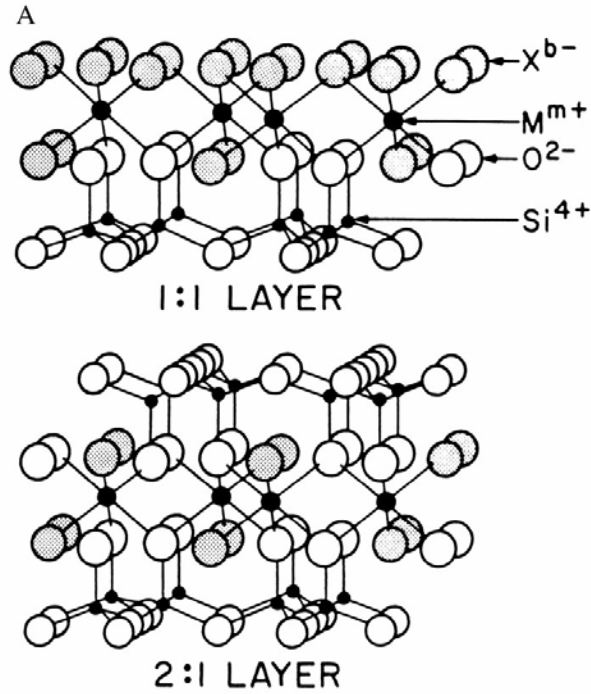
Figure 3: Crystal structure of 1:1 and 2:1 layer type clay minerals.

Clay minerals are divided into several groups. For example, Kaolinite, $Al_2Si_2O_5(OH)_4$, is a common phyllosilicate mineral, the major constituent of kaolin or clay. Kaolinite's structure is composed of silicate sheets (Si_2O_5) bonded to aluminum oxide/hydroxide layers ($Al_2(OH)_4$) called gibbsite layers. Gibbsite is an aluminum oxide mineral that has the same structure as these aluminum layers in kaolinite. The silicate (s) and gibbsite (g) layers are tightly bonded together with only weak bonding existing between the s-g paired layers. The dioctahedral structure of kaolinite is shown schematically in Figure 4 [20].
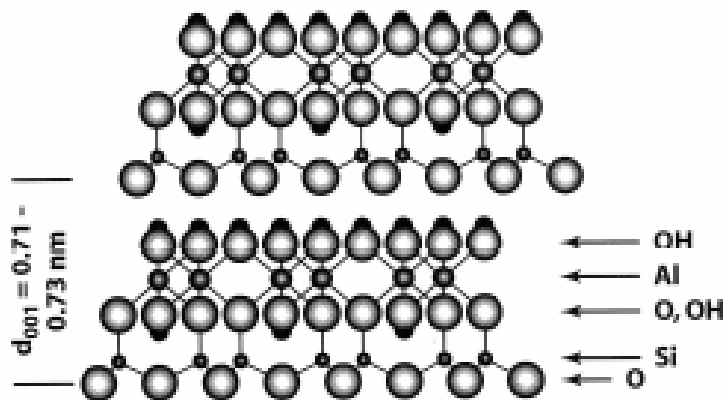
Figure 4: The 1:1 structure of kaolinite, $Al_2Si_2O_5(OH)_4$.

Illite is the only common mineral represented, however it is a significant rock forming mineral being a main component of shales and other argillaceous rocks. The general formula is $K_{0.8}(Al_{1.8}Mg_{0.2})(Si_{3.4}Al_{0.6})O_{10}(OH)_2$. The structure of this group is similar to the montmorillonite group with silicate layers sandwiching a gibbsite-like layer in between, in an s-g-s stacking sequence. The variable amounts of water molecules would lie between the s-g-s sandwiches as well as the potassium ions.

Bentonite is hydrated aluminosilicate clay primarily composed of the smectite-class mineral. It is a 2:1 type aluminosilicate; that is, its crystalline structure presents an alumina octahedral layer between two tetrahedral layers of silica which, by isomorphous substitutions, require cations, denominated exchange cations, to compensate for the negative charges of their laminar edges. Bentonite has the capacity to exchange these cations with the ones present in aqueous solutions. The bentonite mineral structure is shown in Figure 5. Montmorillonite is the dominant clay mineral in bentonite. The ideal mineral formula for montmorillonite is $(Na, Ca)_{0.33}(Al_{1.67}, Mg_{0.33})Si_4O_{10}(OH)_2 \cdot nH_2O$. The characteristic of members of this group is their capacity to absorb water molecules between the sheets, thus producing marked expansion of the structure.
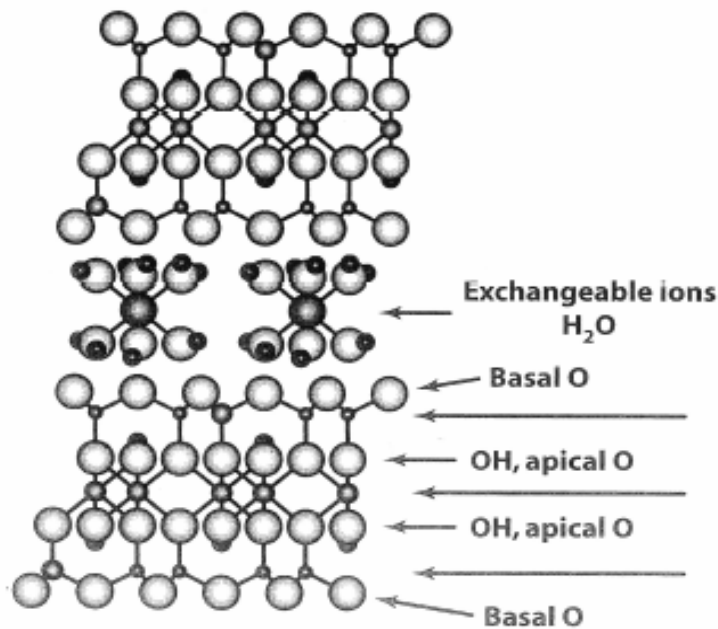
Figure 5: The mineral structures of montmorillonite.

Palygorskite, $(Mg, Al)2Si_4O_{10}(OH) - 4H_2O$, is 2:1 type phyllosilicates. The structure of palygorskite is derived talc-like T-O-T ribbons that expand along the axis of the fibers, with a

width of two pyroxene chains. The octahedral sites are principally occupied by Mg^{2+}, with some replacement principally by Al^{3+} or Fe^{3+} cations. Each ribbon is connected to the next through an inverted Si-O-Si bond, resulting in a continuous tetrahederal sheet and a discontinuous octahederal sheet. The terminal cations that are located at the edges of the octahederal sheets complete their coordination shells with two molecules of water, the structure water. The nanopores run parallel to the fiber axis and are filled at room temperature by zeolitic water that are hydrogen bonded to the structure water. The zeolitic water is easily lost at relatively low temperature, $<120^{o}C$. The cross-sections of the tunnels are about 3.7×6.4 Å. They are responsible for the large specific surface area and excellent sorptive properties of palygorskite, once the zeolitic water has been removed by thermal treatment [21].
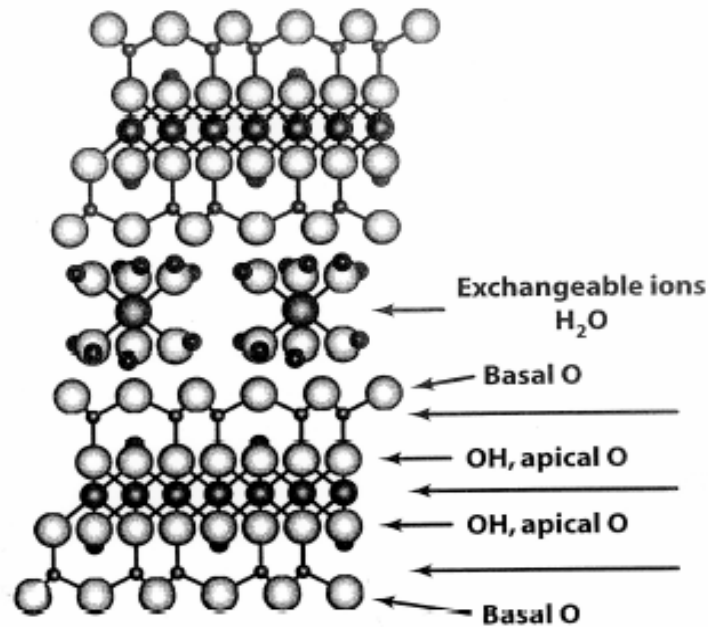
Figure 6: The mineral structures of hectorite.

Hectorite, $Na_{0.40}(Mg_{2.65}Li_{0.35})(Si_{3.95}Al_{0.05})O_{10}(OH)_2$, is a trioctahederal smectite containing Mg and Li as the main octahederal cations with minor amounts of Al and Fe. Incomplete filling of all octahederal sites and hetervalent Li^+ for Mg^{2+} substitution confers a negative charge on the octahederal sheet. The contribution of cation substitution in the tetrahederal sheets to the net negative charge is small due to very low tetrahederal substation. Several properties of hectorite are similar to those of montmorillonite as shown in Figure 6 [22], but some differences have been reported.

Sepiolite is a clay mineral with the formula of magnesium hydrosilicate, $Si_{12}Mg_8O_{30}(OH)_4(H_2O)_4 \cdot 8H_2O$. Sepiolite belongs to the phyllosilicate group of clay minerals. It has peculiar surface properties and important industrial interest due to its high adsorptive capacity. Its structure is quite different from that of smectites. It consists (Figure 7) in the alteration of blocks and tunnels that grow up in the fiber direction. Each structure is built up of two tetrahedral silica sheets "in sandwich" with a central magnesia sheet in a way similar to that which occurs in other 2:1 silicates, although in sepiolite there is a discontinuity of the silica sheets that gives rise to those structural tunnels. This arrangement determines that silanol groups (SiOH) are present at the border of each block at the external surface of the silicate. These silanol groups, together with the water molecules coordinated to the Mg ions at the borders of the structural blocks, are the main active centers for adsorption. These characteristics of sepiolite make it a powerful sorbent for neutral organic molecules and organic cations [23].
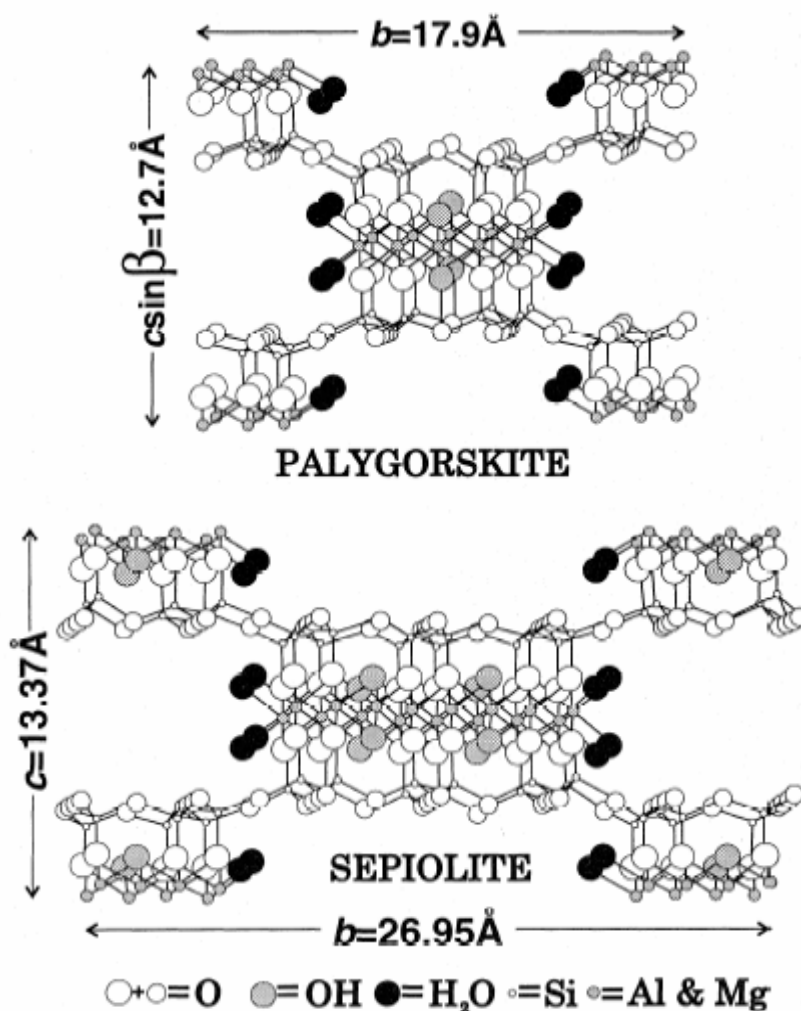
Figure 7: The mineral structures of (a) palygorskite and (b) sepiolite [24].

2.3.2 Adsorption of naphthenic acids from dodecane on metal oxides

Adsorption occurred at metal oxide surfaces plays an important role in several environmental processes including environmental catalysis and remediation, heterogeneous atmospheric chemistry and aqueous geochemistry. The knowledge of surface processes is required for an understanding of such systems. In this report several metal oxides (MOs) were investigated as adsorbents/catalysts for the removal of naphthenic acids (NAs) in the oil. The adsorption of NAs onto metal oxide surfaces generally occurs through coordination via the carboxyl group, which acts as a ligand for vacant coordination sits of surface metal cations. The coordination of a carboxylic acid usually occurs as the deprotonated carboxylate. In general, the more metallic character an element has, the more basic its oxide will be. Likewise, the more non-metallic character an element has, the more acidic its oxide will be. The metallic character of an element can be determined by its position on the periodic table as shown in Figure 8.
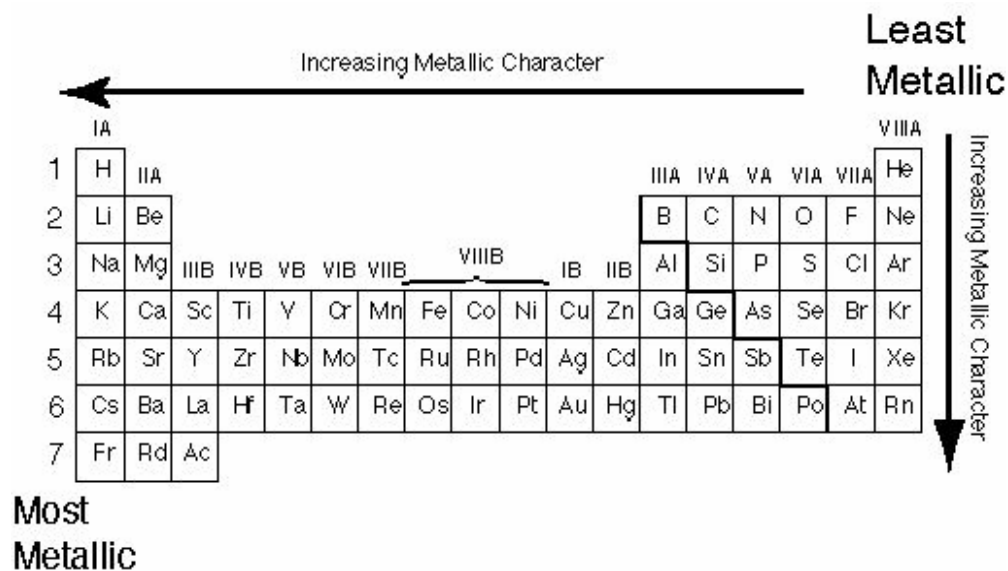
Figure 8: The metallic character of an element.

2.3.3 Methods for adsorption measurements
2.3.3.1 Adsorption of naphthenic acids from dodecane on clay minerals

Crude oil is an extremely complex system. To obtain further insight into the mechanism at the molecular level there is a need for studying simple, well-characterized systems. In this report, we studied the adsorption of NAs from organic/oil phase onto clay minerals and metal oxides. In some cases, the adsorption process was studied in crude oil. Dodecane (C_{12}), purchased from Sigma (>95%), was used as a solvent to simulate the crude oil fraction in which naphthenic acids were present. The model naphthenic acids (i.e. cyclohexanepropionic acid (NA1), benzoic acid (NA2), cyclohexanepentanoic acid (NA3), and 4-heptylbenzoic acid (NA4)) were purchased from Sigma-Aldrich. All chemicals were used without further purification or drying. In addition,

nitrogen-containing model compound (such as quinoline), sulfur-containing model compound (such as 2-phenylthiophene) were added in the NAs solution.

Table 3: Composition of Clay Minerals

Clay code	Description	Chemical composition (%)										Cation exchange capacity (meq/100g)	Surface area (m^2/g)
		SiO_2	Al_2O_3	TiO_2	Fe_2O_3	FeO	MnO	MgO	CaO	Na_2O	K_2O		
KGa-2	Kaolinite, high defect	43.9	38.5	2.08	0.98	0.15	n.d.	0.03	n.d.	<0.005	0.065	3.3	23.5
IMt-1	Illite	49.3	24.3	0.55	7.32	0.55	0.03	2.56	0.43	0	7.83	17.0	28.6
ISCz-1	Illite-Smectite, 70/30	51.6	25.6	0.04	1.11	<0.1	0.04	2.46	0.67	0.32	5.36	n/a	n/a
ISMt-2	Illite-Smectite, 60/40	51.2	26.3	0.17	1.49	0.10	0.01	2.41	1.40	0.04	4.74	n/a	n/a
PF1-1	Palygorskite	60.9	10.4	0.49	2.98	0.40	0.058	10.2	1.98	0.058	0.80	19.5	172.6
SAz-1	Montmorillonite (AZ)	60.4	17.6	0.24	1.42	0.08	0.099	6.46	2.82	0.063	0.19	120	97.4
SAz-2	Ca-Montmorillonite (AZ)	60.4	17.6	0.24	1.42	0.08	0.099	6.46	2.82	0.063	0.19	120	97.4
SCa-3	Montmorillonite (CA)	52.8	15.7	0.18	1.06	<0.10	0.03	7.98	0.95	0.92	0.03	125	76.2
SepSp-1	Sepiolite	52.9	2.6	<0.001	1.22	0.30	0.13	23.6	<0.01	<0.01	0.05	17	307.8
SHCa-1	Hectorite	34.7	0.7	0.038	0.02	0.25	0.008	15.3	23.40	1.26	0.13	43.9	63.2
SWy-2	Na-Montmorillonite (WY)	62.9	19.6	0.09	3.35	0.32	0.006	3.05	1.68	1.53	0.53	76.4	32.2

Several clay samples (from the Source Clay Repository of Clay Mineral Society at Purdue University, West Lafayette, IN), i.e. Kaolin (KGa-2), Illite (IMt-1), Illite-smectite mixed layer 60/40 (ISMt-2), Illite-smectite mixed layer 70/30 (ISCz-1), Palygorskite (PF1-1), Montmorillonite (SAz-1), Ca-Montmorillonite (SAz-2), Montmorillonite, CA (SCa-3), Sepiolite (SepSp-1), Hectorite (SHCa-1), and Na-Montmorillonite (SWy-2), were chosen as model absorbents for this study. The clay samples were mostly used as received for the adsorption isotherms. The chemical compositions, CEC values, and surface areas of clay minerals used are shown in Table 3 [25, 26]. The adsorption experiments were carried out using the batch equilibration technique. Desired amounts of a NAs solution (equal wt% of each compound) were added to different glass centrifuge tubes, which contained known amounts of clay minerals. The tubes were shaken at 25°C for 24 hours. Adsorption reaches a steady state or no longer changes after 24 hours shaking. The adsorptive solution is separated from the adsorbent followed by centrifugation for 20 min. Supernatants were sampled and subject to analysis for NAs concentrations using a Hewlett Packard Gas Chromatography-Mass Spectroscopy (GC-MS). No changes in solute concentrations without clays were detected in the tubes within the experimental period. Therefore, solute mass lost in the supernatant from clay slurries was assumed to be adsorbed by clay. The amount of NAs adsorbed was calculated from the difference between the initial and equilibrium solute concentration in dodecane solution.

2.3.3.2 Adsorption of naphthenic acids from dodecane on metal oxides

In this report, we explored some of the metal oxides as adsorbents at room temperature for the removal of naphthenic acids (NAs). The metal oxides used in this report were Na_2O, MgO, CaO, Al_2O_3, SiO_2, PbO, SeO_2, CuO, Cu_2O, AgO, Ag_2O, ZnO, Y_2O_3, La_2O_3, ZrO_2, MnO_2, Fe_2O_3, and CeO_2. The powders were dried for 24 hours at $100^{o}C$ and stored in a desiccator. In this study, the model NAs solution was prepared by using four model NAs i.e. cyclohexanepropionic acid (NA1), benzoic acid (NA2), cyclohexanepentanoic acid (NA3), and 4-heptylbenzoic acid (NA4) with tetradecane (C14) in equal amount of wt% concentration dissolved in dodecane (C12). The tetradecane is included to verify there is no significant adsorption of solvent, but only NAs. In addition, nitrogen-containing model compound (such as quinoline), sulfur-containing model compound (such as 2-phenylthiophene) were added in the NAs solution. The purpose of this is to observe whether these MOs adsorb NAs preferentially. The concentrations of these NAs were about 0.5 wt% each. The adsorption experiments were carried out using the batch equilibration technique. About 4.5 g of a NA mixture was added to different glass centrifuge tubes, which contained known amounts of MOs (about 0.6 g). The tubes were shaken at $25^{o}C$ for 24 hours, then followed by centrifugation for 20 min. Supernatants were sampled and subjected to analysis for NAs concentrations using a Hewlett Packard Gas Chromatography-Mass Spectroscopy (GC-MS). No changes in solute concentrations without MOs were detected in the tubes within the experimental period. Therefore, solute mass lost in the supernatant from MO slurries was assumed to be adsorbed by MOs. The amount of NAs adsorbed was calculated from the difference between the initial and equilibrium NAs concentrations in the dodecane.

2.4   Advanced theoretical calculation methods
2.4.1   Characterization of naphthenic acids

The most abundant NA components are carboxylic acids with a COOH group attaching to an alkyl-substituted saturated ring with a chemical formula of Ring-$(CH_2)_m$-COOH. Here, the 'Ring' represents a combination of saturated 5-member and 6-member ring structure and the $(CH)_m$ is the carbonyl chain, the COOH group can either directly attach to the ring or to the alkyl-chain. Classifications of this group of NA based on its chemical formula and the ring structure have been made [27] *via* representing their homologues by a general formula $C_nH_{2n+z}O_2$, where n indicates the carbon number and Z specifies a homologous series. The relation between the Z value and number of the saturated ring N can be established [28]:

$$N = - Z/2 \quad \textbf{(saturates)} \tag{2}$$

Although saturated carboxylic acids are the predominant compounds found in most crude oils, aromatic and even heterocyclic compounds have also been reported. For example, an early investigation by the Royal Dutch/Shell Laboratory at Amsterdam of NAs from the lubrication oil found more than 50% of saturates, but also found over 15% of monoaromatics and about 10% of diaromatics1 [29]. A more detailed analysis on the aromatic compounds separated by Elution SiO_2 and Gel Permeation Chromatography (GPC) by Seifert and colleagues [30] found more aromatic compounds, such as naphthalenes, fluorenes, pyrenes etc. A recent ^{13}C NMR analysis [31] also found the chemical shifts in the 120-150 ppm region, which confirms the presence of aromatic carbons. For aromatics we have:

$$N < -Z/2 \quad \textbf{(aromatics)} \tag{3}$$

Another classification method is based on double bond equivalent (DBE)

$$\textbf{DBE} = 1 + \Sigma \; \frac{1}{2} \; [\textbf{Ni} \; (\textbf{V}_i -2)] \tag{4}$$

where N_i is the number of atoms of element i, V_i is the valence of atom i.   Since $V_C = 4$, $V_H = 1$ and $V_O = 2$, a relation between DBE and the Z number for carboxylic acids can be established as:

$$\textbf{DBE} = 1 - Z/2 \textbf{ (carboxylic acids)} \tag{5}$$

It is worth noting that DBE represents more general compositions than that of the Z-number representation, not only for its applicability for aromatics, but also for its extension to more complex compounds containing other elements. For example for the sulfur (S) and nitrogen (N) compounds that widely exist in crude oils. However, the Z-number is more useful to distinguish more detailed isomeric structures of the carboxylic acids. A comparison of the Z-numbers and DBE of some aromatics and their saturated carboxylic acid forms (Figure 9) is listed in Table 4.
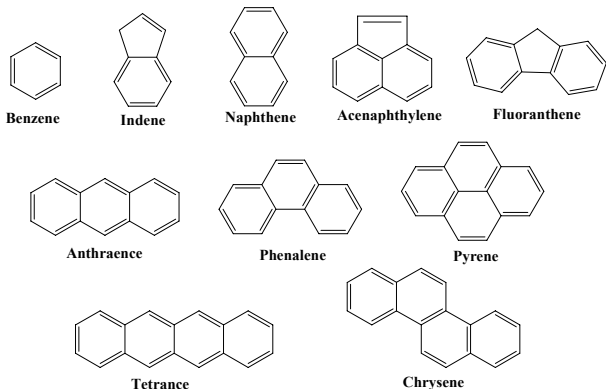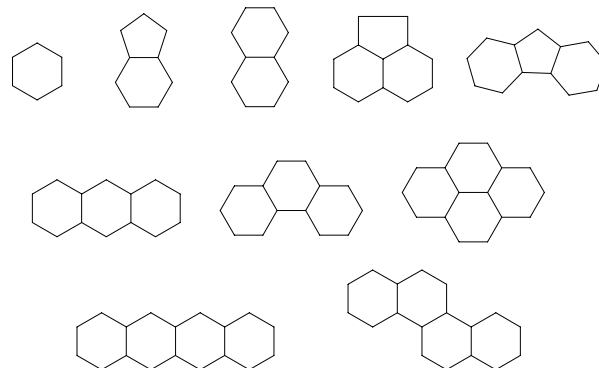
Figure 9: Different ring structures of the hydrocarbon backbones to be attached by the carboxylic acid to form the naphthenic acids.

Table 4 Calculated Z-numbers and the Double Bond Equivalent of Selected Naphthenic Acids

Ring	Saturates			Aromatics		
	Formula	Z	DBE	Formula	Z	DBE
Benzene	$C_7H_{12}O_2$	-2	2	$C_7H_6O_2$	-8	5
Indene	$C_{10}H_{16}O_2$	-4	3	$C_{10}H_8O_2$	-12	7
Naphthalene	$C_{11}H_{18}O_2$	-4	3	$C_{11}H_8O_2$	-14	8
Acenaphthylene	$C_{13}H_{20}O_2$	-6	4	$C_{13}H_8O_2$	-18	10
Fluoranthene	$C_{14}H_{22}O_2$	-6	4	$C_{14}H_{10}O_2$	-18	10
Anthraence	$C_{15}H_{24}O_2$	-6	4	$C_{15}H_{10}O_2$	-20	11
Phenalene	$C_{15}H_{24}O_2$	-6	4	$C_{15}H_{10}O_2$	-20	11
Pyrene	$C_{17}H_{26}O_2$	-8	5	$C_{17}H_{10}O_2$	-24	13
Tetracene	$C_{19}H_{30}O_2$	-8	5	$C_{19}H_{12}O_2$	-26	14
Chrysene	$C_{19}H_{30}O_2$	-8	5	$C_{19}H_{11}O_2$	-26	14

2.4.2   Theoretical calculation of the acidity (pka) of an acidic compound

For a proton-containing compound AH, the gas-phase deprotonation energy can be obtained from the following reaction:

$$AH \rightarrow A^- + H^+ \tag{6}$$

Then:

$$E_{deprot} = E(AH) - E(A^-) - E(H^+) \tag{7}$$

i.e., energies required to remove a proton from an acid in the dilute gas phase, where E(AH) and E(A⁻) are calculated total energies of the AH acid and the conjugate base, respectively. It usually takes a large amount of energy to separate charges because of their Columbic attraction. Even through the gas-phase deprotonation energy does not directly represent the AH acidity in solutions, it predicts the difficulty to remove a photon from the neutral AH compound. We can therefore use E_{deprot} as an initial probe to study the structural dependence of acidity.

The dissociation constant (pKa) in aqueous solutions is calculated from a thermodynamic cycle as indicated in Figure 10. Terms A and E are gas-phase and solution-phase Gibbs' free energies of deprotonation; terms B, C, and D are standard free energies of solvation of AH, A⁻ and H⁺, respectively. The pKa of the AH compound is related to E *via*:

$$pKa = - E / 2.303RT = -0.725 E \qquad (8)$$

$$pKa = -E / 2.30 RT = -0.725 E$$
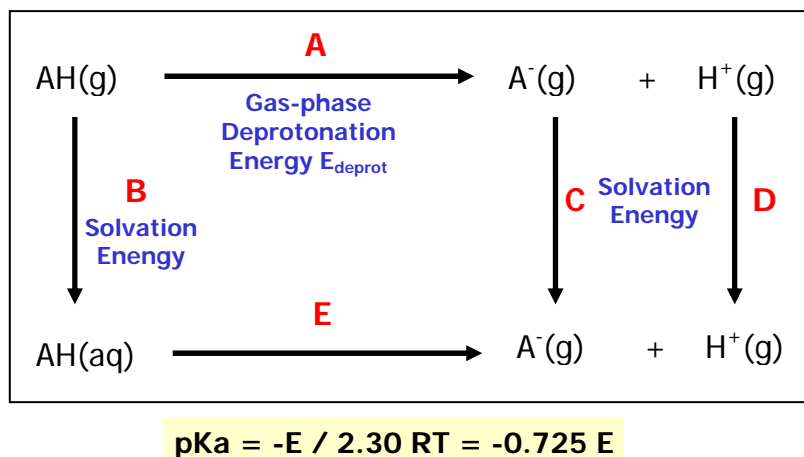
Figure 10: Diagram of theoretical calculations of the pKa value from first principle

All gas-phase quantum mechanism calculations were carried out with the B3LYP version of the density functional theory (DFT) as implemented in the Jaguar v4.0 program [32], This includes the generalized gradient approximation (Becke non-local gradient correction), exact exchange using the Becke three-parameter exchange functional [33], and the non-local correction functional of Lee, Yang, and Parr [34]. The initial geometry of neutral AH and anion A- species were fully optimized at the B3LYP/6-31G* level. The E_{deprot} are calculated using the B3LYP/6-31G(d) basis set, in which a diffusion basis set is added to the oxygen atoms participating in protonated/deprotonated processes. The so-calculated gas-phase E_{deprot} is therefore truly ab initio without introducing additional parameters. The acid-attaching site corresponding to the lowest E_{deprot} on the ring structure is chosen to perform the pKa calculation.

The gas-phase Gibbs' free energy A is calculated by:

$$A = \Delta G^0 [A\text{-}(g)] + \Delta G^0 [H\text{+}(g)] - \Delta G^0 [AH(g)] \qquad (9)$$

The Gibbs' free energy of each term in gas phase is obtained by:

$$\Delta G^0 = E_{0K} + ZPE + \Delta\Delta G_{0 \to 298K} \qquad (10)$$

where E_{0K} is the total energy of the molecule at 0 K, and the zero-point energy (ZPE) and the Gibbs free energy change from 0 to 298K $\Delta\Delta G_{0 \to 298K} = \Delta\Delta H_{0 \to 298K} - T \, \Delta\Delta S_{0 \to 298K}$ were calculated from the vibrational frequency calculation, in which $\Delta\Delta H_{0 \to 298K}$ and $\Delta\Delta S_{0 \to 298K}$ are the

enthalpy and entropy change. All terms in the Eq. (10) can be evaluated from the first-principle quantum mechanical calculations. In our studies, the following computational conditions and scaling factors were used in calculations:

E_{0K}: the optimized geometry from B3LYP/6-31G*, single-point energy calculation at the B3LYP/CC-PVTZ(-f) level;

ZPE: the optimized geometry from B3LYP/6-31G*, single-point vibrational frequency calculation at the HF/6-31G* level, scaled down by 0.9135;

$\Delta\Delta S_{0 \to 298K}$: the optimized geometry from B3LYP/6-31G*, single-point vibrational frequency calculation at the HF/6-31G* level, scaled down by 0.8978;

$\Delta\Delta H_{0 \to 298K}$: the optimized geometry from B3LYP/6-31G*, single-point vibrational frequency calculation at the HF/6-31G* level, scaled down by 0.8905.

The standard free energy of solvation in aqueous solutions is calculated based on the continuum-solvation approach [35]. Three experiment-related parameters are introduced, namely, the inner-space dielectric constant ε_{QM}, the dielectric constant of solvent ε_{sol}, and the probe radius r_0 which is related to the experimental data of the molecular weight and the density of solvent. For water, $\varepsilon_{QM} = 1.0$, $\varepsilon_{sol} = 80.37$, and $r_0 = 1.4$ Å were used to evaluate the standard free energy of solvation of the neutral AH molecule (the "B" term in Figure 10) and for the standard free energy of solvation of the anion A- (the "C" term in Figure 10): $\varepsilon_{QM} = 0.92$, $\varepsilon_{sol} = 80.37$, and $r_0 = 1.4$ Å.

The energy terms of ΔG^0 [H+(g)] and the standard free energy of solvation of a proton in water (the "D" term in scheme I) could not be calculated directly. Following the literature [36], we chose ΔG^0 [H+(g)] = 2.5 RT – T $\Delta S0$ = -6.28 kcal/mol; and $\Delta G^0_{solv}(H+)$ = -258.32 kcal/mol.

2.4.3 Theoretical calculation of 1-octanol/water distribution coefficient (logP)

The caustic washing is the most commonly used technique to reduce the acidity of crude oils. Understanding of the distributions of a naphthenic acid in the water phase and in the oil phase is an important issue in the process design of the caustic washing. 1-octanol/water distribution coefficient (logP) is an important parameter to measure the partition of a molecular compound in both aqueous and oil phases. Current logP calculation methods using the addition of fragment species could not effectively represent the detailed molecular structural dependence. Calculation of logP from first principle has been developed based on the reaction cycle illustrated in Figure 11. Within this method, the distribution coefficients of a molecular compound is determined from

the difference of Gibb's free energy G, which could be calculated from the difference of the solvation energies of this compound in the aqueous (B) and 1-octanol solutions (F).
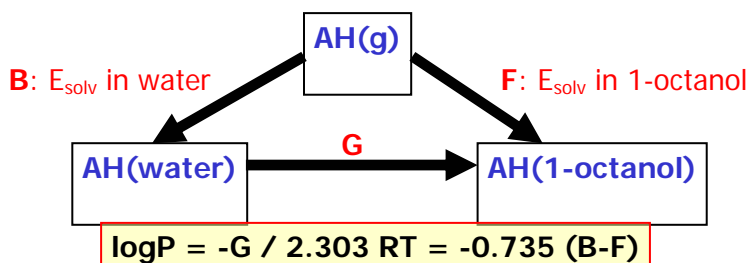
Figure 11: Diagram of theoretical calculations of logP from first principle.

2.4.4   Investigations of the adsorption of naphthenic acids on solid surfaces

Several chemical processes when a naphthenic carboxylic acid adsorbed on the solid surfaces have been investigated using our newly developed Seqquest computational software. The implementation of the Seqquest program allows us to treat a large solid surface as a 2-dimensional slide and study the interaction of a molecule with this slide (Figure 12)
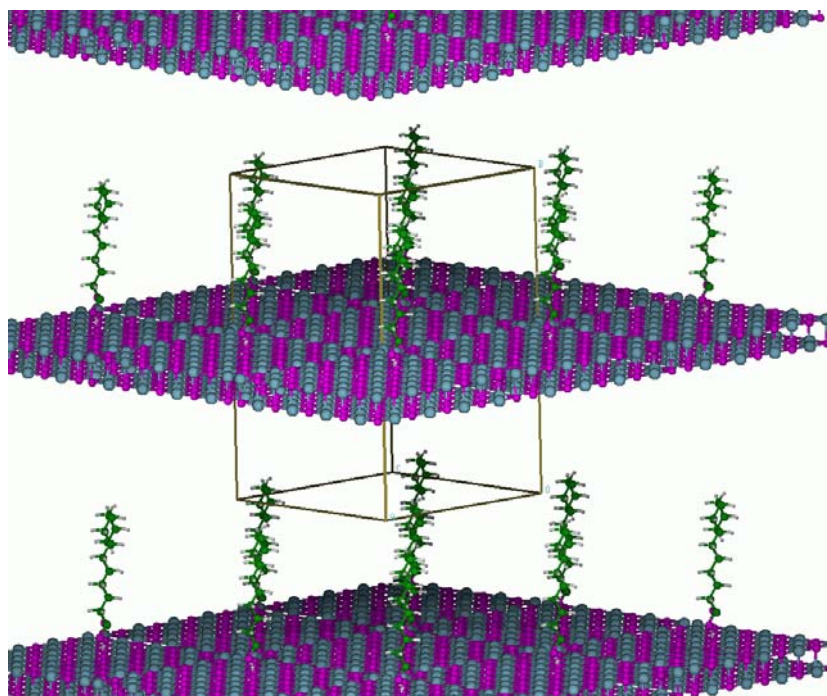
Figure 12: Adsorption of CycloHexane Carboxylate Acid (CHCA) on the MgO(100) Surface – A 2D Slab Model.

The adsorption energy of a molecule on the slide surface is computed from:

$$E_{ads} = E(molecule+slab) - E(slab) - E(molecule) \qquad (12)$$

Where E(slab), E(molecule) are the calculated energies of the slab and a molecule alone, and E(molecule+slab) are the adsorbed system of a molecule on the slide with optimized geometry. For comparison, two metal oxides (CaO and MgO) are selected, and two carboxylic acids (benzoic acid (BA) and Cyclohexane Carboxylate Acid (CHCA)) are used to represent the aromatic and saturated naphthenic acids.

3. Results and Discussion

3.1 Development of effective decarboxylation catalysts
3.1.1 Alkaline earth metal oxides
3.1.1.1 Alkaline earth metal oxides used as the catalysts

Four alkaline earth metal oxides, CaO, MgO, SrO and BaO were tested with a model carboxylic acid, naphthoic acid ($C_{10}H_7COOH$). The catalytic activities of these compounds were determined by the extent of acid conversion and CO_2 yield. Here CO_2 yield is defined as the amount of organic carbon mole converted to CO_2 and it is an indication of the degree of the catalytic decarboxylation.

Figure 13 shows that compared with no catalyst addition, all four alkaline earth metal oxides result in high acid removal rates while CO_2 formation was only detected with MgO.
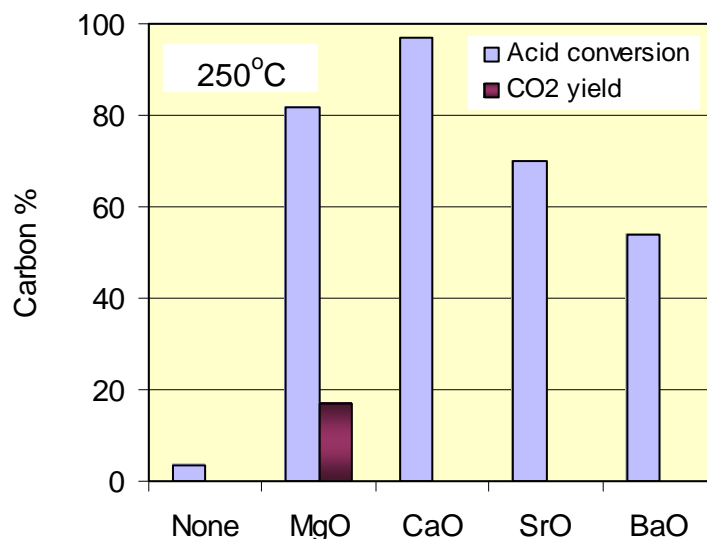
Figure 13: Reaction of naphthoic acid in the presence of alkaline earth metal oxides at 250°C.

Even with the MgO catalyst, the CO_2 yield was much lower than the converted acid amount. Regarding this phenomenon, two factors are considered to be responsible, 1) the strong combination ability of this series of metal oxides with CO_2, (i.e., as CO_2 is formed it tends to be combined with the metal oxides to form stable carbonate minerals (Equ-1)) and, 2) the reaction pathway might be multiple (e.g., in addition to the decarboxylation, other reactions such as neutralization and cracking may occur simultaneously). The high acid conversion obtained from CaO, SrO, and BaO would mainly result from neutralization (Equ-2).

$$RCOOH \longrightarrow RH + CO_2$$
$$\quad\quad\quad\quad\quad\quad \overset{+MeO}{\longrightarrow} MeCO_3 \quad\quad\quad\quad (1)$$
$$2RCOOH + MeO \longrightarrow (RCOO)_2Me + H_2O \quad\quad (2)$$
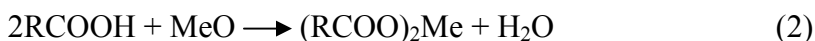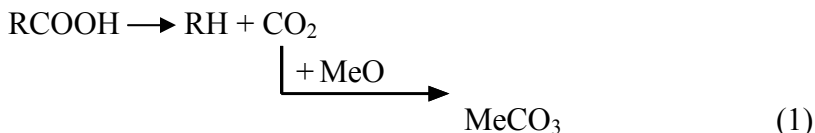
3.1.1.2 Behavior of the MgO catalyst

Intrigued by the unique results from the MgO experiments, we have investigated its catalytic behavior in more detail. The temperature dependence of CO_2 yield and acid conversion are shown in Figure 14. Over a temperature range from 100 to 300°C, a sharp increase in both the CO_2 yield and the acid conversion was observed in the range of 150°C-250°C, suggesting that the main reactions occur at this temperatures range. This temperature is within the acceptable range to meet our objective of identifying a low temperature decarboxylation catalyst. Figure 15 depicts the dependency of CO_2 yield and acid conversion on the MgO loading. It can be seen that for loads of MgO up to 20 wt%, CO_2 yield and acid conversion increased almost linearly with the MgO loading. Further increases in the MgO loading gave little enhancement to CO_2 yield and acid conversion, indicating the latter reaction is reaching saturation.
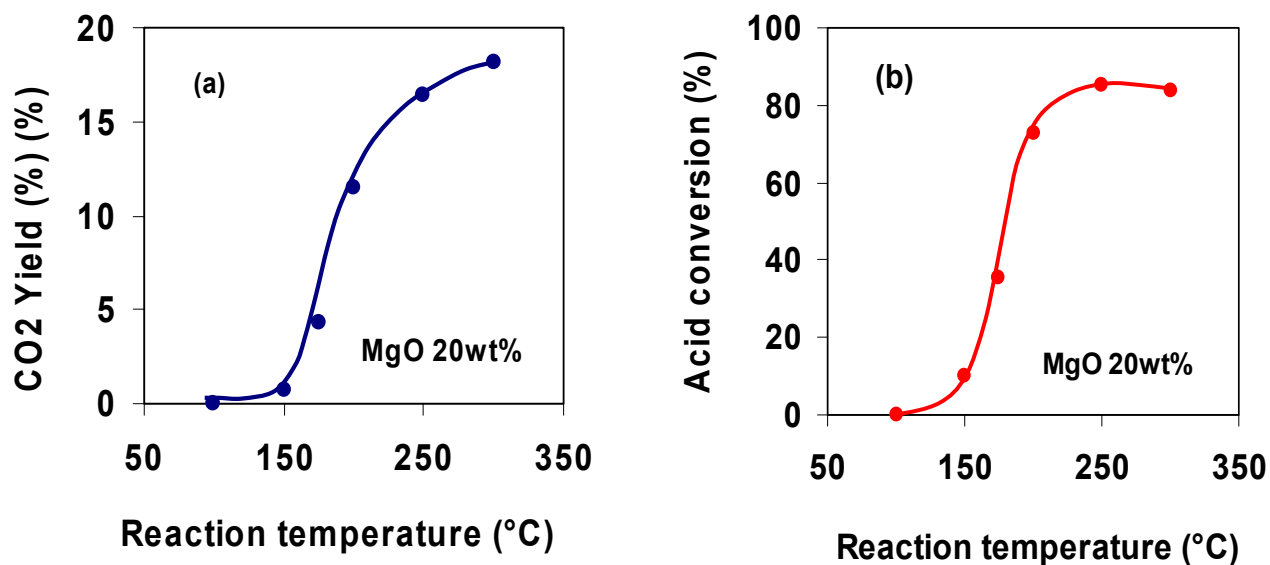
Figure 14: Effects of reaction temperature on naphthoic acid conversion and CO_2 formation in the presence of MgO.
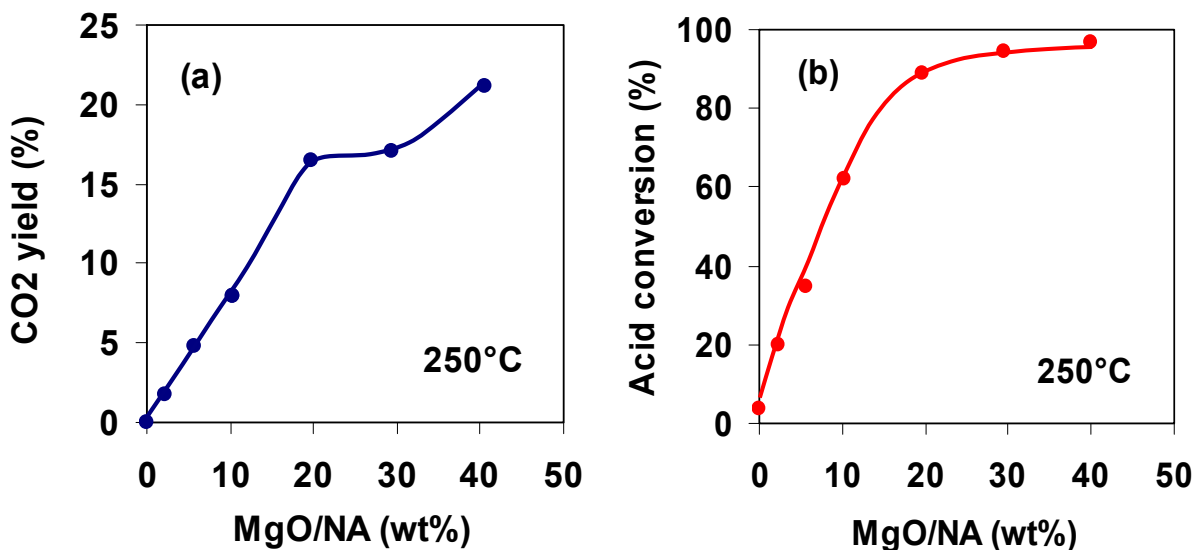
Figure 15: Effects of MgO loading on naphthoic acid conversion and CO_2 formation in the presence of MgO.

3.1.1.3 Applying MgO to different acid substrates

To verify the effectiveness of MgO for decarboxylation of different types of acids, several other acid substrates were tested, including succinic acid (SA, $COOHCH_2CH_2COOH$), cyclohexane carboxylic acid (CHCA, $C_6H_{11}COOH$) and naphthoic acid (NA, $C_{10}H_7COOH$). Figure 16 shows that CO_2 was detected in each reaction, suggesting that the decarboxylation reactivity of MgO is not dependent on acid structure.
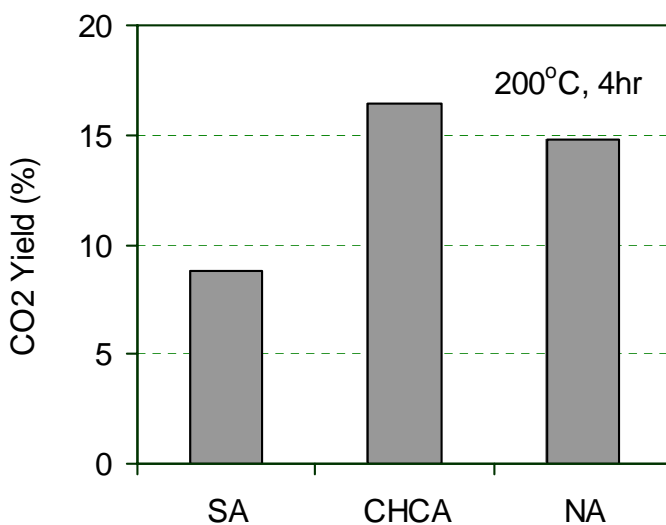
Figure 16: Catalytic decarboxylation of different carboxylic acids in the presence MgO catalysts.

Several mechanisms for the role of MgO in decarboxylation catalysis are considered to be possible. The formation of CO_2, as measured in our experiments, identified the occurrence of the catalytic decarboxylation. Due to its inherent strong basicity, MgO will tend to react with acids through acid-base neutralization. Moreover, there have been previous reports that MgO promotes ketonization [37] and cracking reactions, in particular when MgO underwent high temperature pretreatment [38].

3.1.2 Oxidative metal oxides

Table 5: Catalytic decarboxylation of model carboxylic acid in the presence of oxidative metal oxides

Acid (mg)		Catalyst (mg)		Temp (°C)	RT (hr)	Acid conv (%)	CO$_2$ yield (%)	C$_{10}$H$_8$ Yield (%)	C$_{20}$H$_{14}$
NA	60.0	Ag$_2$O	9.8	230	4	26.0	3.6		
NA	49.7	MnO$_2$	10.0	230	4	34.2	3.3		
NA	50.2	PbO$_2$	11.8	230	4	24.9	4.5		
NA	49.9	CuO	10.2	230	4	53.9	3.5		
NA	53.0			250	4	3.6	0.1		
NA	49.9	Ag$_2$O	10.4	250	4	53.1	53.7	19.4	
NA	54.3	MnO$_2$	10.9	250	4	51.9	14.6		
NA	56.6	Mn$_2$O$_3$	10.2	250	4	20.2	2.8		
NA	57.6	Cu$_2$O	10.7	250	4	59.2	6.7		
NA	49.8	CuO	10.5	250	4	63.3	17.2	1.6	
NA	49.5	Fe$_2$O$_3$	9.7	250	4	40.2	0.0		
NA	55.2	Co$_2$O$_3$	10.7	250	4	16.0	6.0		
NA	57.4			300	4	5.9	0.4		
NA	54.0	Ag$_2$O	10.8	300	4	93.9	96.9	66.2	detected
NA	48.3	AgO	10.2	300	4	16.1	15.4	2.2	
NA	49.7	MnO$_2$	11.5	300	4	74.3	17.1	0.5	detected
NA	52.6	Mn$_2$O$_3$	10.7	300	4	61.8	5.2		
NA	49.9	PbO$_2$	10.8	300	4	38.4	5.2		
NA	52.2	CuO	11.5	300	4	56.5	20.9	4.4	
NA	50.2	Cu$_2$O	10.1	300	4	63.6	22.9	13.7	
NA	50.3	Ag (Powder)	7.2	275	4	16.9	0.5		
NA	50.4	Ag+Air	10.0	275	4	18.7	7.7	0.8	
CHPA	64.0	Ag$_2$O	9.4	250	4	10.6	2.8		
CHPA	65.6	MnO$_2$	10.3	250	4	36.2	5.5		
CHPA	72.2	PbO$_2$	13.9	250	4	24.4	5.3		

NA, C$_{10}$H$_7$COOH, 2-naphthoic acid   CHPA, C$_6$H$_{11}$C$_4$H$_8$COOH, Cyclohexane pentanoic acid

Several metal oxides with multiple oxidative states were investigated in the catalytic decarboxylation of model compounds, naphthoic acid and cyclohexane pentanoic acid, the latter is considered to be more representative as the component of naphthenic acid in crude oil. The tested metal oxides include Ag_2O, AgO, MnO_2, Mn_2O_3, PbO_2, CuO, Cu_2O, Fe_2O_3 and Co_2O_3. Note that all of these metal oxides have variable oxidative states.

The data in Table 5 show that except for Fe_2O_3, all of these metal oxides are effective to the catalytic decarboxylation reaction. Among them, Ag_2O shows excellent decarboxylation reactivity. When increasing reaction temperature from 230°C to 300°C, the acid conversions increased from 26.0% to 93.9% and the CO_2 yields were also correspondingly enhanced. More important, the latter well match the acid conversions. In addition, naphthalene, as another major decarboxylated product, was also detected. The yield of naphthalene, defined as the carbon conversion to naphthalene, reached to 66.2% at 300°C. Moreover, The GC-MS analysis also identified the formation of two dimers of naphthalene, 1, 2'-binaphthalene and 2, 2'-binaphthalene ($C_{20}H_{14}$). These byproducts might be the result of dimerization of naphthalene. This result strongly suggested that the reaction occurred through a radical mechanism.

Comparison of the same metal atoms at different oxidative states does not show a general trend on their decarboxylation efficiency. For instance, Ag(I) is much active than Ag(II), but Mn(IV) yields more CO_2 than Mn(III), while Cu(I) and Cu(II) gave almost equal CO_2 yields at the temperature of 300 ^{0}C.
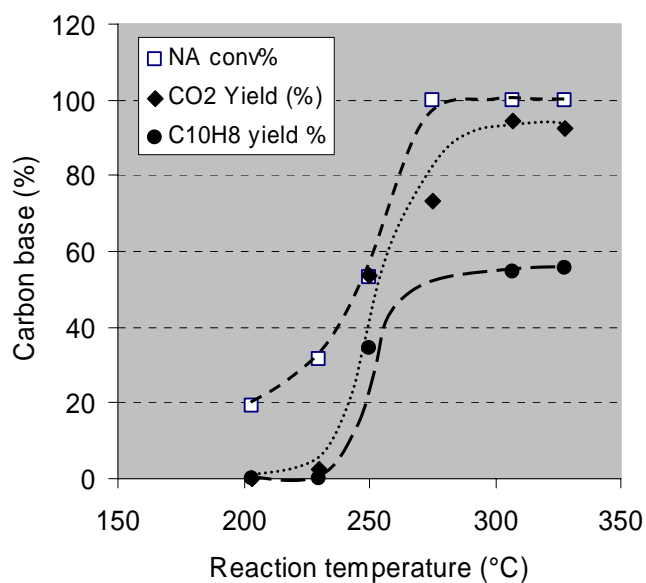
Figure 17: Effects of reaction temperature on acid conversion and product formation in the reaction of naphthoic acid over Ag₂O catalyst.

Regarding the high activities of Ag_2O, there is one concern about the real catalytic active species. The reason is that Ag_2O tend to decompose at the temperature around 200°C. To clarify the doubt, two additional experiments were designed and conducted with pure Ag and Ag+Air. The dada in Table 5 exhibits that Ag powder alone can not catalyze decarboxylation reaction as no CO_2 was clearly detected. The coexistence of air contributed to the formation of CO_2, but the yield could not reach as high as that with Ag_2O. It is assumed that the newly formed oxygen atom from Ag_2O decomposition might be a highly active species that play a key role in acid activation-decarboxylation process.

For Ag_2O, we tested the temperature dependence for acid conversion, CO_2 yield and $C_{10}H_8$ yield. The experiments were carried out in the temperature range of 203~328°C. As shown in Figure 17, the CO_2 yields were roughly close to the acid conversions, in particular, at high temperature range. Rapid increases were found at the temperature around 250°C for both of product formation and acid conversion.

When applying Ag_2O, MnO_2 and PbO_2 to a new acid substrate, cyclohexane pentanoic acid (CHPA), CO_2 was also detected although the yields were not as high due to the lower reaction temperature. These results show promise for the application of oxidative metal oxide catalysts to react with diverse acid substrate structures.

Regarding the mechanism of catalytic decarboxylation on oxidative metal oxides, oxidative decarboxylation via radical intermediate would be the most plausible reaction path. Accordingly, the oxidative abilities of these compounds will be essential to the activities.

3.1.3 Zeolite based catalyst

As C-C cleavage is involved in decarboxylation reaction (R-COOH → RH+CO_2), acidic catalyst becomes one of our choices. On the other hand, the application of acidic zeolite in oil refinery has well been established, typically being represented by the famous FCC process.

As for the application of zeolite in catalytic decarboxylation, there was only one report that discussed the involvement of zeolite in the reaction of benzoic acid. However, the operation condition was relatively too harsh to be realized in practical process. The goral of our work is to look for an effective acidic catalyst that can be operated at mild condition.
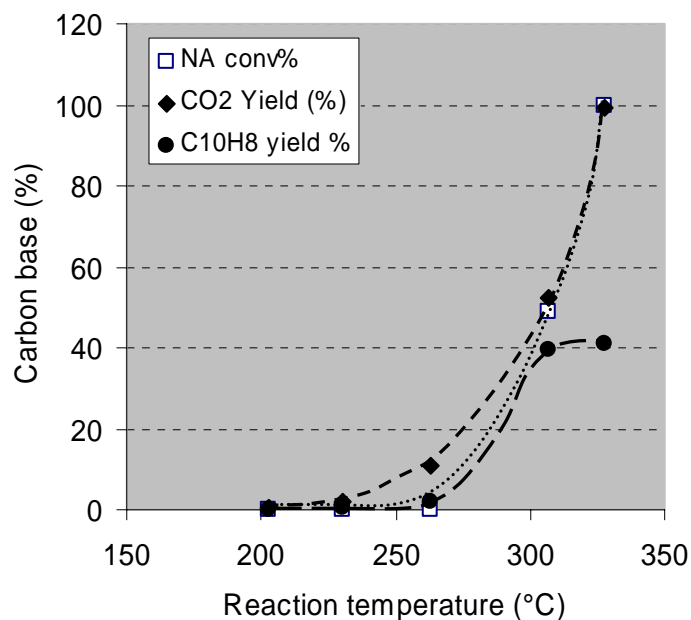
Figure 18: Effects of reaction temperature on acid conversion and product formation in the reaction of naphthoic acid over HZSM-5 catalyst.

A strong acidic zeolite, ZSM-5 type zeolite was targeted in this work. Three samples, CBV 3020E, 3024E and 8014E with different SiO_2/Al_2O_3 ratio, cation form and surface area were purchased from ZEOLYST. Prior to the tests, all the three samples were activated in oven at 450°C overnight. With this treatment, the ammonium type zeolites, CBV3024E and CBV 8014E could be converted to their H-type.

Although the reactivities of the three samples differentiate each other, the strong promotion effects caused by acidic catalyst to decarboxylation reaction are of great significance, not only for the current project but also for general organic reaction chemistry.

Table 6: Catalytic decarboxylation of model carboxylic acid in the presence of the ZSM-5 type zeolite catalysts

Acid (mg)	Catalyst		Temperature (°C)	Reaction time (hr)	Acid conversion (%)	CO_2 yield (%)	$C_{10}H_8$ yield (%)
57.4			300	4	5.9	0.4	0
51.5	CBV 3020E	10.3	300	4	65.4	71.4	41.5
55.3	CBV 3024E	10.0	300	4	49.5	46.1	29.9
67.1	CBV 8014E	11.0	300	4	38.7	34.8	25.6

Using the three zeolites, the decarboxylation experiments were conducted with naphthoic acid at 300°C for 4hrs. As shown in all of the three ZSM-5 catalysts were effective to the catalytic decarboxylation of naphthoic acid. The acid conversions reached from 65.4 to 38.7% for the three zeolites, while the blank run gave only 5.9% conversion CO_2 yields varied in the range of 34.8% to 71.4% and these values were well consistent with the acid conversions. Naphthalene was also significantly formed as another decarboxylation product. The ratios of naphthalene yields to acid conversions fall in around 60%.

Furthermore, we tested the temperature dependence of zeolite 3024E with the same model acid. The experiments were conducted in the temperature range of 203~328°C. As shown in Figure 18 and Table 6, the acid conversion and CO_2 yield were well agreements each other. A rapid increase for both of acid conversion and CO_2 generation took place around 300°C. At 328°C, the acid substrate has almost been converted completely. It is noted that this is also a relatively mild condition compared with the results ever reported.

3.1.4   Supported precious metal catalysts

It is known that Pt has wide application and irreplaceable role in oil and environmental industries due to its excellence catalytic performance for the processes of hydrogenation, dehydrogenation, isomerization etc. and therefore, it.

Being motivated by exploring its more application in organic reaction, we designed two experiments to determine its catalytic activities towards decarboxylation of carboxylic acid. Al_2O_3 supported Pt catalyst was prepared using impregnation method. H_2PtCl_6 was used as the precursor and Pt-loading was controlled at 0.5wt%. The experiment was carried out with naphthoic acid at 275°C for 4hrs. To determine the effect of Pt, the same experiment was run with the support Al_2O_3 alone. Table x listed the experimental condition and results. Compared to the result of blank experiment, CO_2 was clearly formed from Pt/Al_2O_3, and naphthalene was also slightly detected. This result strongly suggests that Pt was effective to catalytic decarboxylation. The data in Table 7 also shows that the acid conversions were almost as high as 100% on both of the catalysts. This might be due to the strong adsorption capacity of Al_2O_3.

Table 7: Catalytic decarboxylation of model acid in the presence of supported precious metal catalysts

Catalyst	Catalyst weight (mg)	Acid	Acid weight (mg)	Reaction Temp (°C)	Reaction time (hr)	CO_2 yield (%)	Acid conversion (%)	Naphthalene yield (%)
Pt/Al_2O_3	58.2	NA	50.5	300	4	9.0	100	1.2
Al_2O_3	58.6	NA	50.7	300	4	0.2	100	0.0

Pt/Al_2O_3: 0.5wt%

As for the practical meaning of this data, it might be less possible to apply Pt-based catalyst in crude oil upgrading directly. However, the importance of this result is that it would add one more example for its application of Pt in organic reactions. This will also prompt the interests of the theoretical scientist to reveal the mechanism on how Pt catalyzes the reaction.

3.1.5   Other catalytic tests

In addition to these effective catalysts we developed in this work, we also conducted a large amount of catalytic tests with other materials. Although we failed to obtain high decarboxylation activities, some of the results were still informative.

Table 8: Reactions of naphthoic acid in the presence of various solid materials

Catalyst (mg)		Acid (mg)		Temp (°C)	RT (hr)	Acid conv (%)	CO_2 yield (%)	Note
$MgSiO_4$	11.0	NA	50.5	300	4	17.0	1.6	$C_{10}H_8$ yield, 0.3%
$MgTiO_3$	10.1	NA	50.5	300	4	0.0	0.4	
$BaTiO_3$	10.5	NA	64.7	300	4		1.2	
$CaZrO_3$	10.7	NA	62.2	300	4		1.0	
$BaZrO_3$	12.1	NA	50.8	300	4		0.6	
$CaTiO_3$	10.4	NA	51.9	300	4		0.7	
$3Al_2O_3·2SiO_2$	9.9	NA	49.3	250	4	2.8	0.0	
Al_2O_3 (acidic)	10.1	NA	49.1	250	4	2.9	0.0	
Al_2O_3 (neutral)	10.2	NA	49.9	250	4	12.5	0.0	
Al_2O_3 (basic)	10.6	NA	48.8	250	4	24.4	0.0	
CaC_2	12.8	NA	48.3	200	4		0.1	C_2H_2 yield ~84%
Mo_2O	10.3	NA	47.4	200	4		0.1	C_2H_2, detected
CeO_2	10.6	NA	47.7	250	4		0.2	
La_2O_3	10.4	NA	49.7	250	4		0.0	
Y_2O_3	10.5	NA	50.6	250	4		0.0	
ZrO_2	11.1	NA	51.2	250	4		0.1	

NA, $C_{10}H_7COOH$, 2-naphthoic acid

Table 8 summarized part of the results including series of perovskite-structured compounds $MgTiO_3$, $BaTiO_3$, $CaZrO_3$, $BaZrO_3$ and $CaTiO_3$; Al_2O_3 with different acid-base properties; metal carbides CaC_2 and Mo_2C; rare earth metal oxides, CeO_2, La_2O_3, Y_2O_3 and ZrO_2 and several other materials. The data in Table X shows that tiny amounts of CO_2 and naphthalene were detected

from MgSiO$_4$; perovskite compounds were inactive to carboxylic acids, so did for rare earth metal oxides. Al$_2$O$_3$ did not result in decarboxylation, but contributed to acid removal to some degree, probably through their adsorption functionalities. Besides, the adsorption capacities of them depend on their acid-base properties, the stronger of the basicity, and the larger adsorption capacity to acid. Metal oxides behaved different from others, they could not promote catalytic decarboxylation but resulted in the formation of C$_2$H$_2$, in particular, when CaC$_2$ was used, the C$_2$H$_2$ yield reached as high as 80%. The reactions occurred here is more possibly hydrolysis.

$$CaC_2 + 2RCOOH \rightarrow C_2H_2 + Ca(RCOO)_2$$
$$2Mo_2C + 2RCOOH \rightarrow C_2H_2 + 2MoRCOO$$
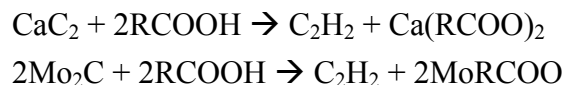
3.2 Reaction of an acid mixture with MgO and other supported catalysts
3.2.1 Results from batch reaction

Table 9: Reaction of mixed acid solution in the presence of various supported catalysts

Catalyst (Ni, Cu 0.5wt%)	None	MgO	Ni/MgO	Cu/MgO	Ni/Al$_2$O$_3$	Ni/SiO$_2$	Cu/Al$_2$O$_3$	Cu/SiO$_2$
Solution amount (g)	2.4870	2.5432	2.5511	2.3960	2.5261	2.5357	2.3755	2.3806
Catalyst loaded (mg)		25.5	25.5	25.4	25.8	25.5	27.2	25.0
Conversion of acid (%)								
CPCA	16.0	39.0	70.8	86.5	5.0	21.5	0.0	12.8
CHCA	15.0	46.7	70.5	83.9	5.7	18.9	0.0	10.5
BA	14.5	78.8	91.2	92.4	15.0	15.4	5.5	10.4
C$_5$H$_{11}$-CHCA	11.3	81.6	92.4	93.2	10.7	16.0	2.4	7.1
C$_7$H$_{15}$-BA	7.0	92.5	97.5	98.0	4.8	8.7	5.3	3.5

CPCA, cyclopentane carboxylic acid; CHCA, cyclohexane carboxylic acid; BA, benzoic acid

Mixed acid solution: Solvent, dodecane

CPCA 2.471%; CHCA 1.927%; BA 0.871%; C5H11-CHCA 1.099%; C7H15-BA 1.107%

Reaction temperature and time: 200°C, 4hr

As the goal of this work is to apply the catalyst developed to crude oil, a mixed acid-hydrocarbon solution experiment was conducted to bridge the model compound and crude oil. MgO and a group of supported metal catalysts were used in these tests. In the mixed acid-hydrocarbon solution, five acid compounds, which represent different acid structures, were dissolved in dodecane to mimic the composition of oil. As listed in Table 9, higher acid conversions were obtained from MgO compared with no catalyst being used and the acid

conversions could be further improved when small amounts of Ni and Cu were loaded with MgO, with the maximum conversion exceeding >90%. However, if the metals were supported on other supports (e.g. Al_2O_3 and SiO_2) no such promotion effect was measured. The amount of acid conversion observed was equivalent to, or even lower than that observed with no catalyst addition. This suggests a synergism that occurs between metals and MgO, which may possibly involve the enhanced cleavage of C-C bonding due to the presence of Cu or Ni.

3.2.2   Results from flow reaction

To obtain understanding of MgO catalyzed decarboxylation process, flow reaction tests were carried out with a new mixed acid solution, which contains four carboxylic acids and two hydrocarbons, which were dissolved in dodecane (Table 10).

Table 10: Composition of mixed acid solution

Components	Wt%
NA1	0.518
NA2	0.518
NA3	0.520
NA4	0.516
n-C14	0.518
n-C16	0.526
Solvent: dodecane (n-C12)	
NA1: Cyclohexanepropionic acid	
NA2: Benzoic acid	
NA3: Cyclohexanepentanoic acid	
NA4: 4-Heptylbenzoic acid	

The flow tests were carried out with the apparatus described in Figure 2 and the hydrocarbon mixed acid solution was placed in one side of the transfer vessel. A stainless loop which connects reactor and sample collection valve was placed in a dry ice-trap to trap the liquid products. The temperature and flow rate were set at 300°C and 0.1ml/hr. For comparison, blank test was also performed under the same experimental condition. GC-MS analysis shows that blank test did not result in significant changes for these carboxylic acid compounds (Figure 19). However, in the presence of MgO, GC analysis shows that four acid peaks vanished rapidly after the reaction. Instead, new peaks were generated and the peak strengths increased gradually with the reaction time (Figure 19)

With GC-MS, we identified the structures of these unknown peaks. To our surprise, all of these products have ketone structures with the general formula of RCOR', where R and R' were contributed by either original acids, cyclohexane propionic acid, cyclohexane pentanoic acid and benzoic acid, or the hydrocarbons, C_{14}, C_{16} and C_{12} (used as solvent). For products No. 6 and 7, the group of $-COC_6H_5CH_3$ would result from the cracking of the raw acid, 4-heptybenzoic acid.
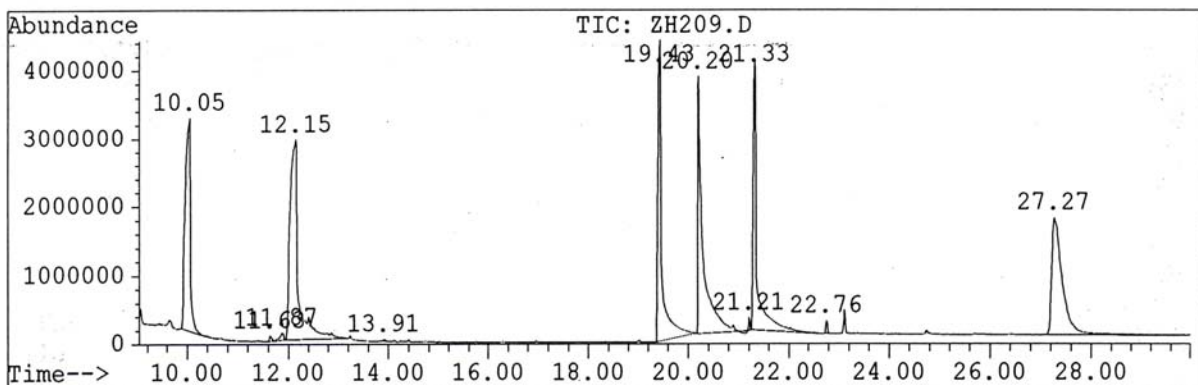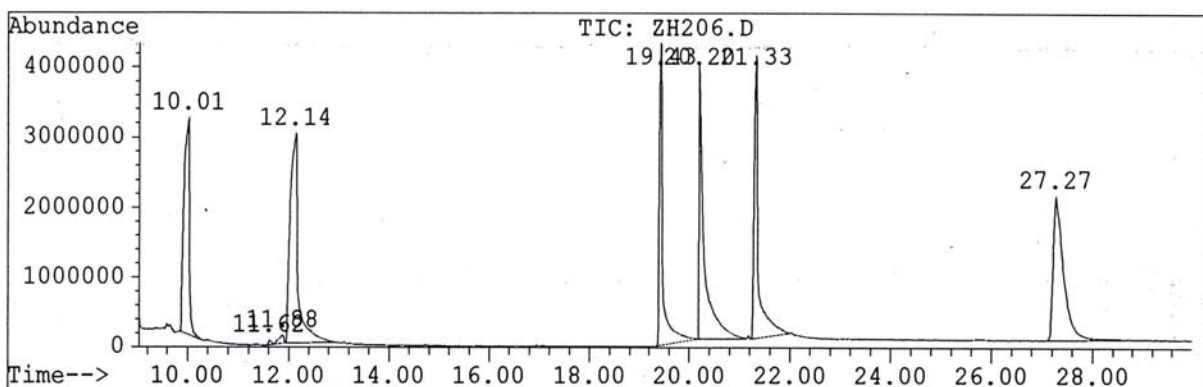
Figure 19: GC-MS analysis for (a) mixed acid raw solution, (b) mixed acid solution from blank.

If labeling all the components of mixed acid solution as a(C_{12}), b(C_{14}), c(C_{16}), d(cyclohexane propionic acid), e(benzoic acid), f(cyclohexane pentanoic acid), g(4-heptybenzoic acid), various combinations such as dd, ae, df, be, ff, bg and cg, were identified in these products (Figure 21) Based on these product characteristics, the reaction equations were correspondingly suggested as shown in Figure 22 and Figure 23.

More important, through analyzing the product structures, we obtained more understanding on the catalytic roles of MgO to carboxylic acid. Instead of direct catalytic decarboxylation ($RCOOH \rightarrow RH + CO_2$), the major reaction promoted by MgO would be ketonization (decarboxylation condensation) accompanied by RCOR' as well as CO_2 and H_2O formation. This speculation also accounts for the low CO_2 yields in contrast to the high acid conversions, which was observed in the single model acid experiments.
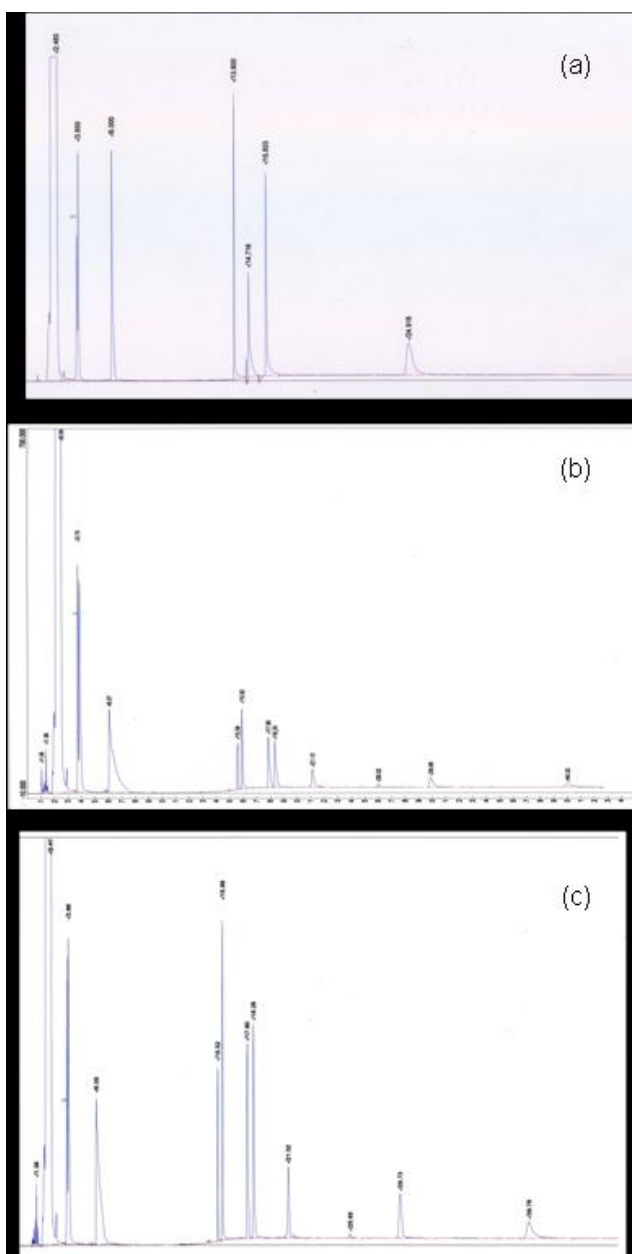
Figure 20: GC analysis for MgO catalyzed mixed acid solution flow reaction (a) mixed acid raw solution; (b) collected during 1.5 ~ 2.5hr; (c) collected during 7.5 ~ 9.5hr
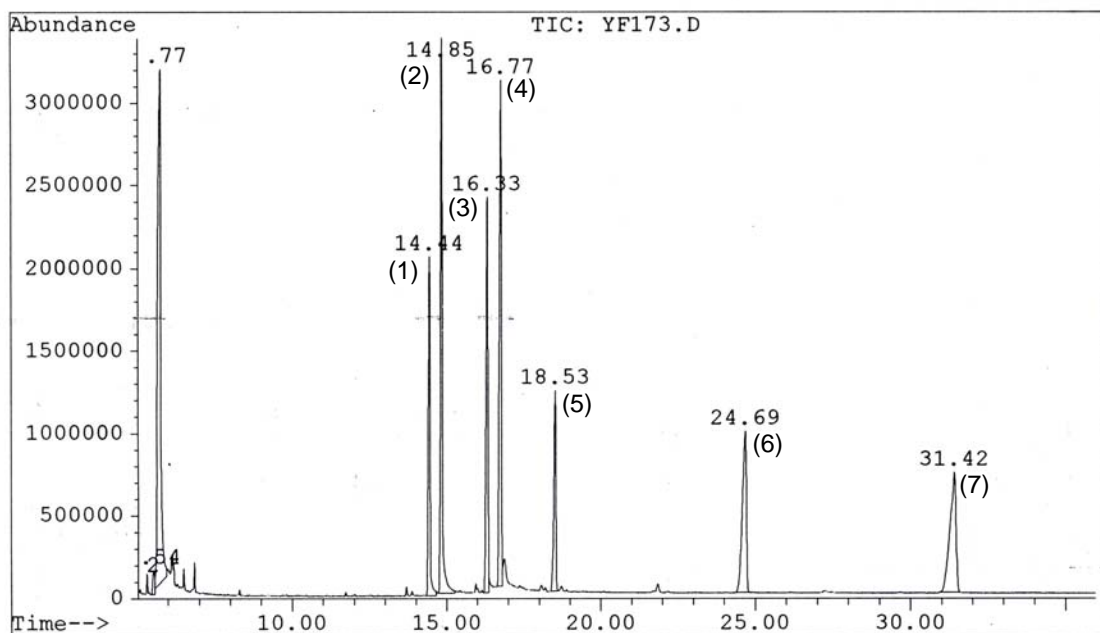
Figure 21: GC-MS chromatogram of the products in mixed acid flow reaction.

Product No.	Structures	Formula	MW
(1)		$C_{17}H_{30}O$	250
(2)		$C_{18}H_{28}O$	260
(3)		$C_{19}H_{34}O$	278
(4)		$C_{22}H_{36}O$	316
(5)		$C_{21}H_{38}O$	306
(6)		$C_{22}H_{34}O$	314
(7)		$C_{24}H_{38}O$	342
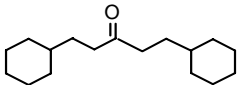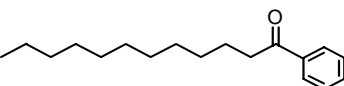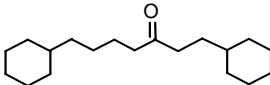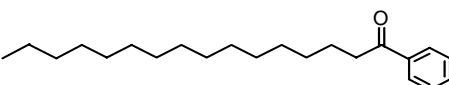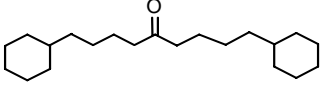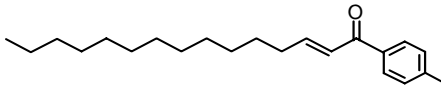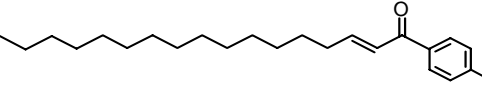
Figure 22: Identified major products in flow reaction of mixed acid solution.

48

(1) [structure] + [structure] → [structure] $+ CO_2 + H_2O$

(2) [structure] + [structure with COOH] → [structure] $+ CH_3OH$

(3) [structure] + [structure] → [structure] $+ CO_2 + H_2O$

(4) [structure] + [structure with COOH] → [structure] $+ CH_3OH$

(5) [structure] + [structure] → [structure] $+ CO_2 + H_2O$

(6) [structure] + [structure with COOH and C_7H_{15}] → [structure] $+ C_6H_{14} + H_2O$

(7) [structure] + [structure with COOH and C_7H_{15}] → [structure] $+ C_6H_{14} + H_2O$
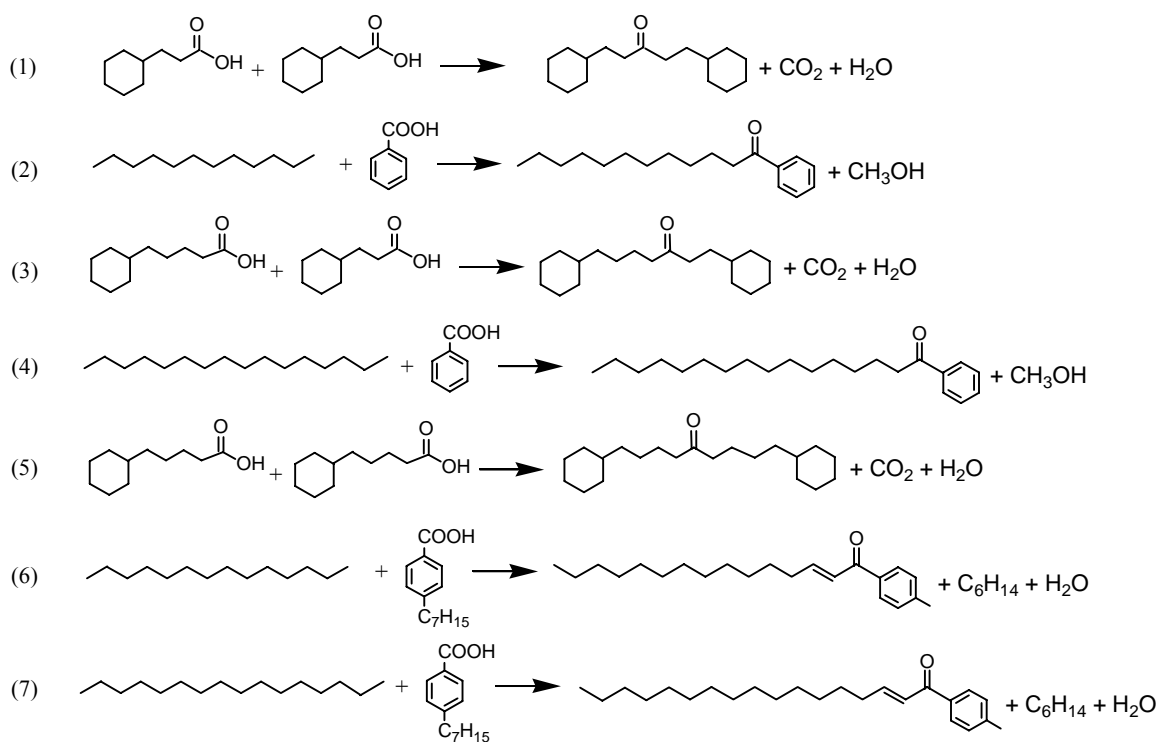
Figure 23: Suggested reactions which result in the formation of the products.

Briefly, the work based on the results of model carboxylic acids and mixed-acid solution, led to the discovery of four-type effective decarboxylation catalysts represented by MgO, Ag_2O and Cu_2O, HZSM-5 and Pt/Al_2O_3. All of them exhibit decarboxylation activities at relatively mild conditions. The major reactions happened in these different catalyst systems are listed in Table 11. To explore their application in organic chemistry as well as in practical processes becomes a new challenge.

Table 11: Four types effective decarboxylation catalysts

Catalyst Type	Representative Catalyst	Major Reactions and Products
Alkaline earth metal oxide	MgO	$RCOOH \rightarrow RCOR + CO_2$
Oxidative metal oxides	Ag_2O, Cu_2O	$RCOOH \rightarrow RH + CO_2 + R\text{-}R$
Acidic zeolite	HZSM-5	$RCOOH \rightarrow RH + CO_2$
Supported precious metal	Pt/Al_2O_3	$RCOOH \rightarrow RH + CO_2$

Reaction temperature: 200~300°C

3.3   Application of the catalyst for naphthenic acid removal from crude oil

3.3.1 Distribution of naphthenic acid in California Midway Sunset crude oil

To investigate the distribution of acidic components in crude oil, the oil fractionation was conducted using a method of silica-gel adsorption, pentane and dichloromethane sequent abstraction. The components of asphaltene, hydrocarbons + aromatics (hydro+Aro) and resin were obtained and their TAN were measured. The separation procedure can be described as the following.

a) Separation of Asphaltene

Dissolve ~20g of crude oil in 150ml of *n*-pentane with continuous stir, separate the insoluble component and collect the solid after drying. The dark brown solid is asphaltene.

b) Preparation of a silica gel column

Mix about 72g silica gel with 300ml *n*-pentane and degas the mixture. Slowly pour the mixture into the column with gentle tapping. Always keep the level of *n*-pentane higher than the silica gel.

c) Recovery of hydrocarbons and aromatics

Add the filtered solution to the prepared silica gel column. Continuously wash the column with *n*-pentane and collect the eluate until the eluate color turn to very slight. Then distill the solvent, collect the distillates and evaporate the remained solvent. The residue is a mixture of hydrocarbons and aromatics.

d) Recovery of resin

Change *n*-pentane to dichloromethane to wash the column again and collect the eluate and then evaporate the solvent to obtain the component of resin.

e) Results

The next table (Table 12) shows the mass balance of different components and their TAN values. The total mass balance reached 95% and this confirmed the reliability of the method employed. It can be seen that asphaltene occupies a small fraction in mass but contributes to the high acidity; hydrocarbon+aromatics are very low acidic; and resin is in between. By adding all the TANs multiplied by their mass percentages, it was seen that this value is much lower than the original TAN for this oil. This suggests that silica gel itself may absorb some strong acidic compounds.

Table 12: Separation of oil components and TAN measurements

Components	Mass Recovered	Mass Percent	Acid Number [a]	Acid Number
Asphaltene	1.60 g	8.0%	8.32	Calculated by the weight distribution
Hydro+Aromatic	12.14 g	60.7%	0.14	
Resin	5.26 g	26.3%	2.34	
Texaco Crude Oil	20.0 g	Total: 95.0%	4.35	1.44

It is known that thermal treatment results in partial cracking for the oil components, accompanied by the formation of gases, lighter oils and coke. Major traditional and newly developed heavy oil upgrading processes such as visbreaking are based on this thermal cracking principle. As thermal treatment will also causes the decomposition for some naphthenic acid or sulfur compounds, the TAN and S concentrations will be reduced correspondingly through this process. In order to figure out a real catalytic or adsorptive effect for NA removal, it is necessary to obtain the data of thermal treatment, which will provide references for the catalytic or adsorptive processes.

(a)   (b)
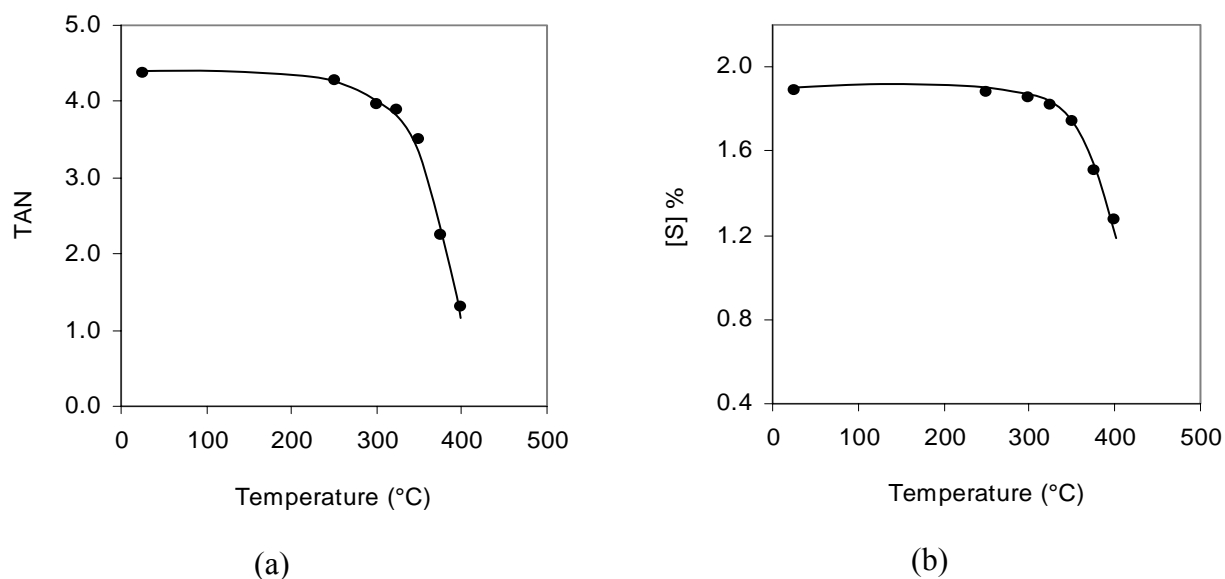
Figure 24: Dependence of (a) TAN change and (b) total S concentration on thermal treatment temperature.

The experiments were carried out in the temperature range from 250 to 400°C at a fixed interval of 25°C between the two points. The bottle-shaped 50 ml autoclaves were used where about 12~13 g oil samples were loaded while this amounts were enough to run TAN and S analysis. The reaction time was set for 4hrs.

Figure 24 shows the TAN and S concentration changes with the thermal treatment temperatures. It was shown that TAN decrease slowly with the temperature increase until 350°C where only about 20% TAN reduction was measured. After this point, TAN dropped dramatically. At 400°C, the TAN decreased to 1.3 and the reduction rate reached to 70.3%. This result suggests that the major decomposition reactions for naphthenic acid compounds take place beyond 350°C. In contrast, the total S concentration changes slower than TAN. Even at 400°C, [S] decreased merely 32.8%, indicating that most of the S compounds in the targeted oil exist in stable forms.

3.3.2 Results from batch reaction
3.3.2.1 On alkaline earth metal oxides (Table 13)

As alkaline earth metal oxides were recognized to be effective to the acid removal and in particular, MgO shows decarboxylation activity for carboxylic acids, their effectiveness for naphthenic acid removal of crude oil needs to be identified as also. Table 13 shows that even with only 1% CaO addition, the TAN decreased from 4.38 to 1.17%, corresponding to 73.3% acid removal rate. On the other hand, the addition of the same amount of MgO lowered the TAN to 3.08, which was not as significant as being expected. Here the stronger basicity of CaO is considered to be responsible for the high TAN reduction rate. As for the S concentration analysis, a slight change, ~6%, was measured only with CaO catalyst. A patent report [39] claimed that CaO contributed to NA and S removal, our results partly support their claims.

Table 13: TAN and S concentration analyses for the oil treated with alkaline earth metal oxides through a batch reactor

Run No.	Oil (g)	Catalyst		Temperature (°C)	Reaction time (hr)	TAN	S (%)
		Composition	Weight (g)				
Raw oil						4.38	
149	12.0			300	4.0	3.95	1.85
150	12.0	MgO	0.12	300	4.0	3.09	1.90
151	12.0	CaO	0.12	300	4.0	1.17	1.77

3.3.2.2 On transition metal oxides (Table 14)

Unlike the excellent behavior of Ag_2O, Cu_2O for the catalytic decarboxylation of model compounds, application of them to crude oil almost did not show positive effect. Regarding this, S-poisoning was considered to be a major reason.

Table 14: TAN and S concentration analyses for the oil treated with transition metal oxides through a batch reactor

| Run No. | Oil (g) | Catalyst | | | Reaction | | | |
		Composition	Weight (g)	Temperature (°C)	time (hr)	TAN	S (%)
Raw oil						4.38	
149	12.0			300	4.0	3.95	1.85
152	12.0	Ag_2O	0.30	300	4.0	4.15	1.84
153	16.0	CuO	0.25	250	4.0	4.10	1.83
154	12.0	Cu_2O	0.24	250	4.0	4.18	1.84

3.3.2.3 On various salts (Table 15)

Table 15: TAN and S concentration analyses for the oil treated with various salts through a batch reactor

| Run No. | Oil (g) | Catalyst | | | Reaction | | | |
		Composition	Weight (g)	Temperature (°C)	time (hr)	TAN	S (%)
Raw oil						4.38	
155	12.0	$4MgCO_3.Mg(OH)_2 \cdot 4H_2O$	0.24	250	4.0	4.06	1.98
156	12.0	Na_2CO_3	0.24	250	4.0	1.87	1.85
189	13.2	K_2CO_3	0.65	300	4.0	4.59	2.00
191	12.6	$CaCO_3$	0.63	300	4.0	1.73	2.00
172	13.4	$AlCl_3$	0.25	300	4.0	8.82	
175	12.7	$FeCl_3.6H_2O$	2.96	300	4.0	6.71	1.79
176	15.6	$CuCl_2.2H_2O$	2.00	300	4.0	10.63	1.41
179	12.8	$NaBO_3$	0.64	300	4.0	4.11	2.01
180	11.7	$Na_5P_3O_{10}$	0.63	300	4.0	5.41	2.09

Several type salt compounds were tested with different added amounts. For carbonates, Na_2CO_3, $CaCO_3$ were found to be very effective for TAN reduction while $MgCO_3$ and Na_2CO_3

behaved differently. It seems that the basicity was not the only reason that can account for this phenomenon as the basicity for these four compounds do not differentiate each other so large. For the metal chlorides being used here, the results were fairly out of our expectation; they could not lower the acidity but instead enhanced the values significantly. As shown in Table 15, the TAN was even enhanced to as high as 10.63 with the addition of $CuCl_2$.

Using acidic catalysts is based on a concept that acidic catalysts can promote C-C cleavage while this cleavage process is involved in decarboxylation process. This feature will have positive effect for decarboxylation process.   However, in the presence of water, the acidic salts will tend to be hydrolyzed, even with trace amount of water; the latter seems to govern the role of these metal chlorides and contribute to the enhanced acidity of the oil.

In spite of the poor behavior for TAN reduction, it was also noted that the presence of $CuCl_2$ lowered the total S concentration to 1.41%, corresponding to about 25% S reduction.

3.3.2.4 On supported metal oxides (Table 16)

Table 16: TAN and S concentration analyses for the oil treated with several solid superbase catalysts through a batch reactor

Run No.	Oil (g)	Catalyst Composition	Weight (g)	Temperature (°C)	Reaction time (hr)	TAN	S (%)
Raw oil						4.38	
165	14.5	NaOH/MgO (15%)	0.24	300	4.0	2.33	1.92
166	13.7	NaOH/Al$_2$O$_3$ (15%)	0.24	300	4.0	3.15	1.94
167	13.6	Na/Al$_2$O$_3$ (5%)	0.24	300	4.0	3.74	1.90
182	12.1	Na/MgO (2%)	0.25	300	4.0	3.45	2.07
168	14.2	Na/MgO (5%)	0.24	300	4.0	1.64	2.11
183	13.3	Na/MgO (10%)	0.26	300	4.0	1.39	2.11
184	15.2	Na/MgO (20%)*	0.27	300	4.0	2.31	2.03
181	12.4	Na/Charcoal (5%)	0.61	300	4.0	3.30	2.08

It is known that solid superbases are a kind of catalyst that can catalyze some organic reactions. The superbases can be either pure compounds such as CaO, SrO or being synthesized by mounting/doping NaOH or Na vapor on the supporters such as MgO and Al_2O_3. To access our goals for this project, we prepared several Na-supported solid superbases catalysts following the procedures of following. 1) Mixing a Na precursor, NaN_3 with the supporters in a flask,

which is being connected to a vacuum pump, with the ratios set to obtain the necessary Na loadings; 2) Heating the flask with a heating mantle to about 350°C while the system was constantly evacuated by the pump; 3) Keeping the flask temperature at this temperature for at least one hour to facilitate the completion of NaN_3 decomposition as the reaction of $NaN_3 \rightarrow Na + 3/2N_2$; while doing this, the flask was gently waved to prevent overheat for some hot spots and uniforming the distribution of Na on the supporters.

The data in Table 16 shows that all of these superbases are effective to TAN reduction. NaOH/MgO (15%) and $NaOH/Al_2O_3$ reduced the TAN to 2.33 and 3.15 respectively. Comparing the three superbase catalysts, Na/MgO, Na/Al_2O_3 and Na/Charcoal, which have the same Na-loading, it was found that Na/MgO has the largest promotion effect, with only 5% Na loading on MgO, it promoted TAN reduction further from 3.09 (MgO only) to 1.64. Increasing the Na loading from 2% to 10% led to consistent TAN reduction from 3.45 to 1.39. However, 20% Na loading showed abnormal tendency, from which the TAN was even higher than those with 5% and 10% loadings.

Even though, the concept of using superbase catalysts for naphthenic acid removal from heavy crude oil is still considered to be a potentially available approach.

3.3.2.5 On zeolite and supported zeolites (Table 17)

Table 17: TAN and S concentration analyses for the oil treated with zeolites or supported zeolites through a batch reactor

Run No.	Oil (g)	Catalyst Composition	Weight (g)	Temperature (°C)	Reaction time (hr)	TAN	S (%)
Raw oil						4.38	
185	12.5	Na/Zeolite (6.3%)*	0.62	300	4.0	1.28	2.15
201	12.9	LZ-Y52	0.63	300	4.0	4.73	
202	15.1	Na/LZ-Y52 (5%)	0.73	300	4.0	3.66	
203	13.1	CBV-500	0.60	300	4.0	5.50	
204	12.9	Na/CBV-500 (5%)	0.60	300	4.0	3.82	

Due to the large surface areas, unique pore structures, adjustable acid-base features for these special group materials, zeolites have extensive applications in petrochemical industry. To explore their application in crude oil upgrading, several runs were conducted with three

commercial available zeolites, 13+4A, LZ-Y52 and CBV-500. Na-doped zeolites catalysts were also investigated. The data in Table 17 shows that LZ-Y 52 and CBV-500 did not show any positive effects to TAN reducing; the introduction of 5% Na improved their performances to some degree, but was not as effective as being loaded on MgO. To our surprise, the addition of Na/13X+4A largely decreased the oil TAN to 1.25 although the supporter themselves 13x and 4A are sorted as inactive to most of the chemical reactions except for their adsorption feature.

3.3.2.6 With other additives (Table 18)

Using organic N-compounds as additives to promote catalytic decarboxylation has been previously reported. Motivated by their excellent performance, the new tests were performed with the combination of MgO and H_2NCONH_2 or 2-hydroxypyridine. The data in Table 18 shows that the addition of both N-compounds contributed to further improvement of MgO to the oil acidity suppression. In the presence of 1.31g H_2NCONH_2, the TAN was reduced to as low as 0.60.

Table 18: TAN and S concentration analyses for the oil treated with MgO in the presence of additive through a batch reactor

| Run No. | Oil (g) | Catalyst | | Reaction | | TAN | S (%) | Additive |
		Composition	Weight (g)	Temperature (°C)	time (hr)			
Raw oil						4.38		
195	14.2	MgO	0.26	300	4.0	0.60	2.06	H_2NCONH_2 1.31g
196	13.2	MgO	0.26	300	4.0	2.40	1.89	2-hydroxypyridine 1.32g

Summarizing all of these results based on batch reaction catalytic tests, several effective TAN suppressing solid catalysts have been sorted out, from which the TAN could be reduced from 4.36~5.0 to 1.0~2.2. These catalysts might be metal oxides, salts and supported solid superbases and others.

3.3.3   Results from fixed-bed flow reaction

3.3.4.1 Naphthenic acid removal from standard acid-added crude oil with MgO

From the point of view of practical application, flow system for heavy oil treatment has indisputable advantages than other processes as in the aspects of oil-catalyst/adsorbent separation, catalyst/adsorbent regeneration. For the lab-scale tests, flow tests can also provide

valuable kinetic information such as activity changes of the catalysts, degrees of carbon deposit on catalyst, features of the treated oils. As an important step for this work, various flow tests were carried out focusing on MgO catalyst that is aimed at optimization of operation condition.

	TAN
Oil only	4.70
Oil+2%CHPA	11.4
80°C, 2hr	11.5
150°C, 2hr	11.1
250°C, 3hr	14.5
300°C, 4.5hr	15.8
350°C, 6hr	10.3
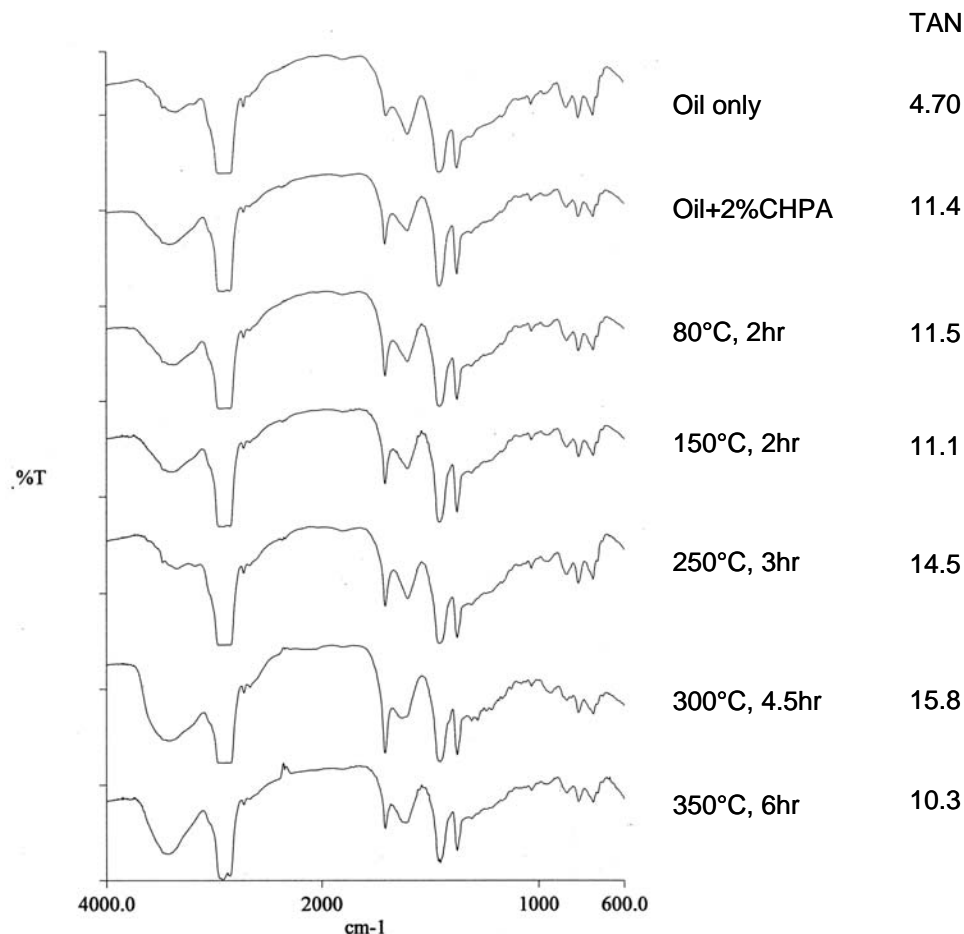
Figure 25: IR and TAN measurements for the oil* treated thermally through a flow reactor (Oil*: oil + 2% CHPA).

Figure 25 is a group of results obtained from the oil feed with 2.0wt% cyclohexane pentanoic acid (CHPA) addition. The purpose to do this is to strengthen the IR adsorption of –RC=OOH. The experiments were conducted with an in-line flow reaction apparatus described in the experimental sections.   About 0.5g of the catalyst (28 to 60 meshes) was loaded into the middle region of the tubular reactor. Glass beads and glass wool were packed into both ends of the reactor to reduce the dead volume and immobilize the catalyst particles. Due to the high viscosity of the oil sample, all the transfer lines and valves were heated to about 80°C to keep the oil flowing. The oil feed was filled in the transfer tank and the flow rate was set at 6ml/hr. During the reaction, the IR adsorption of -RC=OOH group was monitored as a rough estimate of

the effectiveness of the catalyst. If the RCOOH adsorption significantly recovered to the starting condition, this was an indication that the catalyst had been deactivated and the reaction could be hampered. Oil samples were collected at different reaction intervals for measurement of the TAN.

	TAN	Reduction of TAN (%)
Oil+2%CHPA	14.5	
250°C, 2hr	11.3	22.1
250°C, 5hr		
250°C, 9hr	9.3	35.9
250°C, 16hr	17.1	
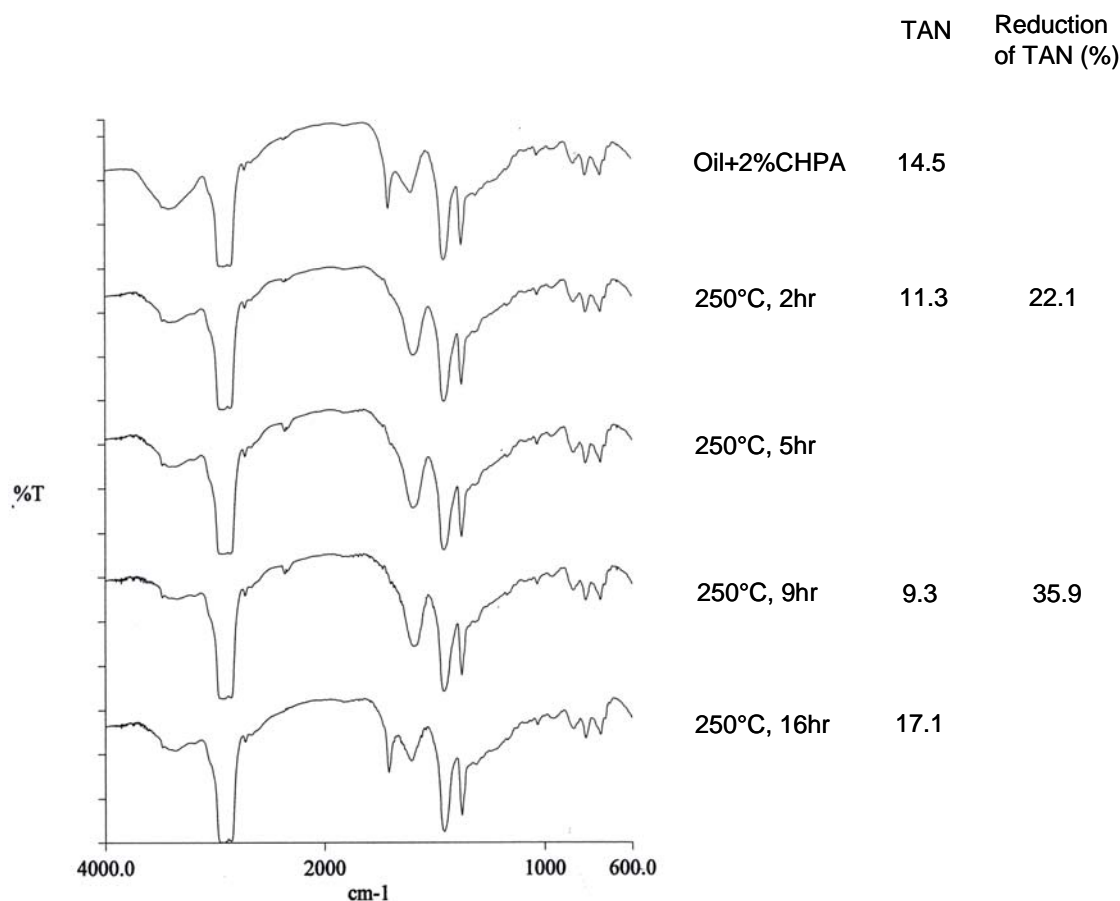
Figure 26: IR and TAN measurements for the oil* treated with MgO through a flow reactor at 250°C (Oil*: oil + 2% CHPA).

The IR spectra for the original crude oil and the oil plus CHPA at different temperatures without the loading of catalyst are shown in Figure 26. This figure clearly shows that IR RC=OOH adsorption at around 1700 cm^{-1} is greatly enhanced due to the addition of 2% CHPA, and the TAN also increased from 4.7 (raw oil) to 11.4 due to the model compound addition. During heating, the RC=OOH adsorption remained at a relatively constant level, suggesting that thermal treatment alone can not significantly remove naphthenic acid under these conditions. In fact, the TANs for the oil heated to 250°C and 300°C were found to be higher than the original

feed. This may have been due to the loss of some light components during heating leading to the concentration of the acidic components.

	TAN	Reduction of TAN (%)
Oil+2%CHPA	15.8	
300°C, 1hr	8.8	44.3
300°C, 3hr	5.6	64.5
300°C, 8hr	7.9	50.0
300°C, 12.5hr	9.1	42.4
300°C, 20.5hr		
300°C, 24hr	12.5	15.5
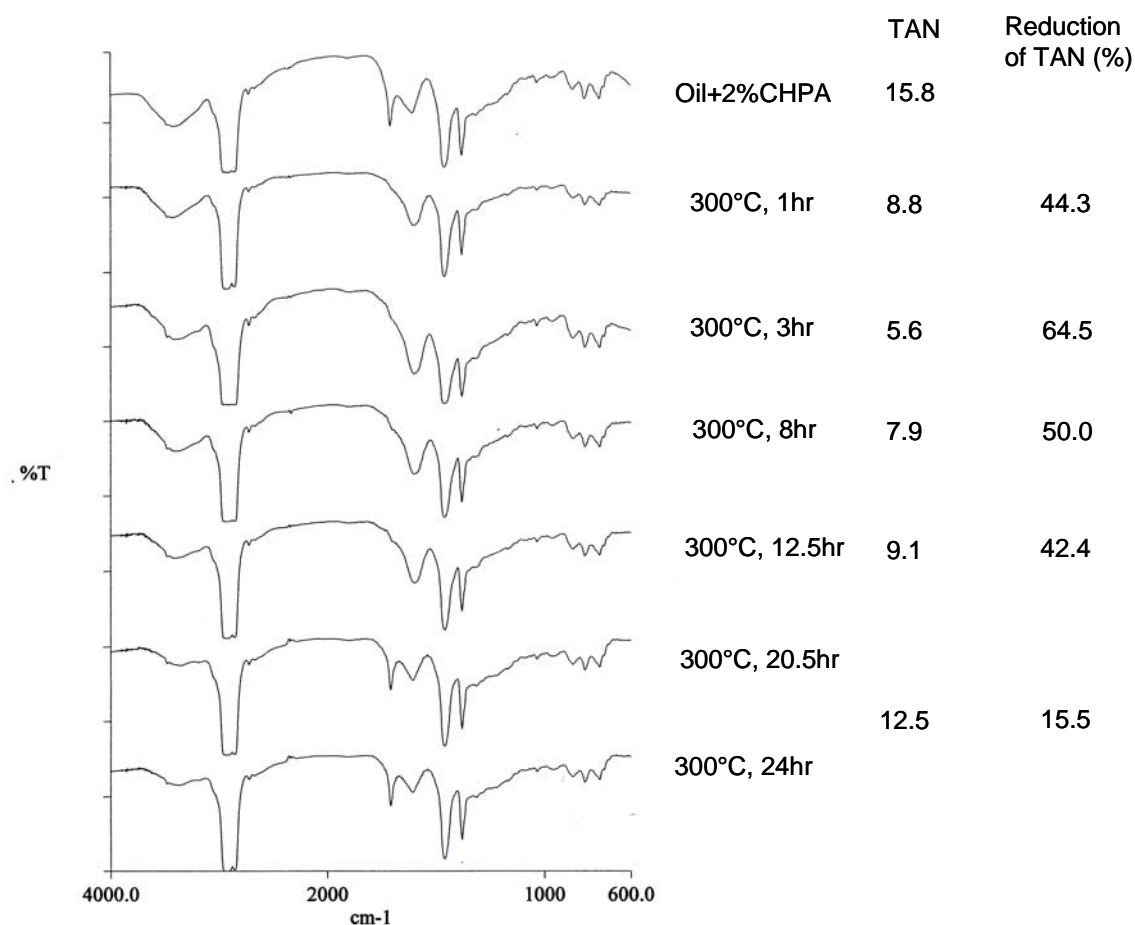
Figure 27: IR and TAN measurements for the oil* treated with MgO through a flow reactor at 300°C (Oil*: oil + 2% CHPA).

An experiment containing MgO catalyst was continuously run for 16hrs at 250°C with the results shown in Figure 27. The IR measurements show that the catalyst was effective for 9hr at 250°C. The quantity of oil that was treated amounted to 47.7g in total and the oil treatment capacity was calculated to be 95.5g-oil/g-MgO. The TAN of the oil decreased more than 30% after 9hr at 250°C. It can be seen in Figure 27 that there were some inconsistencies between the IR measurements and TAN analyses. The reason would be that in addition to the naphthenic acid components in oil, other acidic components such as S compounds might also contribute to the overall acidity for the oil products.

We then ran the same reaction at a temperature of 300°C and the catalytic capacity of the MgO lasted for a longer time (Figure 27). IR measurements show that the deactivation took place between 12.5 and 20.5 hrs. The TAN measurements gave lower values of 5.6 and 7.9 for the oils collected during the reaction time 2-4 and 5-8 hrs periods, respectively. The acid conversion, based on TAN decrease reached 50-64%.

3.3.4.2 Naphthenic acid removal from standard acid-added crude oil with MnO_2

	TAN	Reduction of TAN (%)
Oil+2%CHPA	14.5	
250°C, 1hr	11.0	23.9
250°C, 2hr	12.4	14.3
250°C, 3hr		
	11.9	17.9
250°C, 4hr		
250°C, 6hr		
	15.27	
250°C, 8hr		
250°C, 10.5hr		
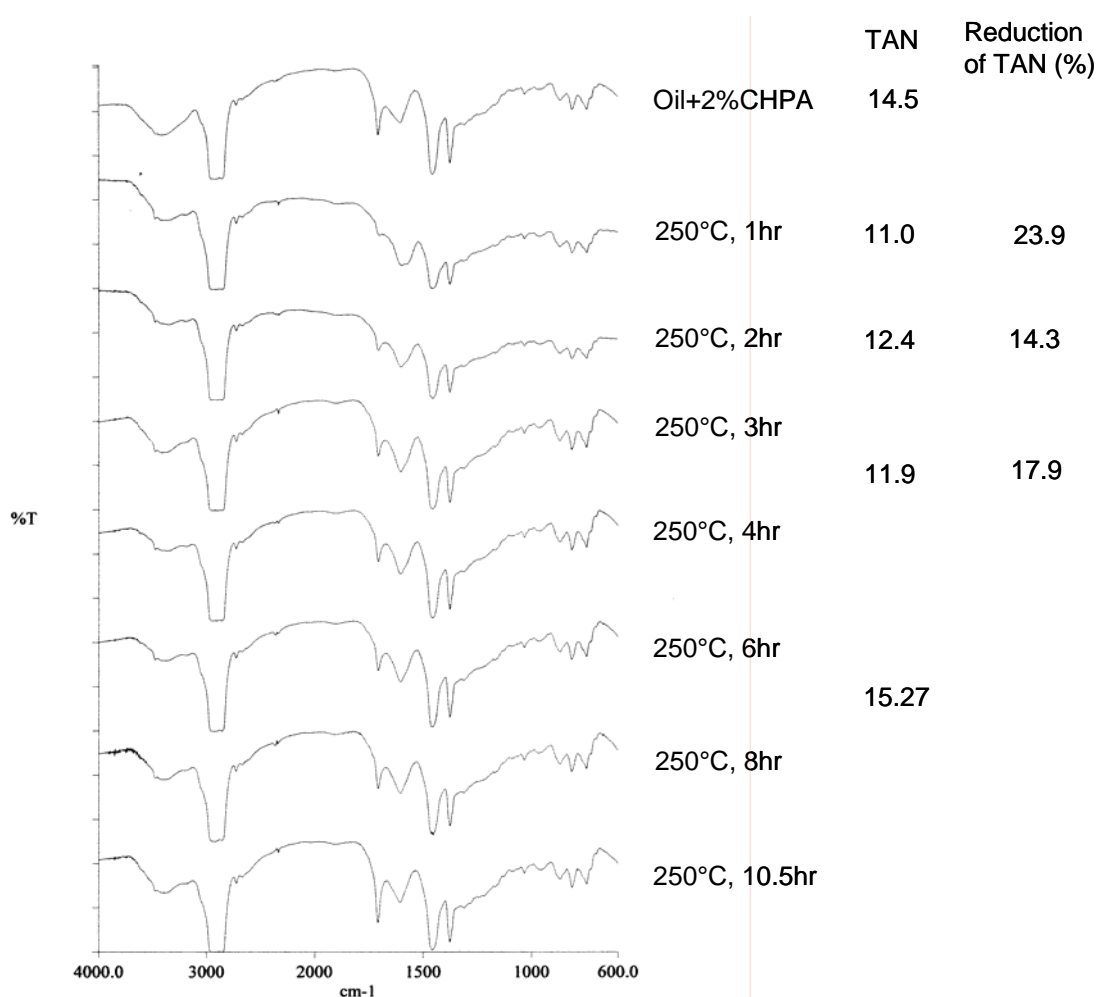
Figure 28: IR and TAN measurements for the oil* treated with MnO₂ through a flow.

In addition to MgO, we also eye on transition metal oxides, inspired by their excellent behavior for model compounds decarboxylation (Figure 28).   Among these candidates, MnO_2 was selected to run flow tests at 250°C for 10hr30min. The IR measurement showed that MnO_2 was effective to RCOOH reduction at the early reaction stage and then the peaks increased gradually with the reaction time. After about 10.5hrs, it was recovered almost completely. The

TAN analysis showed that TAN of the oil decreased to some degree until 4.2hr and the oil treatment capacity was around 51g oil/g-MnO_2.

The preliminary results flow reaction running exposed many practical problems that were not encountered in the experiments involving model compounds. The major difficulties relate to oil diffusion, selective contact between acidic components in oil and the catalyst, poisoning and deactivation of the catalyst caused by heteroatom compounds, and coke deposition. For a heavy oil deed with TAN 4.38, even it is treated as very "acidic", the real NA concentration in oil is still low. Assuming the NA compounds have an average molecular weight of 200, the weight percent of NA is merely 1.6%. Even within this 1.6% NA compounds, the chemical bonding involved in carboxylic acid group are further lower. Accordingly, any decarboxylation catalyst should be highly selective to naphthenic acid. This will ensure the interaction between the catalysts and NA. In addition, the catalyst should be active to C-C cleavage via variable intermediates and mechanisms.

Our work shows that MgO is a basic catalyst that will selectively access the acidic substrates. The result from model acid indicates its effectiveness to catalytic decarboxylation. Meanwhile there was report that MgO was effective to promote cracking reactions at elevated temperatures. All of these information predict that MgO might be a promising catalyst for a practical application of NA removal. Another important reason that drives this work is that MgO is usually considered inactive to react with S-compound. So the S-poisoning issue will be not as serious as other materials such as transition metal based materials. Experimentally, to obtain more effective decarboxylation activities and a prolonged catalyst life, the experimental design as well as operation conditions needs to be improved further.

3.3.4.3 Naphthenic acid removal from crude oil with MgO catalyst

To get the data more close to real condition, instead of the oil feed with standard acid addition, we used real oil to continue the experimental work. The tests were similarly run with MgO and the IR measurement, TAN and viscosity analyses were performed for the treated oil.

With 1g MgO catalyst, whose particle sizes fell in a range of 20-60 meshes, the test was continuously run at 300°C for 54 hr and the flow rate of oil changed from 15.35 to 1.76ml/hr, mostly in the range of 2-5 ml/hr. The contact time of oil feed with the catalyst was calculated roughly to be 200-500 seconds. The total oil collected during the reaction was 206.23g. The TAN changes at different reaction stages were plotted as the Figure 29 (a) and Table 19.

Compared with the value of 4.79 for crude oil, the TANs of treated oil varied in the range of 2.42 to 3.20. The catalyst kept its effectiveness even after 48hr and the TAN reduction rates were in the range of 33.2 to 49.9%. On the other hand, the viscosity measurement did not exhibit significant changes for the treated oil.

To improve the catalytic behavior of MgO catalyst, the experimental condition was further modified. To accumulate longer retention time of the oil in catalyst bed, 2.0g catalyst was loaded into the reactor, and the flow rate was set slower at about 50µl/min. The contact time was calculated to be 33min. As shown in Table 20 and Figure 29 (b),

Table 19: Flow reaction of crude oil over MgO catalysts at 300°C

Texaco Crude oil, TAN 4.79   Catalyst: MgO, 28-65 mesh, 1.0g

Bottle No.	Net hour	Total run hrs	Collected oil weight	Total oil collected	Flow rate (ml/hr)	Temp (°C)	TAN	TAN reduction (%)
1	0.34	0.0	5.22	5.22	15.35	<300	4.79	
2	1.0	1.0	7.36	12.58	7.36	330-300	2.42	49.5
3	2.0	3.0	3.51	16.09	1.76	300		
4	2.0	5.0	13.12	29.21	6.56	300	2.96	38.2
5	3.0	8.0	8.05	37.26	2.68	300		
6	3.0	11.0	8.23	45.49	2.74	300	3.20	33.2
7	3.0	14.0	7.54	53.03	2.51	300		
7.5	5.0	19.0	16.23	69.26	3.25	300	3.03	36.7
8	2.0	21.0	9.97	79.23	4.99	300		
9	3.0	24.0	15.51	94.74	5.17	300		
10	2.0	26.0	3.9	98.64	1.95	300	3.01	37.2
11	3.0	29.0	11.2	109.84	3.73	300		
12	3.0	32.0	8.15	117.99	2.72	300		
13	3.0	35.0	8.65	126.64	2.88	300	2.40	49.9
14	8.0	43.0	24.3	150.94	3.04	300		
15	5.5	48.5	26.03	176.97	4.73	300	2.94	38.6
16	3.5	52.0	15.69	192.66	4.48	300		
17	2.0	54.0	7.53	200.19	3.77	300		

The experiment was continuously run at 350°C for 171.58 hr and the amount of the oil being collected reached 202.74g. For the treated oil, the TAN decreased from 4.74 to 1. 74 ~1.98,

corresponding to about 63%~58% reduction rates. On the other hand, the viscosity measurement shows that the viscosity was also significantly decreased from 6300 cP for raw oil to 420~830 cP at 40°C. If roughly estimating the API values based on a simulated curve of viscosity vs. API, it was found that the API increased about 3~4 units for the treated oil. This greatly contributes to the improvement of the mobility of oil.

(a)

(b)
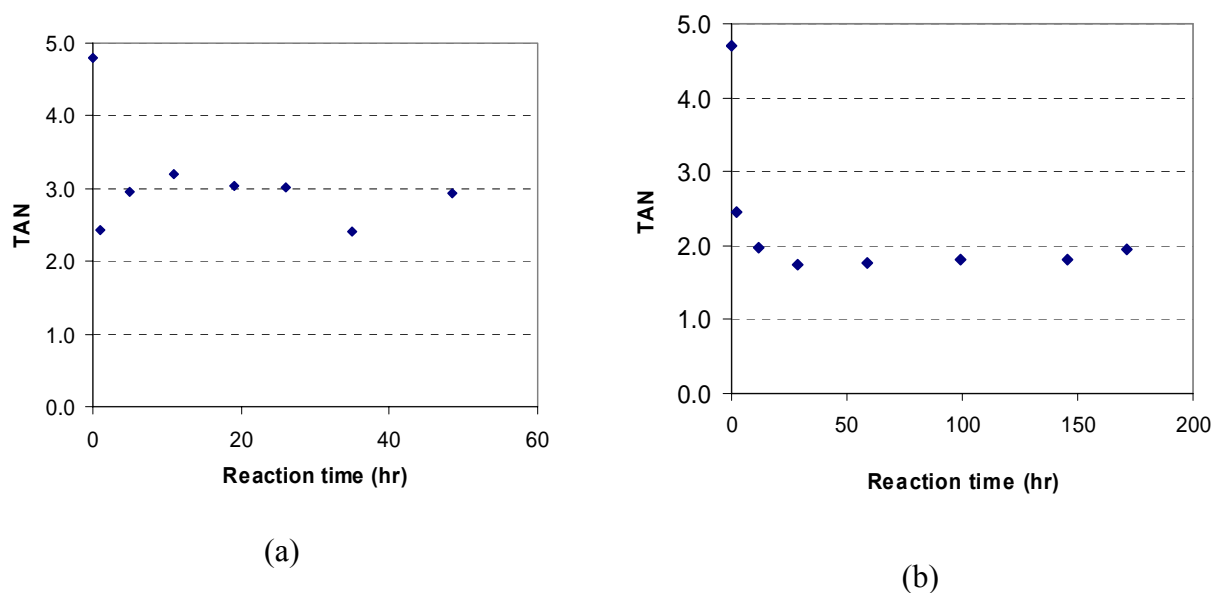
Figure 29: (a) reaction of crude oil over MgO catalysts at 300°C. (b) Flow reaction of crude oil over MgO catalysts at 350°C.

Table 20: Flow reaction of crude oil over MgO catalysts at 350°C

Bottle No.	Net hour	Total run hrs	Collected oil weight (g)	Total oil collected (g)	Temp (°C)	Flow rate (ml/hr)	TAN	TAN Reduction	Viscosity (40°C)	API Gravity	[S]
1	0.42	0	5.73	5.73	<350	13.64	4.71			13.2	
2	2.25	2.25	17.78	23.51	350	7.90	2.45	48.0			1.65
3	9.33	11.58	16.98	40.49	350	1.82	1.98	58.0	605	16.6	
4	17.33	28.91	20.04	60.53	350	1.16	1.74	63.1	282	17.7	1.62
5	29.67	58.58	22.28	82.81	350	0.75	1.77	69.2	420	17.1	
6	20.83	79.41	14.11	96.92	350	0.68			636	16.5	
7	20.17	99.58	20.70	117.62	350	1.03	1.81	68.4	572	16.6	
8	17.00	116.58	19.91	137.53	350	1.17			420	17.1	1.55
9	10.00	126.58	16.03	153.56	350	1.60		34.6	830	16.1	
10	18.67	145.25	25.33	178.89	350	1.36	1.81	68.4	684	16.4	
11	26.33	171.58	23.85	202.74	350	0.91	1.96	65.2	744	16.3	

3.3.5 Results of various measurements and characterization

3.3.5.1 XRD characterization for the used catalysts

XRD is known as an effective approach to characterize the structures of solid materials. For the used MgO catalyst, XRD analysis was performed with a Philips X'Pert Pro Multipurpose X-ray Diffractometer (Figure 30). The scan range of 2θ was set from 10 to 80. Three samples, including pure MgO, pure $MgCO_3$ and a used MgO from flow reaction, were analyzed to see if the structure of the catalyst has changed. It was found that the major diffraction peaks of MgO remained and no typical $MgCO_3$ peaks were detected from the used MgO, indicating that MgO kept its basic structure during the reaction, but no clear evidence showing that carbonate was formed. This dispelled our concern about the formation of $MgCO_3$ that once was formed; it would be very difficult to be decomposed back to MgO. Usually it needs the calcinations temperature as high as 800~1300°C.

3.3.5.2 Carbon deposits on catalysts

Table 21: Carbon and hydrogen concentration analyses for the catalysts exposed to crude oil reaction at different conditions

Run No.	Reactions	Carbon wt%	Hydrogen wt%
FR12	MgO, 300°C, 54hr	8.52	1.38
FR13	MgO, 350°C, 7.7hr	3.63	0.42
FR14	MgO, 300°C 14.5hr + 350°C 5hr	3.73	0.94
FR15	HZSM-5, 300°C, 22.25hr	6.96	1.04
FR16	MgO, 80°C, 10hr	0.79	0.18

Accompanied with the thermal cracking reaction, carbon deposit will occur inevitably on the surface or bulk of the catalyst. To determine the degrees of C-deposit on the catalysts used in this work, the C/H elementary analysis was conducted with several selected catalysts with the results listed in Table 21. The data in Table 22 shows that C-deposit becomes serious when the catalysts exposed in oil feed for longer time (FR12), at higher reaction temperature (FR13) or when strong acidic catalyst was used (FR15). In contrast, lower temperature and short exposed time to oil feed will not result in serious coking and C-deposit (FR16).
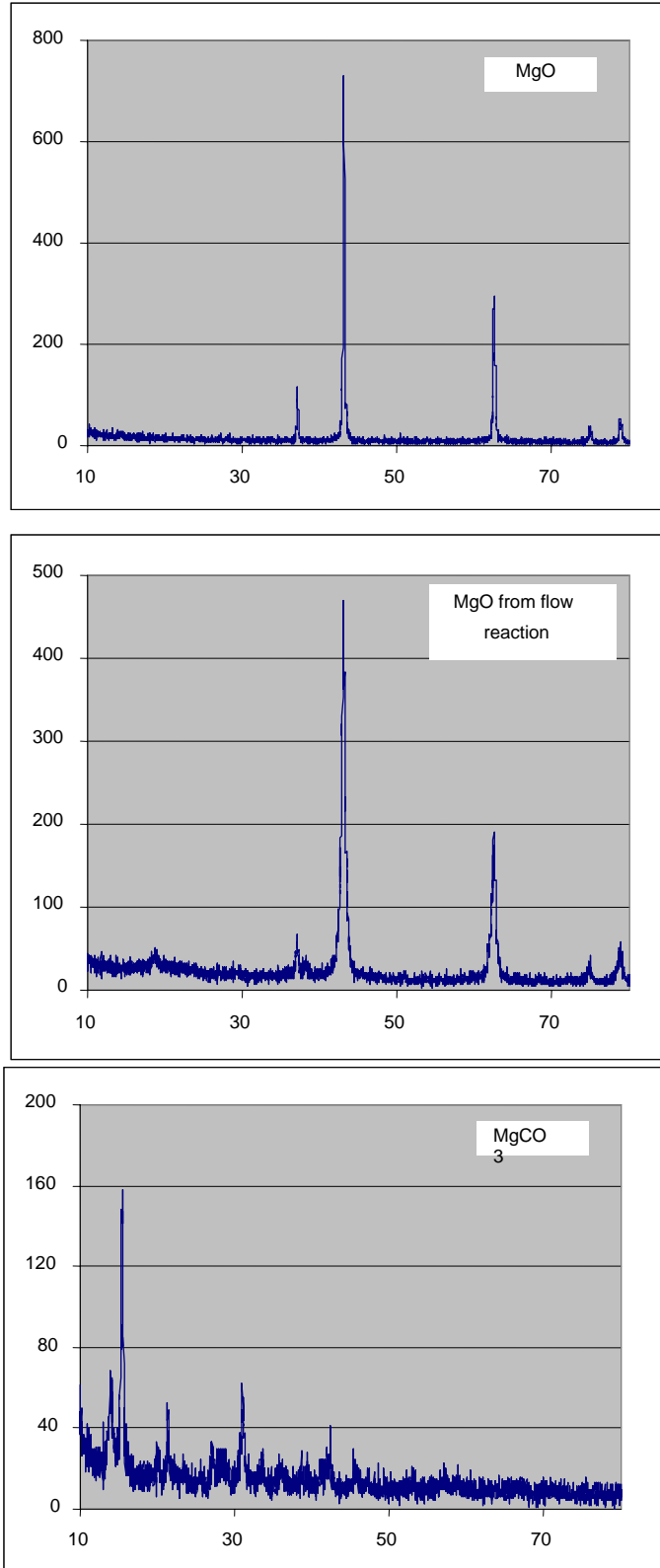
Figure 30: XRD analysis for the selected solid samples.

Then a new concern related to this work is on how to suppress the C-deposit and prolong the catalyst life. Enlightened by the concept of aquaconversion [40-42], where water, being premixed with oil feed, can suppress the formation of coke and heavy residue by capping hydrocarbon radicals via combining with H radical, which was supplied through high temperature catalytic water decomposition, several water addition experiments were conducted with batch reactors at 300°C for 10 hr (B2, B3 and B4) and 325°C (B6, B7and B8). The C-analysis results as shown in Table X clearly indicate that the presence of water can suppress the C-deposits effectively. The carbon concentrations dropped from 7.06% to 2.06% at 300°C and from 8.36% to 1.98% at 325°C. On the other hand, the addition of oxidative additive such as H_2O_2, which produce active atomic oxygen through thermal decomposition, enhanced the C-deposit. In general, a reductive reaction atmosphere is needed to suppress coking and heavy carbon depositing, which is equal to prolong the catalyst life.

Table 22: Carbon and hydrogen concentration analyses for the catalysts exposed to crude oil reaction in the presence of additives

Run No.	Reactions	Carbon wt%	Hydrogen wt%
B2	MgO + Oil, 300°C, 10hr	7.06	2.11
B3	MgO + Oil + H_2O, 300°C, 10hr	2.06	3.39
B4	MgO + Oil + H_2O_2, 300°C, 10hr	11.06	2.54
B6	MgO + Oil, 325°C, 12hr	8.36	16.2
B7	MgO + Oil + H_2O, 325°C, 12hr	1.97	2.26
B8	MgO + Oil + H_2O_2, 325°C, 12hr	16.2	2.39

3.3.5.3 Gas analysis for crude oil gold tube tests

Table 23: Gas product analysis from sealed gold tube experiments at 300°C for 10hr

Catalyst (mg)		Oil (mg)	Gas product (ml/g-oil)			
			C_1	CO_2	H_2S	C_2-C_5
None		210.8	0.233	0.150	0.445	0.155
MgO	5.1	201.0	1.251	0.520	1.267	0.639
Ag_2O	5.2	202.9	0.194	0.733	0.007	0.114
Cu_2O	5.0	200.9	0.473	1.023	0.004	0.179
HZSM-5	5.0	230.2	0.128	0.208	0.367	0.196

Sealed gold tube experiments were a unique technique that has been widely used in fundamental study of geochemistry. The device for gold tube experiments were specially developed in our lab that can serve for multiple projects. To a small gold tube with an internal diameter of 3.5mm and tube length about 6-7 cm, the reactants and catalyst were loaded into. The lower part of the gold tube was inserted into an ethanol- liquid nitrogen bath to trap any possible volatile substances. The gold tube was then flushed with argon to remove the air. After that, the other end of the tube was crimped and sealed using an argon welder. Prior the real test, the sealed gold tube was placed in ultra sonic device to promote the mixing for the added components. The isothermal pyrolysis experiments were conducted in an oven where outer water pressure was added to the gold tubes to balance the expansion of the gold tube volume due to the high temperature reaction.
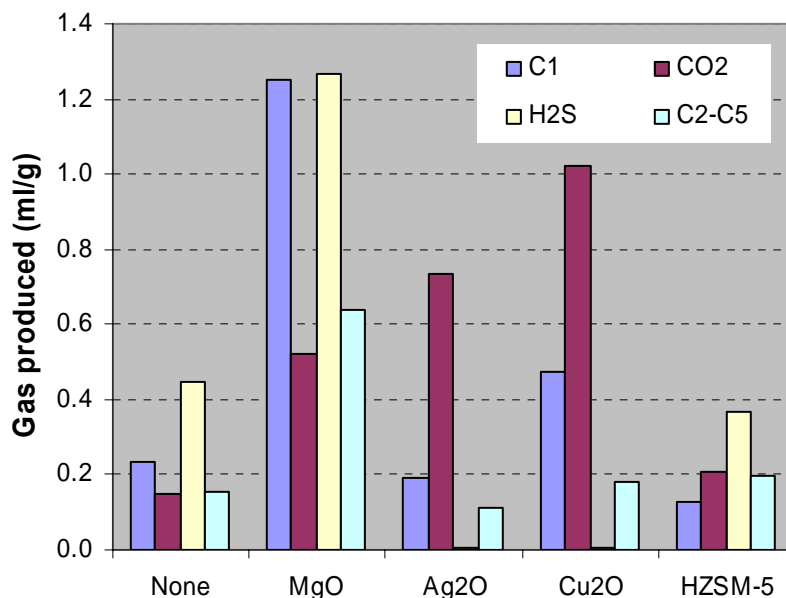
Figure 31: Gas product analysis from sealed gold tube experiments at 300°C for 10hr.

For the crude oil tests with gold tubes, about 200mg oil and 5mg catalyst were loaded in each tube. Four representative catalysts, MgO, Ag_2O, Cu_2O and HZSM-5 with a blank test were run at 300°C for 10hr. After the reaction, the gold tube, placed in a glass tube with an O-ring vacuum valve, was connected to the vacuum line and the tube was pierced with the O-ring sealed vacuum needle valve to release the gases and other fluid products. The gaseous products were transferred and analyzed following the procedure described in 2.1.3.

As shown in Table 23 and Figure 31 compared with blank test, CO_2 amounts were clearly higher from the catalysts of MgO, Ag_2O and Cu_2O. This provides very direct evidence showing that decarboxylation process occurred on these catalysts. The data in Table X also shows that the H_2S amounts were extremely lower from Ag_2O and Cu_2O catalyzed reaction. This was also well consistent with our prediction.

3.4   Development of effective naphthenic acid adsorbents

3.4.1   Adsorption of naphthenic acids from dodecane on clay minerals

Table 24 summarizes the results of NAs adsorbed onto the selected clay absorbents. The order of the affinity of various clays as adsorbents to NAs is: SepSp-1>SWy-2>SAz-1≥PF1-1> SCa-3 ≥SHCa-1 >SAz-2>IMt-1>IScz-1>KGa-2>ISMt-2. In addition, in each test no significant adsorption was observed for tetradecane. This result shows that these clay adsorbents are highly selective toward NAs but not hydrocarbon. The results show that Sepiolite (SepSp-1) and Na-montmorillonite (SWy-2) are potential efficient adsorbent for removing NAs from oil. The capacity of the adsorption of NAs reached 68 and 53 mg-acid/g-clay for SepSp-1 and SWy-2, respectively. On the contrary, illite-smectite mixed layer (ISMt-2) was found to be inactive towards the acid adsorption. NAs adsorption onto the kaolinite (KGa-2) and mixed layer illite-smectite (ISCz-1 and ISMt-2) was much less than for the other clay minerals.

The Na-montmorillonite, SWy-2, effectively adsorbed NAs with high capacity compared to other sources of montmorillonite such as SAz-1, SAz-2, and SCa-3. This suggests that Na cation exchange might enhance NAs adsorption. Montmorillonites (SAz-1, SAz-2, and SCa-3) with higher CEC and surface area did not adsorb as much as 4-heptylbenzoic acid as the other Na-montmorillonite (SWy-2). Hectorite (SCa-3) is analogous to montmorillonite (SAz-1 and SCa-3). Therefore, the adsorption of various NAs by hectorite and montmorillonite is similar.

Both of the fibrous clay minerals (SepSp-1 and PF1-1) have the higher surface areas (307.8 and 172.6 m^2/g, respectively) compared to that of SWy-2 (32.2 m^2/g). However, the high capacity of NAs adsorption was not observed. This may due to most of the surface areas of sepiolite (SepSp-1) and palygorskite (PF1-1) are from micropores inside the channels that might be accessible to N_2, but are too small for NAs. Adsorption of each NA by sepiolite tool place in larger quantities than that of palygorskite, which may be due to the larger surface area of sepiolite.

In some of clays (IMt-1, SAz-1, SAz-2, SCa-3, and SHCa-1) used, the order of the affinity of four NAs adsorbed onto clays is: NA2>NA3>NA1>NA4. NAs can be deprotonated to give

anions, which can coordinate to metal cations to form surface complexes on the edges of clay minerals. The adsorption of benzoic acid onto the clays except onto KGa-2 was more effective in comparison with the adsorption of other NAs. This is because benzoic acid with an aromatic ring showed strong effect on physical-chemical adsorption. In comparison with benzoic (NA2) and 4-hyptylbenzoic acid (NA4), NA4 has a hydrophobic group, heptyl, which destabilizes carboxylate-metal interaction. This results in a weak adsorption onto clay surfaces.

Table 24: Efficiency of acid removal from the selected clay absorbents

Adsorbent	NAs Adsorbed Percentage (%)				Amount of NAs Adsorbed
	NA1	NA2	NA3	NA4	(mg/g)
KGa-2	5.5	6.6	11.1	1.9	9.7
IMt-1	15.7	24.5	19.1	8.1	25.7
ISCz-1	1.6	25.7	3.1	3.6	12.2
ISMt-2	0.0	0.0	0.0	0.0	0.0
PF1-1	20.1	34.3	20.2	26.9	38.9
SAz-1	21.2	46.7	23.7	13.5	40.0
SAz-2	15.4	30.8	22.3	8.5	29.3
SCa-3	16.1	30.6	19.4	8.7	34.1
SepSp-1	37.9	60.0	39.2	40.9	68.0
SHCa-1	17.4	40.4	19.4	11.8	33.9
SWy-2	17.7	47.0	23.3	49.8	53.0

NA1=Cyclohexanepropionic acid, FW = 156.23

NA2=Benzoic acid, FW = 122.1

NA3=Cyclohexanepentanoic acid, FW = 184.28

NA4=4-Heptylbenzoic acid, FW = 220.31

The crude oil (6.1g) with TAN 4.72 was added into a beaker containing 1.2 g of SepSp-1 and SWy-2, respectively shaken for 24 fours at 66°C. We found that the TAN was decreased to 4.03 and 3.80. However, the same amount of oil and clay with CH_2Cl_2 for 24 fours at 25°C, the TAN was dropped to 3.42 and 3.14, respectively. It indicated that the good contact between oil and clay is necessary.

3.4.2 Adsorption of benzoic acids from dodecane on clay minerals

It was shown that the benzoic acid (BA) was strongly adsorbed on clay mineral surfaces. For this reason, the adsorption isotherm of BA with four clays was further studied and the data obtained in this work are shown in Figure 32. The isotherm is characterized by a decreasing

slope as concentration increases since vacant adsorption sites decrease as the adsorbent becomes covered. Such adsorption behavior could be explained by the high affinity of the adsorbent for the BA at low concentrations, which then decreases as concentration increases. All experimental results could be interpreted according the Langmuir equation:

$$\frac{C_{eq}}{\Gamma} = \frac{C_{eq}}{\Gamma_{max}} + \frac{1}{K \cdot \Gamma} \tag{13}$$

Where C_{eq} (mmol/L) is the equilibrium concentration of the acid in solution, Γ (mmol/ m^2) is the amount of acid adsorbed onto solid at equilibrium, Γ_{max} (mmol/g) is the maximum adsorption capacity (mmol/m^2), and K (L/mmol) is the Langmuir equilibrium constant for the adsorption process. From the adsorption isotherm plotted in accordance with equation 1, the equilibrium constant K and the adsorption capacity, Γ_{max}, are obtained by plotting Γ^{-1} versus the reciprocal equilibrium concentration of acid, C_{eq}^{-1}. From K, the molar standard Gibbs free energy, ΔG^O, was determined as –RTlnK as shown in Table 25.

Table 25: the molar standard Gibbs free energy, ΔG^O

Clay	Surface Area (m²/g)	Γ_{max} (μmol/m²)	ΔG (KJ/mol)	nm²/molecule
SepSp-1	307.8	1.7	-14.35	0.98
PF1-1	172.6	2.1	-15.59	0.79
SWy-2	32.2	11.4	-15.83	0.15
IMt-1	28.6	5.0	-13.89	0.33

The results show that the adsorption of BA on SWy-2 was found to be significantly difference. The theoretical value for monolayer coverage of perpendicular and parallel oriented benzoic acid molecules is 0.225 and 0.515 nm²/molecule, respectively (Wright and Pratt, 1974). From Γ_{max}, the area covered by one BA molecule is calculated to cover an area (A) of 0.15 nm². This corresponds to maximum adsorption (Γ_{max}) as calculated from:

$$\Gamma_{max} = \frac{1}{N_a \cdot A}, \text{ where } N_a \text{ is Avogadro's number.} \tag{14}$$

This suggests that the BA form a monolayer on the SWy-2 surface with perpendicular-oriented molecules. The detailed adsorption mechanism should further investigated by the use of spectroscopic techniques.

Benzoic Acid adsorbed onto Clay Minerals
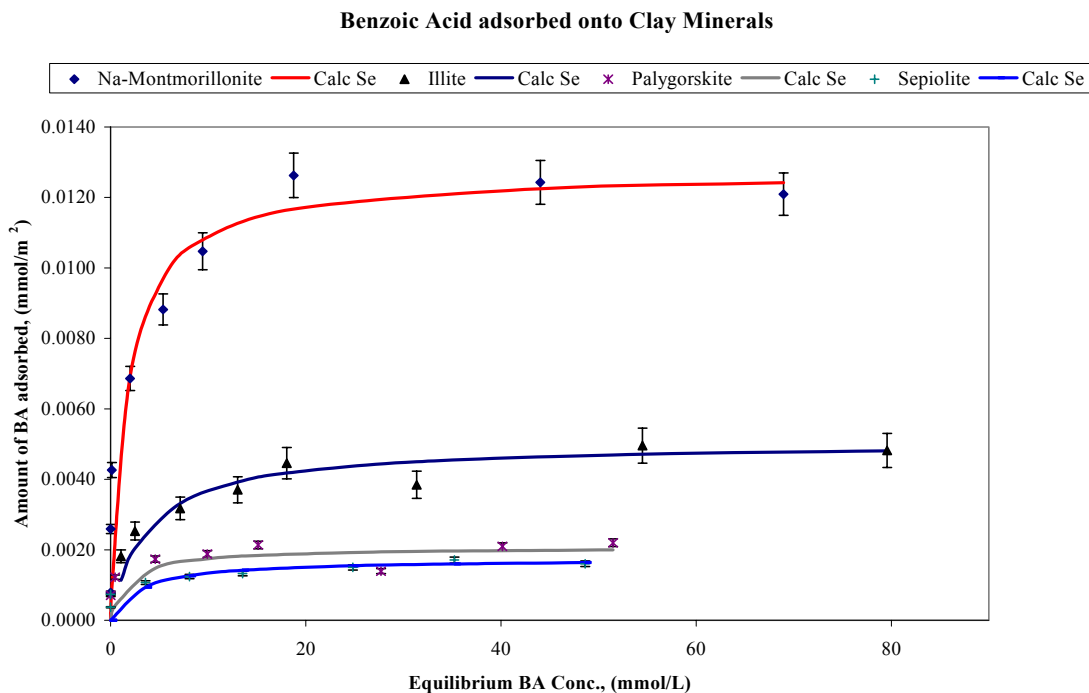
Figure 32: Adsorption isotherm of Benzoic acid on SepSp-1, PF1, SWy-2, and IMt-1.

3.4.3   Adsorption of naphthenic acids from dodecane on metal oxides

Several metal oxides were selected as adsorbents for the removal of naphthenic acids. These results are shown in Table 26. Metal oxides of Group 1A and 2A elements, such as Na_2O, MgO, and CaO are alkaline and can be shown to neutralize NAs. These alkali and alkali earth metal oxides perform as strong base which adsorb substantially all of the NAs onto surfaces based on the stoichiometric ratio. For example, $2RCOOH + MgO \rightarrow (RCOO)_2Mg + H_2O$, i.e. One mole of MgO can adsorb two mole of NA. In this study, we prepared the total 0.098 mole of NAs in dodecane solution with 1.61, 1.78 and 2.48 mole of Na_2O, CaO, and MgO, respectively. After 24 hrs adsorption all of the NAs were removed from the NAs solution. Therefore, the removal efficiency is 100% for these metal oxides.

Aluminum oxide, Al_2O_3, which has specific area of 155 m^2/g, can also adsorb NAs effectively. The amount of NAs being adsorbed by Al_2O_3 is less in comparison with those by MOs of Group 1A and 2A. This would be due to the weaker basicity compared with MOs of Group 1A and 2A. Transition MOs, including CuO, AgO, Ag_2O, ZrO, and MnO_2, were also selected in this study.   It was found that AgO and Ag_2O were very reactive with NAs. They showed great effect on the adsorption of NAs and minor effect on N-containing molecule, but no effect on S-containing molecule, such as 2-phenylthiophene. The adsorption of 2-

71

phenylthiophene is very difficult on the metal oxide surfaces. The rest of MOs have little effect on the adsorption of NAs.

Table 26: Efficiency of NAs removal from the selected metal oxides

Metal Oxide	N-compound	S-compound	NA1	NA2	NA3	NA4	Adsorbed (mg/g)
Al2O3	5.3	0.7	69.4	91.0	69.2	76.7	116.5
SiO2	98.2	3.5	75.3	86.6	74.5	69.4	116.5
PbO	0.0	0.0	0.0	4.2	0.3	2.3	2.4
SeO2	96.0	0.0	5.5	1.0	0.0	2.7	1.1
CuO	0.0	0.0	0.9	6.7	0.0	3.9	4.3
Cu2O	14.7	0.1	3.0	39.0	0.0	23.5	24.2
AgO	33.5	0.0	97.0	99.0	97.5	100.0	153.1
Ag2O	33.6	0.0	100.0	100.0	100.0	100.0	154.4
ZnO	10.6	0.0	62.9	79.7	72.7	97.2	120.4
Y2O3	13.4	1.9	92.0	97.3	91.4	95.9	145.8
La2O3	0.0	0.0	0.0	0.0	0.0	0.0	0
ZrO2	2.9	0.0	0.0	9.1	7.7	6.4	8.3
MnO2	2.3	1.2	0.0	5.6	2.1	1.7	3.3
Fe2O3	7.9	8.8	16.1	16.6	24.4	21.4	30.1
CeO2	0.0	0.0	7.8	4.8	0.0	5.6	5.8

Nitrogen compound=Quinoline, FW = 129.16

Sulfur compound=2-phenylthiophene, FW = 160.24

NA1=Cyclohexanepropionic acid, FW = 156.23;

NA2=Benzoic acid, FW = 122.1;

NA3=Cyclohexanepentanoic acid, FW = 184.28;

NA4=4-heptylbenzoic acid, FW = 220.31

3.5   Theoretical results

3.5.1   Calculated pKa of naphthenic acids
3.5.1.1 Effects of the alkyl-chain position

Whether the carboxyl group is attached directly to the ring structures or to the ring *via* the connection of the alkyl chain is still a matter of debate. Also, there is currently very little information about how the alkyl-chain affects NAs acidities. In order to gain some theoretical insights, four sets of deprotonation energies have been calculated and results are illustrated in Figure 33. Two saturates (a) cyclopentanecarboxylic acid (C_5H_{10}) and (b) cyclohexanecarboxylic acid (C_6H_{12}) and two aromatics (c) benzenecarboxylic acid (C_6H_6) and (d) β-Naphthalenecarboxylic acid ($C_{10}H_{18}$) have been selected.

cyclopentanecarboxylic acid   **cyclohexanecarboxylic acid**

Benzenecarboxylic acid   **β-Naphthalenecarboxylic acid**
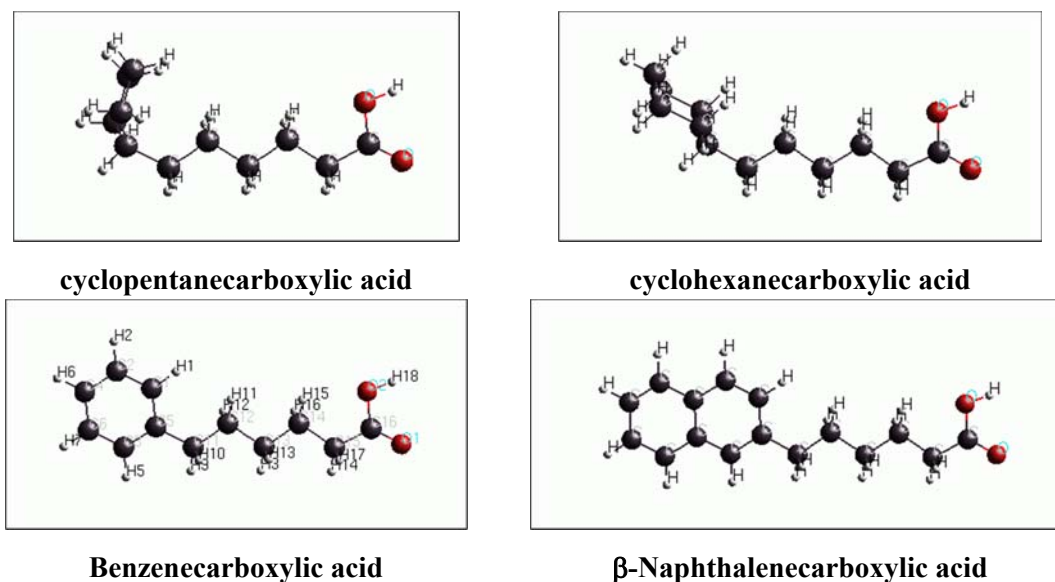
Figure 33: Optimized geometry of a carboxylic acid attaching to saturated and aromatic rings through an alkyl chain.

Calculated E_{deprot} as a function of the alkyl-chain length m are given in Figure 34. The results could be summarized as follows:

i) Geometrically, carboxylic acids tend to maintain a high symmetry in the gas phase as their energetically favored structures. The alky-chain with possibly the most exposed geometry is with hydrogen atoms alternating on each side, and the carboxylic –COOH group located in the same plane as carbon atoms from the alkyl-chain. The H-atom in the carboxylic group can be connected to either oxygen atom. However, it should be in between them such that 'resonance' stabilization can be formed. The saturated rings find it energetically favorable to twist somewhat from a planar conformation to form an envelope-shape structure, while aromatic rings maintain their preferred planar ring structures. For cyclopentanecarboxylic and cyclohexanecarboxylic acids, the saturated rings are perpendicular to the plane defined by COOH and the carbon chain such that overall structures have the reflection-plane symmetry (Cs) as shown in Figure 34 (a) and (b). For 2-naphthalenecarboxylic acids, the naphthalene ring is located in the same plane as COOH to maintain the Cs symmetry (Figure 34 (d)). For benzenecarboxylic acids, both in-plane and perpendicular benzoic ring structures (both have a Cs symmetry) have been examined. We found that the perpendicular conformation as shown in Figure 34 (c) is about ~ 1 kcal/mol systematically more stable than the in-plane position. Therefore only results for the perpendicular configuration are presented.
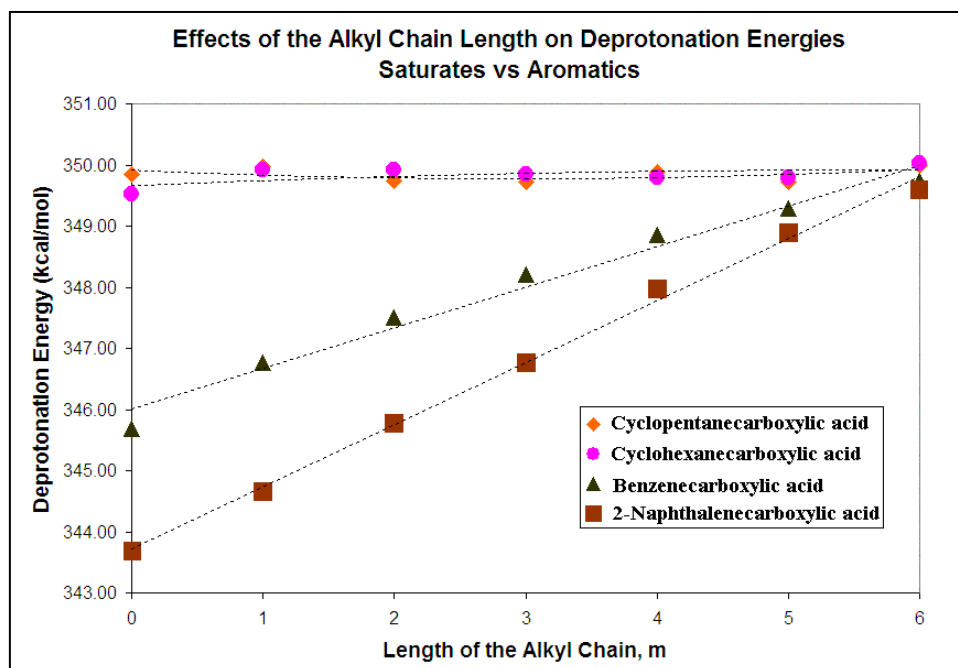
Figure 34: Calculated deprotonation energies (Edeprot) as a function of the chain-length m.

ii) Carboxylic acids exhibit stronger acidities than alcohols because of their abilities to form a "resonance" hybrid. A negative charge equally distributes in between the two oxygen atoms significantly reduces their attractions for a positively charged proton. As a reflection of this resonance stabilization, the energy required to remove a proton from the carboxylic acid is substantially less than from alcohols. When the carboxyl group is directly attached to an aromatic ring, the inductive effect of the aromatic ring withdraws electron densities from oxygen atoms and has a marked acid-strengthening effect, resulting in a decrease of the deprotonation energy E_{deprot} ~ 4 to 6 kcal/mol. Addition of the second ring in aromatics increases the electron-withdrawing ability, rendering a smaller E_{deprot} (1~2 kcal/mol) for naphthalenecarboxylic acids than for benzenecarboxylic acids in the small m region. This effect, however, is only significant in the small m region; it fades quickly as the alkyl chain length increases. When m > 6, E_{deprot} becomes independent to the ring structure. Since most of NAs in crude oils are believed to have much longer alkyl-chain, m is usually considerably greater than 6, we conclude that if the carboxylic group is attached to the alkyl chain, its acidity will be nearly the same for both saturates and aromatics.

3.5.1.2 Effects of the side chain

Instead of forming an aliphatic carboxylic acid, the carboxylic group might directly attach to the aromatic ring with a substituted alkyl side-chain. Both saturates and aromatics, represented

by cyclohexanecarboxylic and benzenecarboxylic acids, with an alkyl side-chain on various substituted positions (denoted as Sub-1, Sub-2 and Sub-3 in Figure 35) have been considered. Dependences of calculated E_{deprot} on the chain length were illustrated in Figure 35. The presence of the substituted side-chain causes a decrease of 1~2 kcal/mol of E_{deprot}, smaller in magnitude than the aromatic effect (4~6 kcal/mol). For saturated ring structures, the side-chain effect is stronger when the side-chain locates closer to the carboxylic group (sub-1), indicating that the steric hindrance is the predominant effect. For aromatics, the electronic effect competes with the steric hindrance effect resulting in a more complex E_{deprot} relation. As an electron donor, the substituted side-chain reduces the electron-withdrawing ability of the aromatic ring to the carboxylic group, which gives rise to an initial increase of E_{deprot}. But with the increase of the alky side chain length, the repulsion becomes dominant again resulting in the decrease of E_{deprot}.
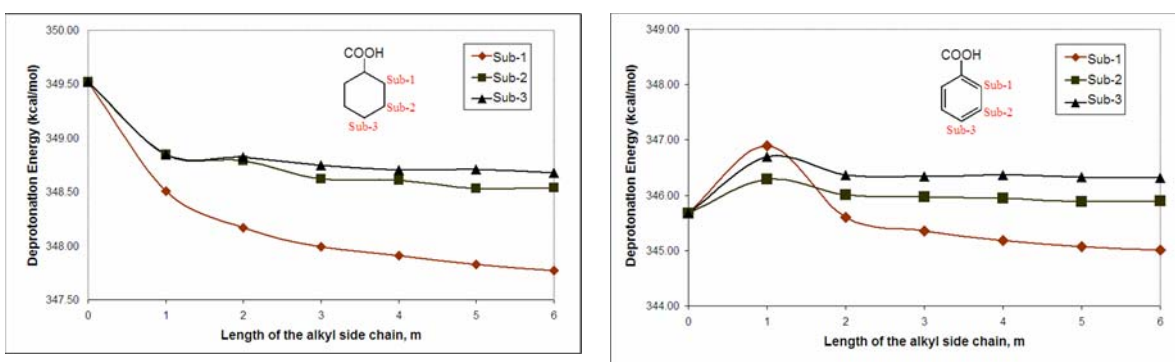
(a)   (b)

Figure 35: Effects of the alkyl side chain on the deprotonation energies.

3.5.1.3 Effect of ring structures

Another complexity of NAs structures originates from the possibility of various ring combinations for both saturated and unsaturated. In the present work, E_{deprot} of a carboxylic group attaching to 10 different ring structure *(ref. Figure 9)* for both saturates and aromatics have been calculated. Evidently, we can a systematic increase of acidity for aromatics. However the predicted acidity difference between aromatics and saturates is smaller (~1.0 difference in pKa value, corresponding to a 1.5 kcal/mol difference in the Gibbs' free energy) compared to that determined from the gas-phase E_{deprot} (4~6 kcal/mol). This produces a more reasonable value compared with the experimental measurement. For example, the experiment pKa value for saturated cyclohexane carboxylic acid (B1) is 4.91 and 4.20 for aromatic benzoic acid (b1), a difference of 0.71. Our calculated pKa difference of 4.4 −3.6 = 0.8 with the solvent effect taken into account is much closer than that directly determined from the gas-phase deprotonation

energy difference of $0.725 * (349.52 – 345.67) = 2.8$. This suggests that the solvent effect is important for a more accurate pKa calculation.

Table 27: Comparison of calculated Edeprot and pKa, effects of the different ring structures

Ring	E_{deprot}		pKa	
	Saturates	Aromatics	Saturates	Aromatics
Benzene	349.52	345.67	4.4	3.6
Indene	349.50	347.92	4.2	3.0
Naphthalene	348.95	343.75	4.8	4.1
Acenaphthylene	348.88	345.11	4.6	3.1
Fluoranthene	348.80	344.51	4.9	3.9
Anthraence	348.36	342.28	4.3	4.1
Phenalene	348.16	342.71	4.5	4.3
Pyrene	348.12	340.71	5.1	4.4
Tetracene	347.66	341.18	5.1	4.2
Chrysene	348.44	340.76	5.1	3.9
Average	348.64	343.46	4.7	3.9

3.5.1.4 Summary of the calculated acidity of naphthenic acids

A brief summary of calculated results of the acidity of naphthenic acids are as follows:

- Despite their complex chemical compositions, naphthenic acids, possessing the same functional group (-COOH), have relatively smaller variation on their acidity;
- Calculated pKa for most naphthenic acid compounds are in the range of $3.0 \sim 5.0$. This indicates that naphthenic acids are relatively weak acids compared with the stronger acids such as the sulfuric acid (pKa $= 0.5 \sim 2.0$).
- Hydrocarbon structure, to which a carboxylic group is attached, has a moderate effect on the acidity of the associated naphthenic acid. Aromaticity substantially increases the pKa value of some naphthenic acid up to 1.0 unit.
- For saturates, the magnitude of the acidity change, mainly due to the steric hindrance effect, is in the order of $0.2 \sim 0.4$ unit. Significantly less than the aromatic effect.
- In the cases that the carboxylic group attaching to the ring structure through an alkyl group with m > 6, both aromatic and steric effects on the acidity could be negligible.

3.5.2 Oil/water distribution coefficients (logP) of naphthenic acids

A set of organic molecules has been selected and the calculated logP values are compared with the experimental measurements (Table 28). An excellent correlation between the calculated logP and experimental data has been established (Figure 36).

Table 28 Comparison of Calculated logP of Selected Compounds with Experimental Data

Chemical Name	CAS #	Formula	Exp. logP	Calc. logP
Benzoic Acid	000065-85-0	$C_7H_6O_2$	1.87	1.82
1-Napthoic Acid	000086-55-5	$C_{11}H_8O_2$	3.10	2.94
2-Naphthoic Acid	000093-09-4	$C_{11}H_8O_2$	3.28	3.00
Antheracene-9-Carboxylic Acid	000723-62-6	$C_{15}H_{10}O_2$	3.85	4.01
Cyclohexanecarboxylic Acid	000098-89-5	$C_7H_{12}O_2$	1.96	1.84
Phenol	000108-95-2	C_6H_6O	1.46	1.39
1-Naphthol	000090-15-3	$C_{10}H_{8O}$	2.85	2.71
2-Naphthol	000135-19-3	$C_{10}H_8O$	2.70	2.73
Anthranol	000529-86-2	$C_{14}H_{10}O$	3.86	3.65
Cyclopentanol	000096-41-3	$C_5H_{10}O$	0.71	0.69
Cyclohexanol	000108-93-0	$C_6H_{12}O$	1.23	1.29
Decahydro-2-Naphthol	000825-51-4	$C_{10}H18O$	2.66	2.78
ThioPhenol	000108-98-5	C_6H_6S	2.52	2.39
1-Naphthalenethiol	000529-36-2	$C_{10}H_8S$	3.86	3.77
2-Naphthalenethiol	000091-60-1	$C_{10}H_8S$	3.86	3.99
Cyclopentanethiol	001679-07-8	$C_5H_{10}S$	2.55	2.33
Cyclohexanethiol	001569-69-3	$C_6H_{12}S$	3.05	2.94
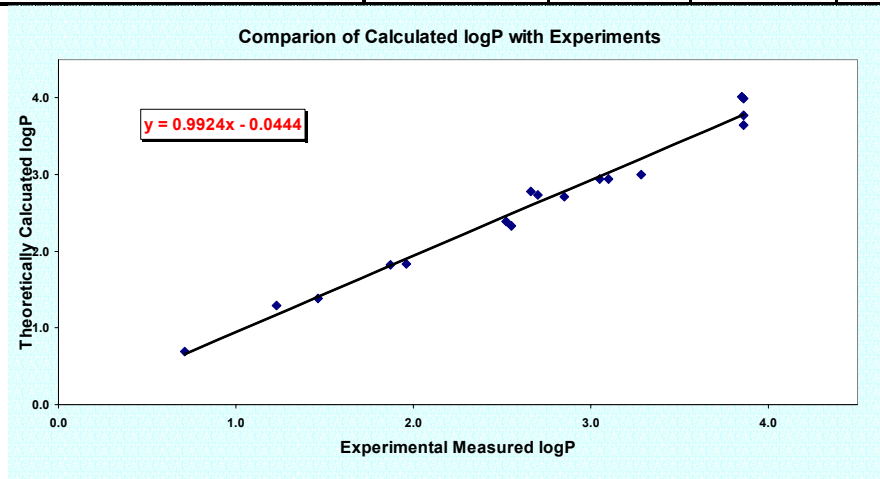
Figure 36: Comparison of calculated logP with experimental measurements.

LogP values of an acidic group attaching to various sites on different ring structures (Figure 37) both aromatics and saturates, have been calculated from first principle. For comparison purpose, a stronger acidic group (-SH) and a non-acidic group (-OH) have also been selected to replace the carboxylic group (-COOH).
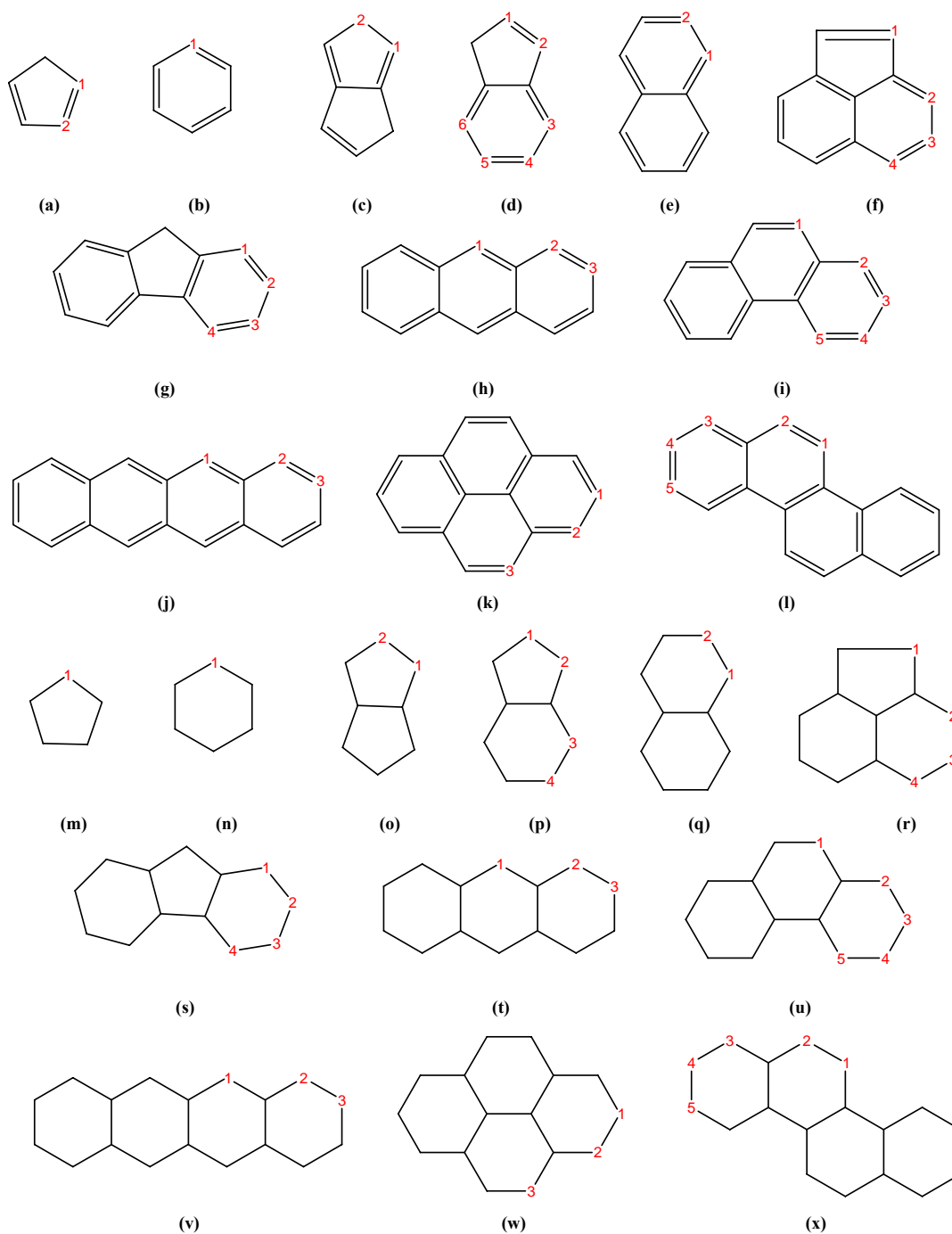
Figure 37: Selected ring compounds and possible attaching sites for the logP calculations.

Table 29 Calculated values of logP for three different function groups attaching on various sites of different ring structures (*ref*. Figure 37 for positions)

	-COOH	-OH	-SH		-COOH	-OH	-SH
a1	0.88	0.17	1.49	g4	4.66	3.51	3.18
a2	1.00	0.27	1.50	h1	4.21	3.76	4.61
b1	1.82	1.39	2.19	h2	4.14	3.77	4.53
c1	2.40	2.14	2.99	h3	4.23	3.80	4.54
c2	2.53	2.16	3.05	i1	4.10	3.75	4.53
d1	2.10	2.02	3.28	i2	4.11	3.74	4.53
d2	2.12	2.10	3.34	i3	4.21	3.78	4.54
d3	2.21	2.12	3.70	i4	4.19	3.77	4.54
d4	2.33	2.19	3.71	i5	4.09	3.75	4.54
d5	2.29	2.17	3.70	j1	5.32	4.75	6.34
d6	2.17	2.09	3.67	j2	5.46	4.80	6.45
e1	2.94	2.71	3.45	j3	5.55	4.83	6.53
e2	3.00	2.73	3.43	k1	5.21	4.46	5.47
f1	3.68	3.35	4.14	k2	4.95	4.36	5.49
f2	3.66	3.33	4.13	k3	4.93	4.37	5.46
f3	3.72	3.36	4.17	l1	4.75	4.75	6.36
f4	3.66	3.33	4.13	l2	5.34	4.74	6.38
g1	3.64	3.45	3.19	l3	5.41	4.75	6.44
g2	4.75	3.54	3.26	l4	5.51	4.79	6.52
g3	4.76	3.56	3.24	l5	5.48	4.78	6.50
	-COOH	-OH	-SH		-COOH	-OH	-SH
m1	1.14	0.69	2.13	t1	4.08	2.72	4.24
n1	1.64	1.19	2.64	t2	4.01	2.73	4.45
o1	1.89	1.65	3.03	t3	4.06	2.72	4.47
o2	2.05	1.75	3.15	u1	3.99	2.72	4.39
p1	2.53	2.24	3.61	u2	4.00	2.73	4.43
p2	2.40	2.15	3.50	u3	4.06	2.72	4.46
p3	2.33	2.10	3.48	u4	4.02	2.72	4.44
p4	2.39	2.16	3.54	u5	3.97	2.73	4.45
q1	2.92	2.70	4.05	v1	4.54	3.98	6.34
q2	2.87	2.65	4.00	v2	4.16	3.97	6.38
r1	3.03	3.01	3.43	v3	4.20	3.94	6.38
r2	3.04	3.00	3.47	w1	3.22	3.15	5.34
r3	3.03	3.03	3.47	w2	3.45	3.19	5.53
r4	2.96	2.94	3.49	w3	3.44	3.18	5.50
s1	3.55	3.52	3.86	x1	4.51	3.96	6.32
s2	3.59	3.59	3.92	x2	4.17	3.97	6.32
s3	3.58	3.58	3.89	x3	4.18	3.97	6.32
s4	3.54	3.53	3.88	x4	4.22	3.95	6.36
				x5	4.20	3.95	6.36

lists all calculated logP values three different functional groups, -COOH, -SH and –OH, attaching on various sites of selected aromatic and saturated ring structures. A brief summary of our calculations is as follows:

- The surface area of a molecule is the predominant factor to its logP value. This is reflected in our calculated results that the larger of a molecular compound, the bigger logP value is.
- Unlike pKa values of naphthenic acids which exhibit a certain degree of structural dependency. The variation of calculated logP values attaching to the different site on the same ring structure is much smaller than that of pKa.

There is virtually no correlation between logP and pKa values, i.e, distributions of an acidic compound in the aqueous phase and in the oil phase is independent to its acidity.

3.5.3 Mechanistic studies of the decarboxylation of aromatic carboxylic acids
3.5.3.1 Decarboxylation of aromatics is an energetically favorable process

Our thermodynamic calculation results indicate that the decarboxylation of a benzoic acid (C_6H_5-COOH) to form benzene (C_6H_6) and carbon dioxide (CO_2) is an energetically favorable process. The calculated gas-phase Gibbs' Free Energy Difference (ΔG) for this reaction is -7.3 kcal/mol at room temperature (T = 298.15 K) ()

$$C_6H_5\text{-COOH} \rightarrow C_6H_6 + CO_2$$

Table 30 Thermodynamic calculations of the decarboxylation reaction of the benzoic acid

Compounds	E_0	ZPE	dG	G
	(Hartree)	(kcal/mol)	(kcal/mol)	(kcal/mol)
C_6H_5-COOH	-420.946837	75.231	-35.784	-264108.69
C_6H_6	-232.310025	68.976	-15.688	-145723.46
CO_2	-188.646591	7.272	-22.279	-118392.53
$C_6H_6+CO_2$	-420.956616	76.248	-37.966	-264115.99
Gibbs' Free Energy Difference =			**-7.30**	kcal/mol

3.5.3.2 Thermal decomposition of simple carboxylic acids are not easy

Without catalyzed, most of the carboxylic acids could not be easily decarboxylated. As a matter of fact, the thermal decomposition energies for same simple carboxylic acids have been found to be very high (). This indicates the transition barriers for the decarboxylation reaction without the presences of the catalyst requires much high temperature, which is not applicable in our naphthenic acid removal process.

Table 31 Most of carboxylic acids are not easy to thermal decomposition

Acid	Chemical Formula	Thermal Decomposition Reaction	Products	Energy Barrier (kcal/mol)
Formic Acid	HCOOH	Dehydration	$CO + H_2O$	66
	HCOOH	Decarboxylation	$CO_2 + H_2$	68
Acetic Acid	CH3COOH	Dehydration	$CO + H_2O$	67.5
	CH3COOH	Decarboxylation	$CO_2 + H_2$	62

3.5.3.3 Reactions of the Mg(R-COO)$_2$ salt

In the present of the MgO catalyst, the formation of the Mg-salt through base-acid neutralization reaction has been detected in several occasions. It has been long speculated that the salt formation could have played an important role in the catalyzed decarboxylation reaction. i.e, the Mg-(R-COO)$_2$ as an intermediate. To examine this hypothesis, a series of calculations has been performed to determine the most energetically favorable path (Figure 38). Several possible reaction paths for the reaction of the Mg-salt to form the phenol as the final product are considered. The numbers (in unit of kcal/mol) represent the calculated Gibbs' Free Energy Differences. Clearly, the reaction path I + II, with the reaction energy of +18.75 kcal/mol, is the most energetically favorable. The reaction path IV + V + VII has slightly higher reaction energy of + 24.96 kcal/mol, but the reaction path III + VII requires much higher energy with the reaction energy of + 44.40 kcal/mol.
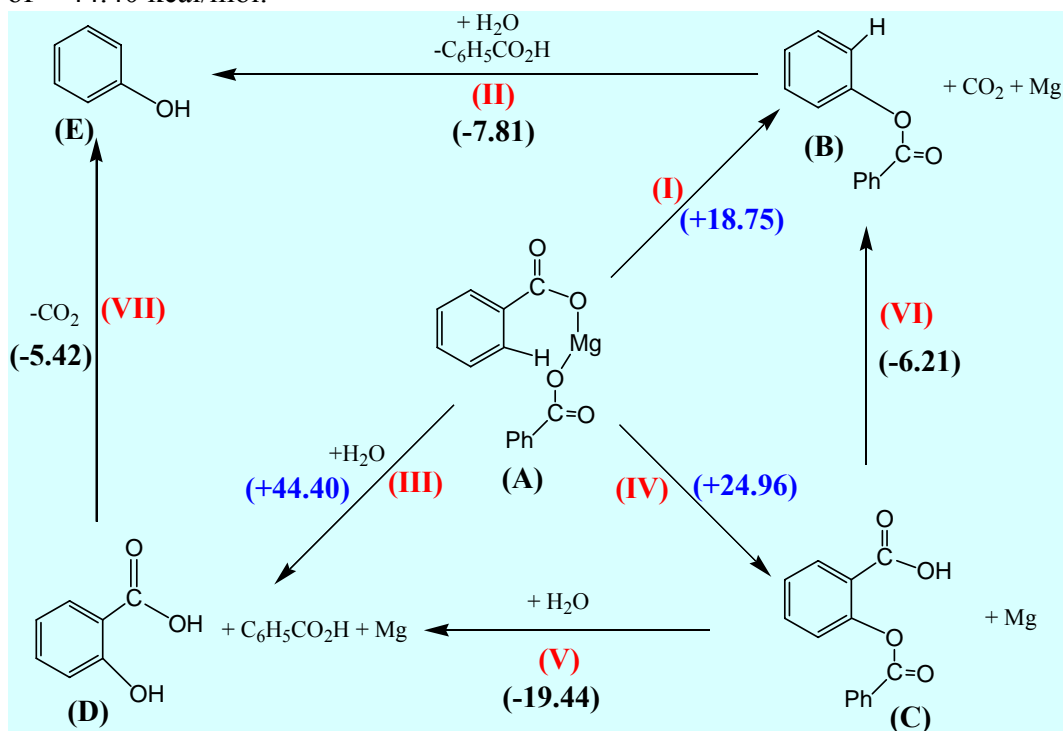
Figure 38: Theoretic energy profiles of the reaction of the Mg-salt.

3.5.3.4 MgO-catalyzed decarboxylation of aromatic naphthenic acids

In the path I mentioned above, the initial nucleophilic attack on the *–ortho* site of the aromatic ring is responsible for the potential lower reaction energy. Intrigued by this observation, we studied a reaction pathway of MgO-catalyzed decarboxylation of aromatic carboxylic acid (benzoic acid) to form phenol. Two transition states are successfully located. The first one features a 4-membered ring transition of the OH group to attack the *–ortho* position of the benzene ring (TS-OH), and the second one is a classical 1,2-shift of a proton from *–ortho* position to the *–ipso* position, accompanied by the formation of the CO_2 and phenol (TS-H). The calculated transition barriers are 30.85 and 48.66 kcal/mol, respectively for TS-OH and TS-H (Figure 39).
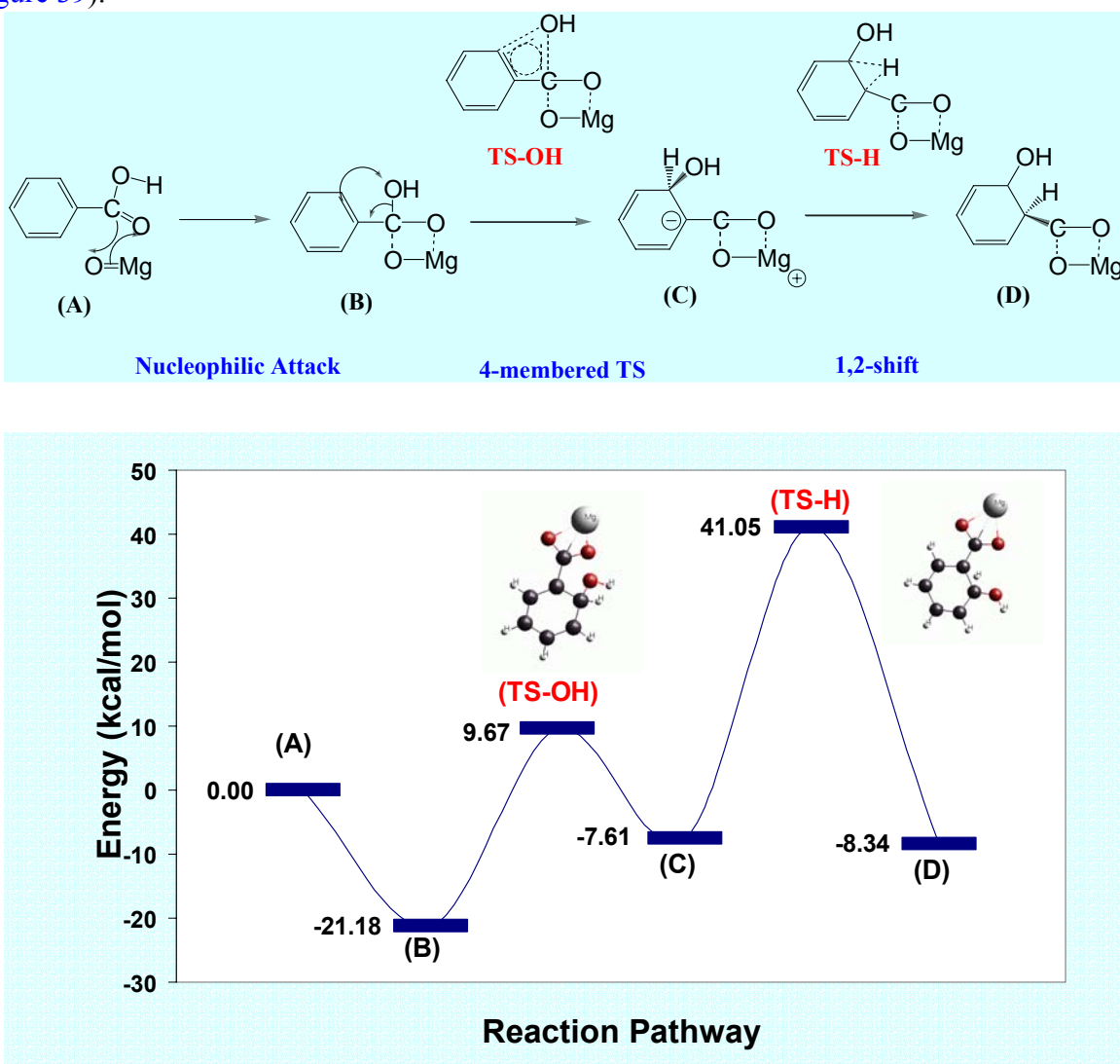
Figure 39: Reaction pathway of a MgO-catalyzed decarboxylation of the benzoic acid.

3.5.4 Theoretical studies of chemical processes on the oxide surfaces

3.5.4.1 Adsorption of acids on the oxide surface

Calculated energies of the CaO and MgO slab, BA and CHCA molecules, as well as the molecule + slab systems are given in Table 32. From these results, the adsorption energies of BA and CHCA on CaO and MgO surfaces could be obtained as in Table 33

Table 32 Calculated energies in both atomic unit (a.u.) and eV

Compound	Calculated Energy	
	a.u.	eV
MgO-Slab	-580.7883	-7898.72
CaO-Slab	-1230.469	-16734.38
BA	-150.8614	-2051.72
CHCA	-157.7015	-2144.74
MgO-Slab+BA	-731.6973	-9951.08
MgO-Slab+CHCA	-738.7742	-10047.33
CaO-Slab+BA	-1381.593	-18789.67
CaO-Slab+CHCA	-1388.657	-18885.73

Table 33 Adsorption energies (eV) of a BA or a CHCA on MgO(110) and CaO(100) slab

	Adsorption Energy (eV)	
	BA	CHCA
MgO-Slab	-0.65	-3.87
CaO-Slab	-3.57	-6.61

From these calculations, we can see that:

- Adsorption of an acid on both MgO and CaO surface result in a more stable state (E_{ads}<0), indicating both MgO and CaO could be served as solid adsorbents.
- E_{ads} on CaO is more negative than on MgO, indicating CaO is a stronger adsorbent than MgO
- Adsorption of saturate on the oxide surface is in general stronger than aromatics.

3.5.4.2 Deprotonation of acids on the oxide surfaces

Once an acid is adsorbed on the oxide surface, it could readily loss the proton, the deprotonation process (Figure 40) Calculated energies of a combination of the adsorption of a

proton (H^+) on the O and the adsorbed carboxylate on the metal center are list in Table 34. From these the adsorption energies and the deprotonation energies can be computed as in Table 35.
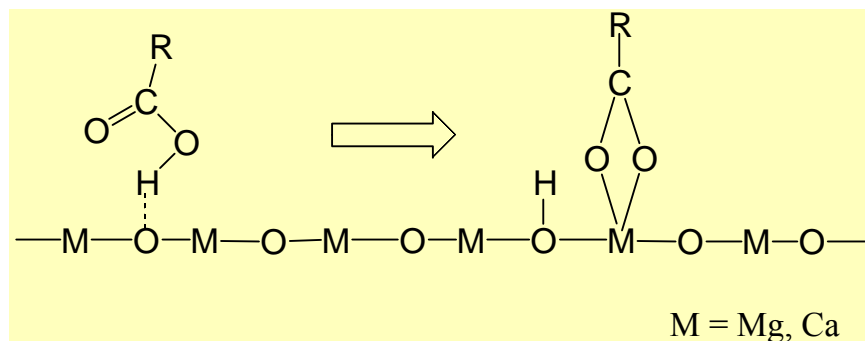
Figure 40: The Deprotonation process of an adsorbed acid on the oxide surface.

Table 34 Calculated energies (eV) of the deprotonated configurations

Compounds	Calculated Energy	
	(a.u)	(eV)
MgO-slab+BA+H	-731.7075	-9951.22
MgO-slab+CHCA+H	-738.7289	-10046.71
CaO-slab+BA+H	-1381.5338	-18788.86
CaO-slab+CHCA+H	-1388.5684	-18884.53

Table 35 Adsorption energies and deprotonation energies of acids on the oxide surfaces

	Adsorption Energy (eV)		Deprotonation Energy (eV)	
	$BA^- + H^+$	$CHCA^- + H^+$	$BA^- + H^+$	$CHCA^- + H^+$
MgO-Slab	-0.79	-3.25	-0.14	0.62
CaO-Slab	-2.76	-5.41	0.81	1.20

From these calculations, we conclude that the deprotonation of an adsorbed acid on the oxide surface is a relative easy process. Furthermore, the acid could loss its proton easier on MgO than on CaO. For the benzoic acid on MgO, the protonation energy is negative, suggesting this could be a spontaneous process.

3.5.4.3 Decarboxylation of acids on the oxide surfaces

Energy profiles of the decarboxylation of the adsorbed carboxylate to form CO_2 have also been calculated (Figure 41). The calculated adsorption energies are listed in Table 36, and from these, the decarboxylation energies are obtained (Table 37).

M = Mg, Ca
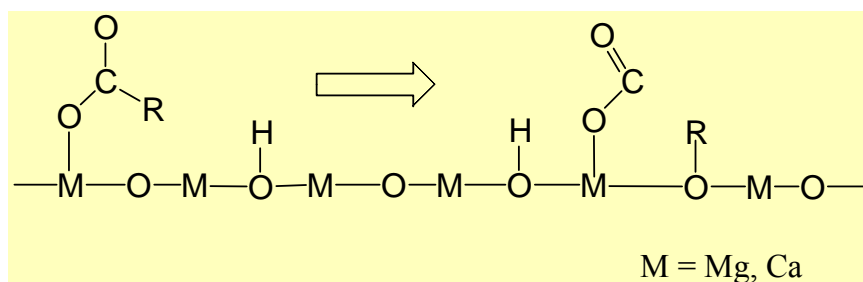
Figure 41: The decarboxylation Process of the adsorbed carboxylate on the oxide surfaces.

Table 36 Calculated energies (eV) of decarboxylated compounds

Compound	Calculated Energy	
	a.u.	eV
MgO-Slab+ph+CO_2+H	-731.4029	-9947.08
MgO-Slab+CHC+CO_2+H	-738.322888	-10041.19
CaO-Slab+ph+CO_2+H	-1381.06957	-18782.55
CaO-Slab+CHC+CO_2+H	-1387.93026	-18875.85

Table 37 Adsorption and decarboxylation energies of adsorbed carboxylates on the oxide surfaces

	Adsorption Energy (eV)		Decarboxylation Energy (eV)	
	$BA^- + H^+$	$CHCA^- + H^+$	$BA^- + H^+$	$CHCA^- + H^+$
MgO-Slab	3.36	2.27	4.14	5.52
CaO-Slab	3.55	3.27	6.31	8.68

As one would have expected, the decarboxylation process is the most energetically demanded process. Comparison indicates that decarboxylation of the adsorbed carboxylate on MgO will be easily than on CaO. This result suggests that CaO could be a good solid adsorbent for naphthenic acids, but could not perform catalysis decarboxylation. MgO might have dual functions (adsorption and decarboxylation).

3.5.4.4 Desorption of acids on the oxide surfaces

To complete the overall reaction path, desorption of forming products from the oxide surfaces has also been calculated (Figure 42). The calculated energies are listed in Table 38, and from those, desorption energies are given in Table 39.


Figure 42: The desorption process on the oxide surfaces.

Table 38 Calculated energies (eV) of desorption on the oxide surfaces

Compound	Calculated Energy	
	a.u.	eV
MgO-Slab+ph+CO_2	-731.666612	-9950.67
MgO-Slab+CH+CO_2	-738.555241	-10044.35
CaO-Slab+ph+CO_2	-1381.34751	-18786.33
CaO-Slab+CH+CO_2	-1388.23614	-18880.01

Table 39 Adsorption and desorption energies on the oxide surfaces

	Adsorption Energy (eV)		Desorption Energy (eV)	
	ph+CO_2	CH+CO_2	ph+CO_2	CH+CO_2
MgO-Slab	-0.23	-0.89	-3.59	-3.16
CaO-Slab	-0.23	-0.89	-3.78	-4.16

Desorption of the forming products, namely CO_2 and phenol (ph) or Cyclohexane (CH) from the oxide surface is an energetic downhill process. It should not require additional energy for separation.

3.5.4.5 Summary of chemical processes of carboxylic acids on the oxide surfaces

Figure 43 highlights the overall calculated energy profile of the benzoic acid (BA) and Cyclohexane Carboxylic Acid (CHCA) interact with the MgO(100) and CaO(100) surfaces. From these calculations, we conclude that:

- Adsorption of a carboxylic acid on CaO is much stronger than on MgO, indicating that CaO is a good solid adsorbent for the naphthenic acid;
- Decarboxylation is the most energetically demanded process, so it will be the rate-determining step in the overall reaction path;
- MgO could have a dual function characterization for both adsorption and decarboxylation for naphthenic acids.
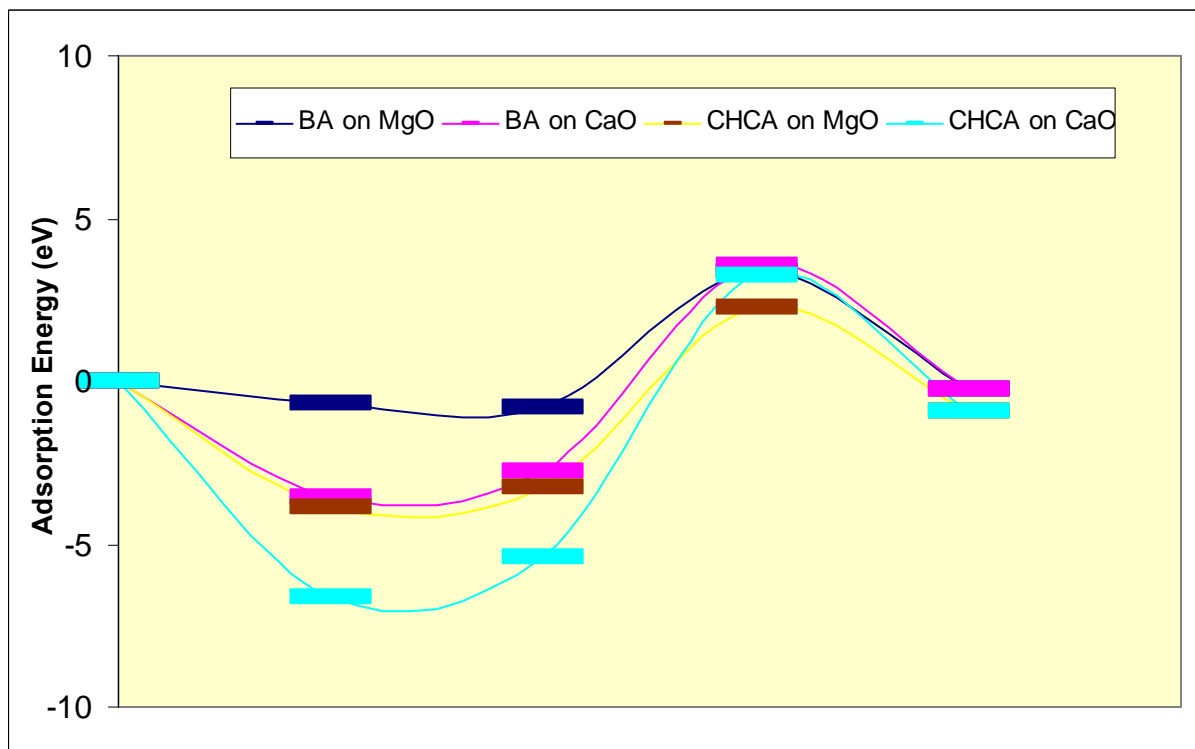

Figure 43: Summary of the calculated energy profile of carboxylic acids on the oxide surfaces.

3.5.5 MgO-catalyzed ketonization – a reaction toward the process design

In light of our recent experimental observations that various ketonic intermediates have been identified in non-stationary flow reactor condition with the presence of the MgO catalyst, theoretical studies have been carried out to provide a mechanistic view of the ketonic decarboxylation as an effort to optimize the process design. Even though the bimolecular coupling of the carboxylic acids for the formation of ketones has been a well-known biological and chemical process for almost 150 years [43], its reaction mechanism is still under discussions [44, 45]. In contract to the oxidative decarboxylation which is believed to be mostly radical mechanism predominant [46], ketonization involving di-carboxylic acids is considered to occur in a more concerted fashion. Depending on the promoter type, the reaction could be either catalytic (T < 300 ^{0}C) [47-49] or pyrolytic (T > 400 ^{0}C) [50, 51] or both [52]. Therefore, our

experimental results that indicating that MgO is capable of catalyzing decarboxylation at low-temperature (200 ~ 300 ^{0}C), are therefore of special industrial interests for the development of a low-temperature catalyzed decarboxylation process for the naphthenic acid removal.

3.5.5.1 Ketonization without catalyst is very difficult

A typical ketonization reaction involves two carboxylic molecules to form a ketone, accompanied by water and carbon dioxide formations.

$$RCOOH + R'COOH \rightarrow RC=OR' + CO_2 + H_2O \qquad (11)$$
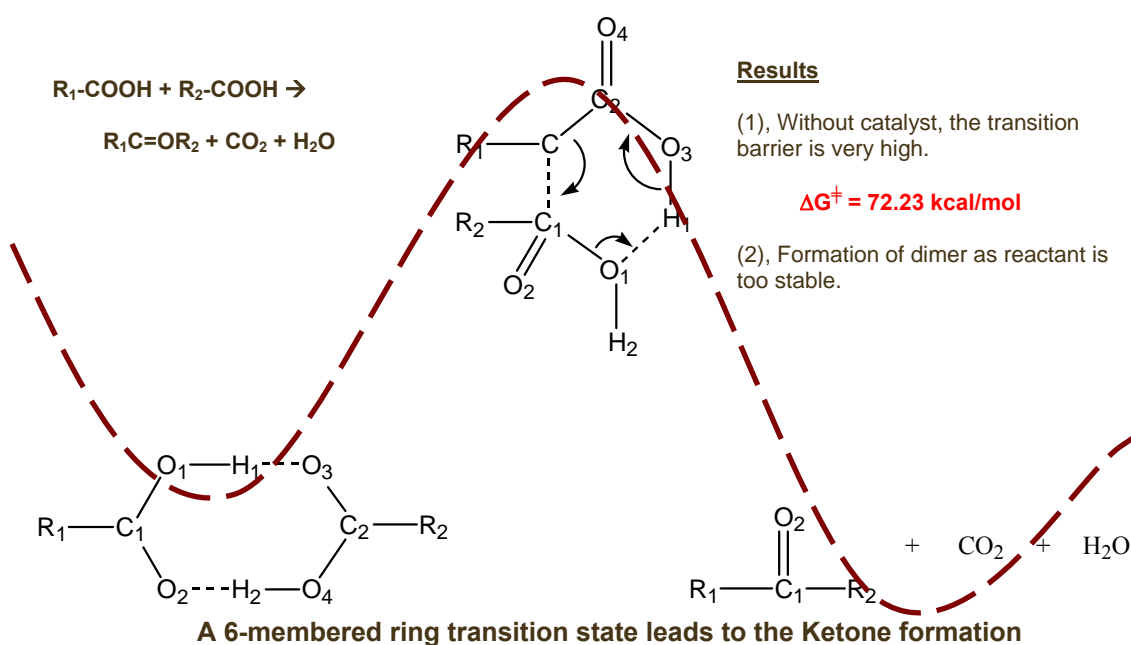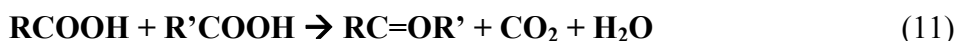
Figure 44: Ketonization with catalyst is very energetically demanded.

Even without the presence of the MgO catalyst, a bimolecular concerted reaction pathway between two acidic compounds exists. TS for this reaction is characterized by a nucleophilic attack from the β-Carbon ($C_\beta 1$) of one acid to the α-Carbon ($C_\alpha 2$) of the second acid. Decarboxylation (breaking of the $C_\alpha 1$-$C_\beta 1$ bond to form CO_2) is accomplished by a proton transfer forming a H_2O leaving group. Even though this reaction features a 6-membered ring transition, the calculated transition barrier ($\Delta\Delta G^{\ddagger} = 72.2$ kcal/mol) is substantially high. The tendency to form a dimer (Figure 44) of two acids yields an extra stability in the reactant configuration (an -18.0 kcal/mol energy gain compared to two separated acetic acids) is

responsible for this high transition barrier. It is worth mentioning that the energies for the thermal decomposition of the acetic acid are in the range of 62 ~ 68 kcal/mol (*ref* Table 31). Therefore, the ketonic decarboxylation of two acetic acids without the assistant of catalyst is very unlikely.

3.5.5.2 Formation the mg-salt results is even difficult to break

Despite of the relative high lattice energy of MgO, the bulk acetate formation has been detected when the MgO catalyst is used as catalyst. The Mg-acetate salt could form via the acid-base neutralization reaction:

$$\textbf{RCOOH + R'COOH + MgO} \rightarrow \textbf{RCOOMgCOOR' + H}_2\textbf{O} \qquad (12)$$

(1)   Acid-Base Neutralization

MgO + 2 CH$_3$COOH $\rightarrow$ Mg(CH$_3$COO)$_2$ + H$_2$O

(2)   Thermal Decompostion of Salt

Mg(CH$_3$COO)$_2$ $\rightarrow$ CH$_3$COCH$_3$ + CO$_2$ + MgO

Results

(1)   Transition barrier is even higher

$\Delta G^{\ddagger} = 87.56$ kcal/mol

(2)   Once a Mg(R-COO)$_2$ salt is formed, it is very stable.
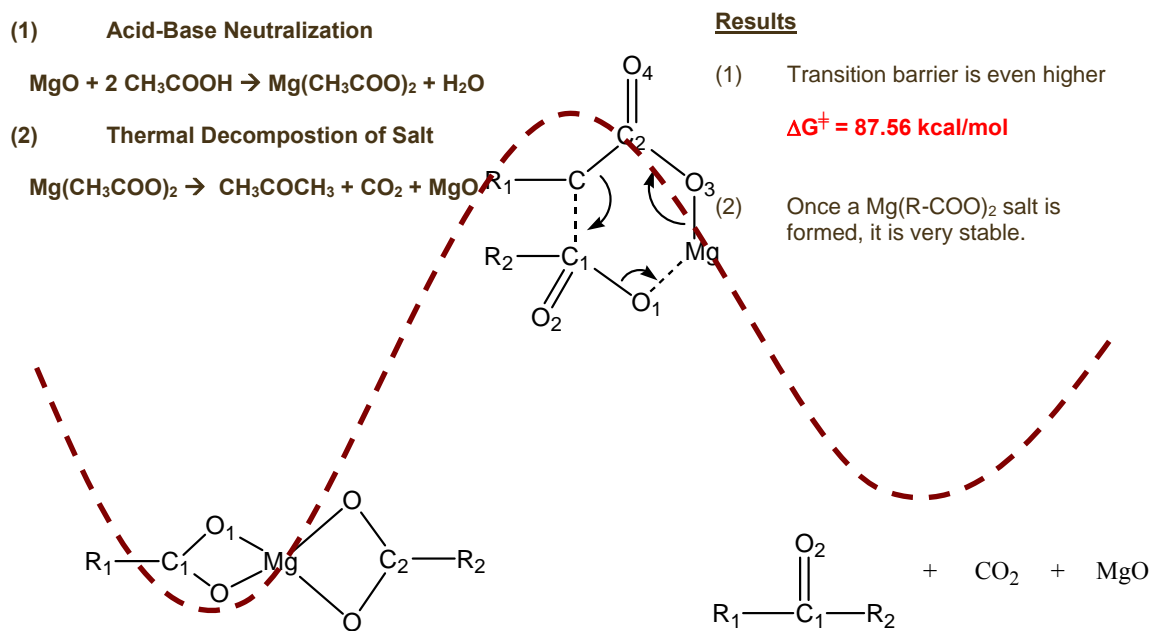
Figure 45: Formation of Mg-Salt is even difficult to break.

A 6-membered ring transition state analogous to the di-acid mechanism has also been located (Figure 45). The transition barrier is found to be even higher ($\Delta\Delta G^{\ddagger} = 87.6$ kcal/mol). This clearly indicates that the Mg-acetate salt is very stable and can only be decomposed through the high-temperature pyrolytic process, but is not responsible for the ketonic decarboxylation observed in the low-temperature range (~300 ^{0}C). In this sense, the salt formation is very unlikely to be an intermediated step of the catalytic ketonization reaction, instead, it behaviors

more likely to be a 'dead' end of the process. Once the Mg-acetate salt is forming, it will need much high energy to break it.

3.5.5.3 A novel ketonization mechanism with significantly lower transition barrier

To account for the experimentally observed low-temperature MgO-catalyzed ketonization, we propose a new reaction path as follows: first, one carboxylic acid adsorbs and deprotonates on MgO; then a second acid in its 'free' form reacts with this associated acidic compound undergoing a concerted 6-membered ring transition (Figure 46) The so-calculated transition barrier is significantly lower ($\Delta\Delta G^{\ddagger} = 42.4$ kcal/mol) than those in dimer and salt forms, indicating that this is much energetically favorable. A less stable reactant configuration is responsible for this dramatic transition barrier reduction. Furthermore, the $C_\alpha 1$-$C_\beta 1$ bond related to the decarboxylation process on the associated acid compound has also been substantially weakened ($C_\alpha 1$-$C_\beta 1 = 1.512$ Å compared to $C_\alpha 2$-$C_\beta 2 = 1.494$ Å), also contributing to the transition barrier lowering.
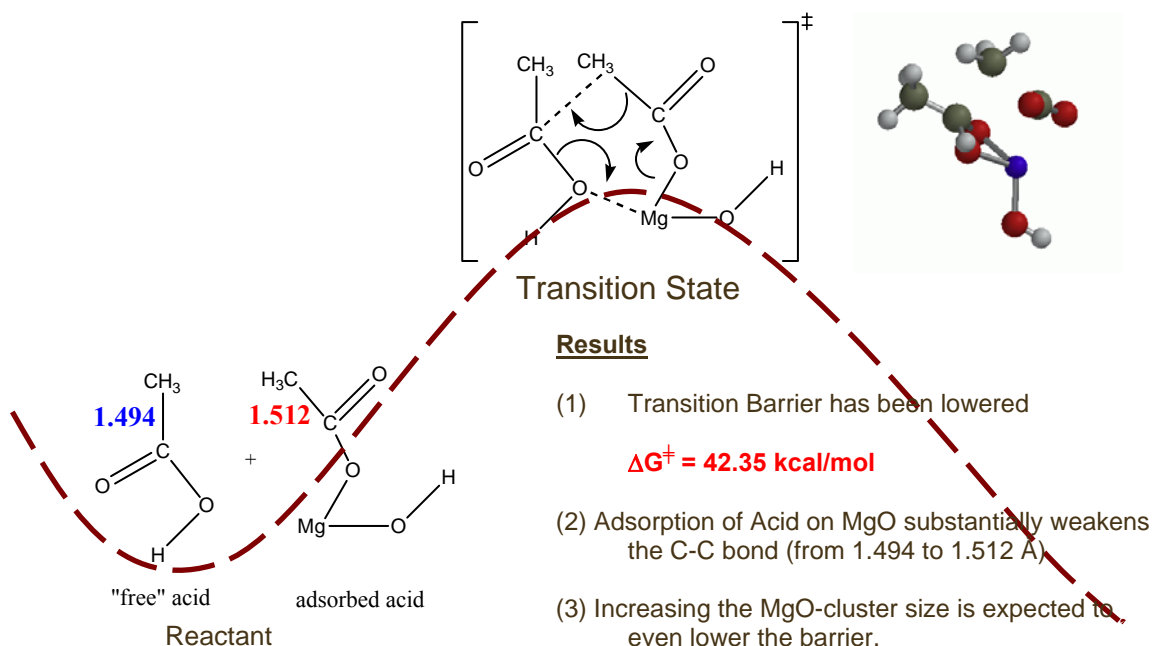

Figure 46: A Novel ketonization reaction mechanism.

90

3.5.5.4 Discussions and implications

A brief summary of above calculations is as follows:

- All three transition states follow a typical concerted S_N2 reaction mechanism. The methyl group ($H_3C_\beta1$) transfers from $C_\alpha1$ (decarboxylation, breaking the $C_\beta1$-$C_\alpha1$ bond) to $C_\alpha2$ (ketonization, forming the $C_\beta1$-$C_\alpha2$ bond), undergoing a chiral inversion with a nearly planar structure at TS.

- The structure of the Mg-O ion-pair, used in the proposed model to simulate MgO, does not change during the reaction. Therefore, the proposed model could be easily extended to the interaction of a 'free' acid with the adsorbed acetate on the MgO surface. This suggests that the ketonization reaction favor the gas-surface interaction model (the so-called Eley-Rideal Model), rather than the Langmuir-Hinshelwood Model [53], in which both reacting species are bonded to the solid surface.

- Formation of the metal salt has long been speculated to be an important step in the decarboxylation reaction. Several hypotheses on the concerted decarboxylation reaction mechanism have been based on the initial formation of the metal salt compound. Our calculations clearly indicate that the Mg-salt is a very stable species that requires very high energy to break. Therefore avoid the formation of the metal salt is important in the naphthenic acid removal process design.

- Our novel ketonization reaction mechanism features the interaction of an associated carboxylate ion on the solid surface with an unassociated 'free' acid. Availability of both associated and non-associated acidic molecules is an important controlling factor for the ketonic decarboxylation. Adsorption and deprotonation of an acidic molecule on MgO could be readily due to the strong basicity of MgO. Our flow reactor design also facilitates the reaction by ensuring the continuous supply of 'free' acids.

4.   Conclusions

Through our continuous effort working with this "Improved Processes to Remove Naphthenic Acid" project, we developed effective low temperature decarboxylation catalysts, obtained profound understanding on catalytic decarboxylation process, and also explored the possibility of creating a real naphthenic acid removal process.

Based on a large amount of experimental investigation with model carboxylic acid compounds, we discovered four type effective decarboxylation catalysts, which are alkaline earth metal oxide, transition metal oxides, strong acidic zeolite and supported precious metal catalysts. The representative catalysts for these four types include MgO, Ag_2O/Cu_2O, HZSM-5 zeolite and Pt/Al_2O_3. All of these catalysts show excellent catalytic decarboxylation activities at relative low temperature ca. 200-300°C. The decarboxylation mechanism was investigated through theoretical calculation and product/intermediate analyses. It has been clear that MgO catalyze decarboxylation reaction through a ketonization mechanism with two moles of carboxylic acid, which give rise to the formation of one mole of CO_2. Ag_2O and Cu_2O are, most possibly, involved in decarboxylation process via a free radical mechanism. On the other hand, the high activities of zeolite towards decarboxylation would be caused by C-C cracking catalyzed by the strong acidic sites on zeolite. Due to the complexity of the oil composition and poison issues, not all of these catalysts can be directly applied in crude oil. However, their applicability in organic chemistry as well as other functional group modification would be highly predicable.

To explore the applicability of the catalysts developed from the model carboxylic acid tests to heavy oil upgrading, more experimental investigation were performed with real oil through a batch and flow reaction systems. The NA removal efficiency was characterized by TAN measurement. The results of batch reaction catalytic tests revealed the effectiveness of several solid catalysts that can suppress TAN from 4.36~5.00 (raw oil) to 1.0~2.0 in the temperature range of 250~300°C. These catalysts might be metal oxides, salts, supported solid superbases and others, represented by CaO, $CaCO_3$, Na_2CO_3, Na/MgO and Na/13X+4A zeolite etc.

Focusing on MgO catalyst, which was identified to be effective to catalytic decarboxylation, naphthenic acid adsorption, flow reaction tests with a fixed bed tubular reactor were performed and the results revealed the effectiveness of MgO to naphthenic acid removal. At 300°C, with contact time in the range of 200-500 seconds, the TAN reduction rates could reach about 30~50% while the catalyst could keep its activity for more than 50hrs. Furthermore at 350°C with longer contact time ~ 33min, the TAN reduction rate reached as high as 70% while the

catalyst kept the high activity until 171hr. Meanwhile, the viscosities of the treated oils were found to be reduced significantly through this process, which results in API value upgraded from 13.2 to 17.7, about 4 units improvement.

The results of other measurements and catalyst characterization such as C/H analysis, XRD measurement indicate that MgO catalyst basically keep its raw structure during the reaction without the formation of magnesium carbonate. Carbon deposition occurred on the catalysts depending on the catalyst types and the operation condition. The presence of water can suppress the coking or heavy residue deposition on catalysts effectively. The enhanced CO_2 formation over MgO, Ag_2O, Cu_2O catalysts from gold tube crude oil tests provided direct evidence showing the occurrence of catalytic decarboxylation.

Our adsorption experiments revealed that clay minerals, such as sepiolite and montmorillonite, have the potential to be used as adsorbents for the removal of naphthenic acids. In order to enhance the efficiency of adsorption of NAs by mineral clays, various species, such as metal-oxide pillars and organic or organometallic complexes should be incorporated into the structure of clay minerals to improve the adsorptive and/or catalytic properties of the products.

In summary, combining our catalytic and adsorptive approaches developed in this work; the NA in crude oil can be effectively removed and the quality of the oil can be upgraded.

Theoretical studies based on the modern molecular modeling techniques have played an essential role in this project. Using a variety of state-of-the-art computational simulation tools, we have carried out a number of theoretical works to provide insights of the physical and chemical properties of different naphthenic acids, as well as the fundamental views of the decarboxylation processes. A brief summary of our theoretical achievements is as follows:

- To select NA model by theoretically evaluating the acidity (pKa) and 1-octane/water distribution coefficient (logP) – a large number of different naphthenic acid compounds have been studied, and their pKa and logP values have been calculated from first-principle. From these studies, we concluded that the variation of the acidity of naphthenic acid compounds is relatively small (~ 1.0 pKa value). This provides a theoretical foundation to our selection of the mixture of model compounds as a represent of the naphthenic acid in our early experimental tests.

- To study decarboxylation reaction mechanisms with key transition states located and thermodynamic properties taking into account – Different reaction catalyzed decarboxylation mechanism have been investigated utilizing Quantum Mechanics Density Functional Theory (DFT) with the stable, intermediated and transition states located. Combining with our experimental efforts, we have identified a novel concerted ketonic decarboxylation mechanism which provides a significant insight to our experimental observations of the formation of the various ketonic compounds.

- To provide the theoretical guidance on catalyst selections and designs – In conjunction with our experimental efforts to screen and select proper catalysts, theoretical studies have been carried out to provide theoretical guidance. Most of the transition metal and precious metal oxides exhibit certain degrees of decarboxylation capabilities, suggesting that a radical or an ionic reaction mechanism will be predominant. On the other hand, magnesium oxide (MgO), which is of our most interest, will follow a most concern reaction pathway due to its lack of empty d-orbits.

- To investigate the adsorption of NA on metal and/or alloy solid surfaces – Using our newly developing 3-dimension computational software (SeqQuest), different chemical processes occurring on metal oxide surfaces have been theoretically studied. By Comparing of the calculated energy profiles of the selected aromatic and saturated naphthenic acids interacting with a CaO and MgO surface, we found that CaO could be a good chemical adsorbent towards naphthenic acids, but could not catalyze the decarboxylation. MgO, however, exhibits both good qualities of adsorption and decarboxylation.

- To help develop and optimize a process of effectively removing NA – Our theoretical studies of the MgO-catalyzed ketonic decarboxylation mechanism indicates that a reaction pathway corresponding to the lowest transition barrier comes from the interaction of a bonded carboxylate (adsorbed and deprotonated acid on the MgO surface) with an unbonded ("free") acid compound. Therefore, availability of both associated and non-associated acid compounds will be essential to facilitate this reaction. Furthermore, our studies clearly indicate that the formation of metal-salt, which has been long speculated as an important step in the overall decarboxylation reaction, is actually a 'dead' end of the process. Once a metal-salt is formed, it requires much higher energy to break it. These results strongly support our flow reactor process design.

References

1) B. Region, in: API Proceedings, vol.11, Russia, 1930, P.102.
2) N.A. Tomczyk, R.E. Winans, J.H. Shinn, R.C. Robinson, Energy & Fuels 15 (2001) 1498-1504.
3) M.P. Barrow, L.A. McDonnell, X. Feng, J. Walker, P.J. Derrick, Anal. Chem. 75 (2003) 860-866.
4) W.A. Derungs, Corrosion 12 (1956) 617-622.
5) Gutzeit, J. Mater. Perform. 16 (1977) 24-35.
6) Piehl, R.L., NACE Conference, Corrosion / 87, 1987, paper No. 196.
7) 1999 Annual Book of ASTM Standards, Section 5, Petroleum Products, Lubricants, and Fossil Fuels, D664-95, Standard Test Method for Acid Number of Petroleum Products by Potentiometric Titration. pp. 261-267.
8) US Patent, 5,434,329 (1995).
9) S. Ozvatan, Y. Yurum, Energy Sources 24-6 (2002) 581-589.
10) D.J. Darensbourg, M.W. Holtcamp, E.M. Longridge, B.Khandelwal, K.K. Klausmeyer, J.H. Reibenspies, J. Am. Chem. Soc.117-1 (1995) 318-328.
11) D.J. Darensbourg, E.M. Longridge, B. Khandelwal, J.H. Reibenspies, J. Coordination Chem. 32,1-3 (1994) 27-37.
12) B.H. Muller, J. Spitzer, J, Enantioselective Catalysis 100, Monatshefte Fur Chemie 127, 8-9 (1996) 845-858.
13) M. Watanabe, H. Inomata, R.L Smith, K. Arai, Appl. Catal. A-General 219, 1-2 (2001) 149-156.
14) D.J. Darensbourg, J.A. Chojnacki, E.V. Atnip, J. Am. Chem. Soc. 115-11 (1993) 4675-6782.
15) Y. Takemura, A. Nakamura, H. Taguchi, K. uchi, Ind. Eng. Chem. Prod. Res. & Develop. 24-2 (1985) 312-215.
16) F. Behar, P. Ungerer, S. Kressmann, J.T. Rudkiewicz, Revue De Linstitut Francais Du Petrole, Mars-Avril 46-2 (1991) 151-182.
17) Sposito, G. The chemistry of soils. Oxford University Press, New York (1989)
18) Kowalska, M., Güler, Hülya, Cocke, D. L., The Sci. of the Total Environ., 1994, 141, 223-240.
19) Sparks, D. L. Environmental soil chemistry. Academic Press, San Diego (1995)
20) Grim, R. E. Clay Mineralogy, McGraw-Hill Book Co., New York (1968)
21) Kuang, W.; Facey, G. A.; Detellier, C. Dehydration and rehydration of palygorskite and the influence of water on the nanopores. Clays and Clay Minerals, 52, 635 (2004)
22) Essington, M. E. Soil and Water Chemsitry, CRC Press, Boca Raton (2004)
23) Bilgic, C. Investigation of the factors affecting organic cation adsorption on some silicate minerals. J. Colloid Interface Sci. 281, 33 (2005)
24) Galan, E. Properties and applications of palygorskite-sepiolite clays. Clay Minerals, 31, 443 (1996)

25) Van Olphen, H.; Fripiat, J. J. Data handbook for clay minerals and other non-metallic minerals. Pergamon Press, New York (1979)

26) Jaynes, W. F.; Zartman, R. E.; Green, C. J.; San Francisco, m. J. Castor toxin adsorption to clay minerals. Clays and Clay Minerals, 53, 268 (2005)

27) Dzidic, A. C. Somerville, J. C. Raia and H. V. Hart, Anal. Chem, 60 (1988) 1318.

28) T. P. Fan, Energy & Fuels, 5 (1991) 371.

29) W. A. Derungs, Corrosion, 12(2) (1956) 41.

30) W. K. Seifert, Anal. Chem., 41(12) (1969) 1638.

31) C. S. Hsu, G. J. Dechert, W. K. Robbins and E. K. Fukuda, Energy & Fuels, 14 (2000) 217.

32) B. H. Greeley, T. V. Russo, D. T. Mainz, R. A. Friesner, J-M. Langlois, W. A. Goddard III, R. E. Donnolly and M. N. Ringgnalda, J. Chem. Phys., 101 (1994) 4028.

33) D. Becke, J. Chem. Phys., 98 (1993) 5648; 96 (1992) 2155; 97 (1992) 9173.

34) Lee, W. Yang, and R. G. Parr, Phys, Rev. B., 37 (1988) 785.

35) Y. H. Jang, L. C. Sowers, T. Cağin, and W. A. Goddard, J. Phys. Chem. A, 105 (2001) 274-280.

36) Y. H. Jang, L. C. Sowers, T. Cağin, and W. A. Goddard, J. Phys. Chem. A, 105 (2001) 274-280.

37) R. Pestman, R.M. Koster, A.V. Duijne, J.A.Z. Pieterse, V. Ponec. J. Catal.168 (1997) 265-272

38) T. Ushikuba, H. Hattori, K. Tanabe, Chemistry Letters (1984) 649-652.

39) U.S. Patent 5,985,137

40) Pedro Pereira, Roger Marzin, Luis Zacarias et al., Vision Tecnologica, 6 - 1 (1998) 5-14

41) Petro Pereira, Cauri Flores, Huge Zbinden, Jose Guitian et al., The Oil and Gas Journal, 99-20 (2001) p79

42) U.S. Patent 5,885,441

43) C. Friedel, Justus Liebigs Ann. Chem. 1858, 108, 12

44) M. Renz, Eur. J. Org. Chem. 2005 979

45) G.A.H. Mekhemer, S.A. Halawy, M.A. Mohamed, M.I. Zaki, J. Catal. 2005, 230, 109

46) For review of the oxidative decarboxylation reaction, see: J. March ed. Advanced Organic Chemistry, 4th ed. John Wiley & Sons, New York, pp 1185 and references therein

47) K. M. Parida, A. Samal, N. N. Das., Appl. Catal. A, 1998, 166, 201;

48) E. Mueller-Erlwein, B. Rosenberger, Chem. Ing. Tech. 1990, 62, 512

49) N. P. Matsota, V. D. Mezhov, Z. S. Novocherk, Zh. Pril, Khim (Lenin-grad) 1971, 44, 1823

50) M. I. Zaki, M. A. Hasan, L. Pasupulety, Langmuir 2001, 17, 4025

51) R. A. Hites, K. Biemann, J. Am. Chem. Soc. 1972, 94, 5772

52) J. Bigeleisen, A. A. Bothner-By, L. Friedman, J. Am. Chem. Soc. 1953, 75, 2908

53) J.C. Kuriacose, J. Sci. Ind. Research (India) 20B, 1961, 82